IN-LB	Inch-Pound Units
SI	International System of Units

Guide for Precast Concrete Tunnel Segments

Reported by ACI Committee 533

ACI 533.5R-20

American Concrete Institute
Always advancing

First Printing
April 2020
ISBN: 978-1-64195-097-8

Guide for Precast Concrete Tunnel Segments

The technical committees responsible for ACI committee reports and standards strive to avoid ambiguities, omissions, and errors in these documents. In spite of these efforts, the users of ACI documents occasionally find information or requirements that may be subject to more than one interpretation or may be incomplete or incorrect. Users who have suggestions for the improvement of ACI documents are requested to contact ACI via the errata website at http://concrete.org/Publications/DocumentErrata.aspx. Proper use of this document includes periodically checking for errata for the most up-to-date revisions.

ACI committee documents are intended for the use of individuals who are competent to evaluate the significance and limitations of its content and recommendations and who will accept responsibility for the application of the material it contains. Individuals who use this publication in any way assume all risk and accept total responsibility for the application and use of this information.

All information in this publication is provided "as is" without warranty of any kind, either express or implied, including but not limited to, the implied warranties of merchantability, fitness for a particular purpose or non-infringement.

ACI and its members disclaim liability for damages of any kind, including any special, indirect, incidental, or consequential damages, including without limitation, lost revenues or lost profits, which may result from the use of this publication.

It is the responsibility of the user of this document to establish health and safety practices appropriate to the specific circumstances involved with its use. ACI does not make any representations with regard to health and safety issues and the use of this document. The user must determine the applicability of all regulatory limitations before applying the document and must comply with all applicable laws and regulations, including but not limited to, United States Occupational Safety and Health Administration (OSHA) health and safety standards.

Participation by governmental representatives in the work of the American Concrete Institute and in the development of Institute standards does not constitute governmental endorsement of ACI or the standards that it develops.

Order information: ACI documents are available in print, by download, through electronic subscription, or reprint and may be obtained by contacting ACI.

Most ACI standards and committee reports are gathered together in the annually revised the ACI Collection of Concrete Codes, Specifications, and Practices.

American Concrete Institute
38800 Country Club Drive
Farmington Hills, MI 48331
Phone: +1.248.848.3700
Fax: +1.248.848.3701

www.concrete.org

ACI 533.5R-20

Guide for Precast Concrete Tunnel Segments

Reported by ACI Committee 533

David Wan, Chair

Mehdi Bakhshi*†
George F. Baty
Harry A. Chambers‡
George F. Baty

Benjamin Lavon
James Lewis
Donald F. Meinheit
Brian D. Miller

Verya Nasri†
Karen Polanco
Larbi M. Sennour
Venkatesh Seshappa

Michael H. Weber
Dennis M. Wittry
Wael A Zatar

*Chair of task group who prepared this report.
†Members who prepared this report.
‡Deceased.

Consulting Members

Aaron W. Fink
Sidney Freedman

Ava Shypula
Weilan Song

The worldwide trend in construction is toward mechanization and automation. This trend has led to continued rapid progress of mechanized tunneling. Advantages over conventional tunnel construction methods include, but are not limited to, occupational health and safety, faster advance rates, and reducing construction labor requirements. Mechanized tunneling in soft ground using tunnel boring machines is often associated with installing precast concrete segmental lining. However, very little industry-wide guidance has been provided by practice and code organizations. This document provides guidelines for precast concrete tunnel segments, including the most recent developments and practical experience, in addition to information on all aspects of design and construction. These guidelines are based on the knowledge and the experience gained on numerous precast tunnel projects in the United States, and available national and international guidelines often used as industry references.

Keywords: design; durability; fiber; gasket; joint; lining; precast; segment; tolerance; tunnel.

CONTENTS

ACI 533.5R-20 was adopted and published April 2020.

CHAPTER 1—INTRODUCTION AND SCOPE

1.1—Introduction

Precast concrete segments are installed to support the excavation behind the tunnel boring machine (TBM) in soft ground, weak rock, and fractured hard rock applications. As shown in Fig. 1.1, the TBM advances by reacting against the completed rings of precast concrete segments that typically provide both the initial and final ground support as part of a one-pass lining system. These segments are designed to resist the permanent loads from the ground and groundwater as well as the temporary loads from production, transportation, and construction. Currently, very little guidance is provided for tunnel designers and contractors by local or international authorities, and there is an acute need for a document to clearly highlight the practical design principles, advances in construction, and the research needs in this area. Tunnel segments are generally reinforced to resist the tensile and compressive stresses at the ultimate limit states (ULS) and the serviceability limit state (SLS). Special attention is paid in this document to common methods in ULS and SLS designs of these elements. In addition, detailed design considerations are presented, such as concrete strength and reinforcement. Gasket design as sealing elements against groundwater inflow, connection devices, and fastening systems are introduced, followed by segment tolerances, measurement, and dimensional control systems.

1.2—Scope

This document provides analysis, design, and construction guidelines exclusively for one-pass precast segmental lining that is installed almost instantaneously with excavation inside TBM shields only a few yards behind the TBM cutterhead. Linings that are installed long after passing of an open-mode TBM, cast-in-place concrete linings, and segments of other materials such as steel and cast-iron segments do not fall within the scope of this guideline. Two-pass lining systems, which are no longer popular in modern tunnels, are not specifically discussed but can still benefit from the guidelines. More information about the two-pass linings can be found in ITA WG2 guidelines. This guideline provides methods of design and construction for TBM tunneling in soft ground as well as weak and fractured hard rock tunneling. The guidelines and recommendations in this document can be applied to tunnels of different types, such as road, railway, and subway tunnels; headrace, water supply, and waste water tunnels; and service, gas pipeline, and

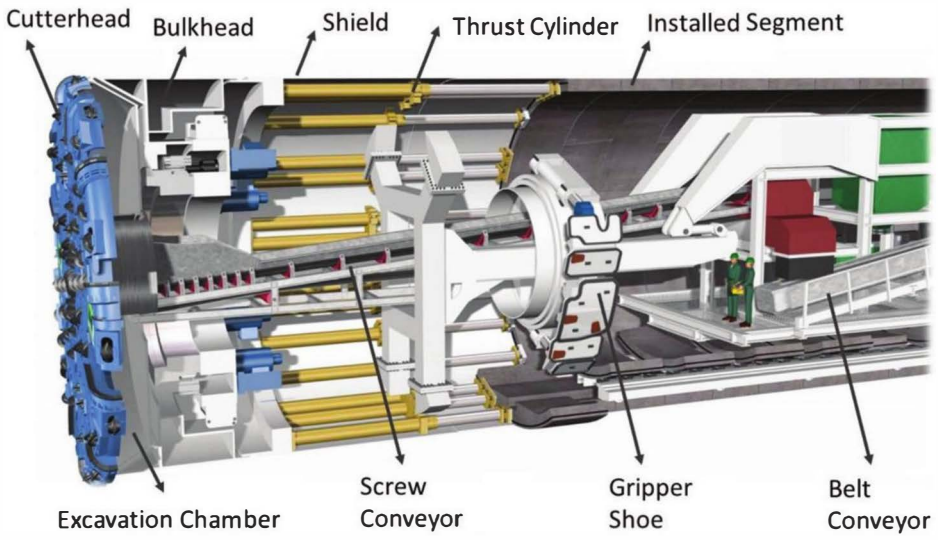

Fig. 1.1—Main parts of a typical TBM of earth-pressure balance (EPB) type, which is used for soft ground tunneling.

power cable tunnels. The structural design part of this document pertains to procedures for designing concrete tunnel segments to withstand the commonly encountered temporary and permanent load cases occurring during the production, transportation, construction, and final service phases. The procedure was developed based on global practice and review of major available design codes, standards, and guidelines related to precast segments in tunneling and concrete industries. The construction aspects presented in this guideline including segmental ring geometry and systems, gasket systems, and connection devices, and segment tolerances reflect global practice perspectives such as ACI 544.7R, AFTES:2005, BS PAS 8810:2016, DAUB:2013, JSCE 2007, LTA 2010, ÖVBB 2011, and STUVAtec:2005. This document does not address the actions of thermal variations, fire loads and explosion, or internal loads such as train loads within the tunnels. While some structural design parts of this guideline may only consider the procedures adopted by ACI, they can be extended to other structural codes such as BS EN 1992-1-1:2004.

CHAPTER 2—NOTATION AND DEFINITIONS

2.1—Notation

A = effective tension area of concrete around reinforcing bar divided by number of steel bars, in.^{2} (mm^2)
A_d = load distribution area inside segment under thrust jack forces, in.^{2} (mm^2)
A_g = gross area of concrete section, in.^{2} (mm^2)
A_j = area of contact zone between jack shoes and the segment face, in.^{2} (mm^2)
A_s = area of reinforcing bars, in.^{2} (mm^2)
a = distance from edge of vacuum lift pad to edge of segment in the load case of stripping (demolding), or dimension of final spreading surface under thrust jack forces, in. (mm)
a_l = transverse length of contact zone between jack shoes and the segment face, in. (mm)
a_t = transverse length of stress distribution zone at the centerline of segment under thrust jack forces, in. (mm)
b = width of tunnel segment or width of tested specimen, ft (m)
C_c = compression force in the concrete section, lbf (N)
C_t = tensile force in the section due to fiber reinforcement, lbf (N)
D_e = external diameters of the tunnel segmental lining, ft (m)
D_i = internal diameter of the tunnel segmental lining, ft (m)
d = thickness of tested specimen, or total width of the segment cross section, in. (mm)
d_1 = length of load transfer zone for the case of longitudinal joint bursting load, in. (mm)
d_{burst} = centroidal distance of bursting force from the face of section, in. (mm)
d_c = concrete cover over reinforcing bar, in. (mm)
d_k = width of the hinge joint or thickness of contact surface between segment joints for the case of longitudinal joint bursting load, in. (mm)
d_s = distributed width of stress block inside the segment for the case of longitudinal joint bursting, in. (mm)
E = modulus of elasticity of concrete, psi (MPa)
E_r = modulus of elasticity of surrounding ground, psi (MPa)
E_s = stiffness modulus of the surrounding ground determined by oedometer test, psi (MPa); or modulus of elasticity of reinforcing bar, psi (MPa)
EH = horizontal earth pressure, psi (MPa)
EV = vertical earth pressure, psi (MPa)
e = eccentricity, in. (mm)
e_{anc} = eccentricity of jack pads with respect to the centroid of cross section, or maximum total eccentricity in longitudinal joints consisting of force eccentricity and eccentricity of load transfer area, in. (mm)

F = forces acting on bottom segment due to self-weight of segments positioned above when segments are piled up within one stack during storage or transportation phases, lbf (N)
F_{sd} = bursting tensile forces developed close to longitudinal joints, lbf (N)
$F_{sd,r}$ = spalling tensile forces developed close to longitudinal joints, lbf (N)
$F_{sd,2}$ = secondary tensile forces developed close to longitudinal joints, lbf (N)
f_1 = first peak flexural strength, psi (MPa)
f_{bot} = stress at the extreme bottom fiber of concrete section, psi (MPa)
f_c' = specified compressive strength of concrete segment, psi (MPa)
f_{co}' = compressive strength of partially loaded concrete surface, psi (MPa)
f_{cd} = concrete design compressive strength according to BS EN 1992-1-1:2004, psi (MPa)
f_{ctd} = fiber-reinforced concrete design tensile strength, psi (MPa)
$f_{ct,eff}$ = concrete tensile strength, psi (MPa)
f^D_{150} = residual flexural strength at net deflection of $L/150$, psi (MPa)
f^D_{600} = residual flexural strength at net deflection of $L/600$, psi (MPa)
f'^D_{150} = specified residual flexural strength at net deflection of $L/150$, psi (MPa)
f'^D_{600} = specified residual flexural strength at net deflection of $L/600$, psi (MPa)
f^D_{150r} = required average residual flexural strength at net deflection of $L/150$, psi (MPa)
f^D_{600r} = required average residual flexural strength at net deflection of $L/600$, psi (MPa)
f_{Ftu} = fiber-reinforced concrete tensile strength at ultimate limit state, psi (MPa)
f_{R1} = residual flexural strength of FRC beam corresponding to crack mouth opening displacement of 0.02 in. (0.5 mm), psi (MPa)
f_{R3} = residual flexural strength of fiber-reinforced concrete beam corresponding to crack mouth opening displacement of 0.1 in. (2.5 mm), psi (MPa)
f_s = stress in reinforcing bar, psi (MPa)
f_t = specified splitting tensile strength, psi (MPa)
f_y = yield stress of required reinforcing bars, psi (MPa)
g = self-weight of the segments per unit length, lbf/in. (N/mm)
H = overburden depth, ft (m)
H_w = groundwater depth, ft (m)
h = thickness of tunnel segment, in. (mm)
h_{anc} = length of contact zone between jack shoes and the segment face, in. (mm)
I = moment of inertia of FRC segment, in.^{4} (mm^4)
J = tunnel boring machine thrust jack forces, kip (kN)
k = coefficient of subgrade reaction or subgrade reaction modulus, lb/ft^3 (kg/m^3)
k_{jr} = Janssen rotational spring stiffness in longitudinal joints, lb.in./rad (N.mm/rad)
k_r = radial component of subgrade reaction modulus or stiffness of radial springs simulating ground-structure interaction, lb/ft^3 (kg/m^3)
k_t = subgrade reaction modulus in the tangential direction, lb/ft^3 (kg/m^3); or in crack width analysis, a factor depending on the duration of loading (0.6 for short-term loading and 0.4 for long-term loading)
k_θ = tangential component of subgrade reaction modulus or stiffness of tangential springs simulating ground-structure interaction, lb/ft^3 (kg/m^3)
L = distance between the supports, in. (mm)
l_t = full length of contact area between segments in longitudinal joints, in. (mm)
$M_{distortion}$ = bending moment due to additional distortion effect, lbf.ft (N.m)
M_n = nominal resistance bending moment, lbf.ft (N.m)
N = axial hoop force in segments, lbf (N)
N_{Ed} = maximum normal force due to permanent ground, groundwater, and surcharge loads, lbf (N)
n = number of segments per ring excluding the key segment ($n \geq 4$); or number of layers of tensile reinforcing bar in crack with analysis
P_0 = surcharge load, lbf (N)
P_{e1} = vertical earth pressure at crown of lining applied to the elastic equation method, psi (MPa)
P_{e2} = vertical earth pressure at invert of lining applied to the elastic equation method, psi (MPa)
P_g = segment dead load, psi (MPa)
P_{gr} = radial grouting pressure, psi (MPa)
P_{pu} = factored jacking force applied on each jack pad in circumferential joints, or maximum factored normal force from the final service loads transferred in longitudinal joints, psi (MPa)
P_{w1} = vertical water pressure at crown of lining applied to the elastic equation method, psi (MPa)
P_{w2} = vertical water pressure at invert of lining applied to the elastic equation method, psi (MPa)
q_{e1} = horizontal earth pressure at crown of lining applied to the elastic equation method, psi (MPa)
q_{e2} = horizontal earth pressure at invert of lining applied to the elastic equation method, psi (MPa)
q_{w1} = horizontal water pressure at crown of lining applied to the elastic equation method, psi (MPa)
q_{w2} = horizontal water pressure at invert of lining applied to the elastic equation method, psi (MPa)
R = radius from centerline of lining, ft (m)
r_o = radius of excavated tunnel, ft (m)
S = distance between stack supports and free edge of segments in the load case of segment storage, ft (m)
s = maximum reinforcing bar spacing, in. (mm)
$s_{r,max}$ = maximum crack spacing, mm
s_s = sample standard deviations of test results
T_{burst} = bursting force, lbf (N)
WA_p = groundwater pressure, psi (MPa)

w = segment self-weight, lb/ft (kg/m); or maximum crack width, in. (mm)
y = distance from extreme tension fiber to the neutral axis, in. (mm)
y_c = distance from extreme compression fiber to centroid of equivalent compression force in the section, in. (mm)
β = dimension of the loaded surface under thrust jack forces according to Iyengar diagram, in. (mm); or in crack width analysis ratio of the distance between neutral axis and tension face to the distance between neutral axis and centroid of reinforcing bar
$\Delta P_{g,\ invert}$ = vertical gradient of radial grout pressure between the crown and invert of tunnel, psi (MPa)
δ = displacement of lining applied to the elastic equation method, in. (mm)
δ_d = diametrical distortion, in. (mm)
ε'_{csd} = compressive strain due to shrinkage and creep equal to 150×10^{-6}
ε_{cu} = ultimate tensile strain
ε_{tu} = ultimate compressive strain
ϕ = strength reduction factor; or reinforcing bar diameter, in. (mm)
γ = material safety factor
λ = slenderness defined as the ratio between the developed segment lengths and its thickness
θ = angle from crown in the elastic equation method, or rotation in the longitudinal Janssen joint, radians
$\rho_{concrete}$ = specific weight of concrete, lb/ft^3 (kg/m^3)
ρ_{eq} = equivalent specific weight of grout, lb/ft^3 (kg/m^3)
$\sigma_{c,j}$ = compressive stresses developed under jack pads because of axial effects of thrust jack forces, psi (MPa)
σ_{cm} = fully spread compressive stress in method of the Iyengar diagram, psi (MPa)
σ_{cx} = bursting tensile stresses using the Iyengar diagram, psi (MPa)
σ_p = specified post-crack residual tensile strength of fiber-reinforced concrete (FRC) segment, psi (MPa)
τ_{yield} = shear yield strength of grout, psi (MPa)

2.2—Definitions

Please refer to the latest version of ACI Concrete Terminology for a comprehensive list of definitions. Definitions provided herein complement that resource.

annular gap—space between the surrounding ground and the outer surface of the segments.

circumferential joint—joint approximately perpendicular to the tunnel axis between two adjacent segment rings.

connections—devices for temporary or permanent attachment of two segments or segment rings in the longitudinal and circumferential joints.

counter key segments—two segments installed adjacent to key segment with at least one tapered joint with respect to tunnel longitudinal axis in plan view.

crosscut—connecting structure between two tunnel tubes or between a tunnel tube and the ground surface or a shaft, with special passages in the connecting area of the main tube.

crown—highest part of a tunnel in cross section.

earth-pressure balance tunnel boring machine—one type of tunnel boring machine used in soft ground tunneling; uses a screw conveyor and with controlling muck removal from the excavation chamber, the earth pressure in the chamber is maintained to balance the face pressure.

extrados—outer surface of the segment or the segment ring on the side in contact with the ground.

gasket—sealing system consisting of sealing strips placed in one or more layers around the individual segment, ensuring permanent sealing of the tunnel tube against the ingress of water from the surrounding ground.

guiding rod—segment accessories in the shape of rods, often 1 to 2 in. (25 to 50 mm) in diameter; placed in longitudinal joints along the centroid of two adjacent segments to fulfill the functions of guidance and locking adjacent segments during installation of a full ring inside tunnel boring machine shield.

ground—soil, rock, and fill into which the tunnel is placed.

intrados—inner surface of the segment or the segment ring on the tunnel side.

invert—lowest part of a tunnel in cross section.

joint misalignment—eccentricity between end of two segments at longitudinal or circumferential joints that results in limited contact areas between segment ends at joints.

key segment—last installed segment of a ring with a trapezoidal shape in plan view, which is often smaller than and accounted for as a proportion of ordinary segments such as one-third, two-thirds, or half.

longitudinal joint—joint between adjacent segments in a ring with an axis parallel to the longitudinal axis of tunnel; also known as radial joint.

one-pass lining—all static and structural requirements of the tunnel lining are handled by the segmental ring; no further internal lining is installed that contributes to load bearing or sealing.

ovalization—deformation of an initially circular segmental ring; for example, to a vertical or horizontal oval shape due to earth pressure, grout pressure, segment self-weight, or uplift.

packer—semi-rigid boards made of polyethylene or fortified asphalt core pressed between two layers of weather-proofed fiberglass plies or timber materials that are placed between tunnel segmental ring joins; they are used to relieve the stresses between segments and therefore prevent cracking and spalling. Packers are not used as often in modern segmental lining construction.

portal—entrance from the ground surface to a tunnel.

reverse key segment—first installed segment of a ring, in rectangular or trapezoidal shape, located opposite to key segment in segmental ring side view and often placed on or very close to tunnel invert.

ring width (ring length)—dimension of the segment ring in its center axis in the longitudinal direction of the tunnel.

segment—curved prefabricated elements that make up a ring of support or lining.

segment thickness—radial distance between the inner and outer sides of a segment.

shield—steel tube, usually cylindrical, shaped to fit the excavation line of a tunnel.

soft ground—residual soil or deteriorated rock with limited compressive strength and stand-up time.

springline—opposite ends of the horizontal centerline of tunnel.

tail void—annular space between the outside diameter of the shield and the outside of the segmental lining.

tunnel boring machine—consisting of a cutterhead, shield, and gantries used to excavate tunnels with a circular or rectangular cross section through different rock and soil strata, and to install the tunnel lining at the end of the shield.

tunnel boring machine backup—area behind tunnel boring machine shields in the shape of an equipment train that is used for providing a final staging area for feeding segments to the installation erectors as well as housing tunnel boring machine ancillary equipment such as transformers, power supply, hydraulic pumps, control room, ventilation, trail skin grouting, and spoil (muck) removal systems needed for the tunnel boring machine operation.

test ring—complete segment ring, usually assembled in horizontal orientation in segment precast plant, for test purposes.

thrust jacks—hydraulic jacks serving to transmit the thrust forces of the tunnel boring machine to the segment ring, facilitate installation, or both.

tunnel cover—perpendicular distance to nearest ground surface from the tunnel exterior.

two-pass lining—tunnel lining consisting of two shells with different structural and constructional requirements that are produced in independent operations and with different construction methods.

CHAPTER 3—DESIGN PHILOSOPHY AND SEGMENTAL RING GEOMETRY

3.1—Load and resistance factor design

The design engineer should use load and resistance factor design (LRFD) method to design concrete precast tunnel segments. LRFD is a design philosophy that takes into account the variability in the prediction of loads and the variability in the properties of structural elements. LRFD employs specified limit states to achieve its objectives of constructability, safety, and serviceability. In BS EN 1992-1-1:2004, this is defined as limit state design.

Even though force effects may often be determined using elastic analyses, the resistance of elements using LRFD design methods is determined on the basis of inelastic behavior. Concrete precast tunnel segments should be designed using load factors and strength reduction factors specified in concrete design codes such as ACI 318. For load cases not covered in these codes, load factors, load combinations, and strength reduction factors from other resources such as ACI 544.7R or AASHTO DCRT-1 can be used.

3.2—Governing load cases and load factors

The current practice in the tunnel industry is to design segmental tunnel linings for the following load cases, which occur during segment manufacturing, transportation, installation, and service conditions:

a) Production and transient stages
   i. Segment stripping (demolding)
   ii. Segment storage
   iii. Segment transportation
   iv. Segment handling

b) Construction stages
   i. Tunnel boring machine (TBM) thrust jack forces
   ii. Tail skin back grouting pressure
   iii. Localized back grouting (secondary grouting) pressure

c) Service stages
   i. Ground pressure, groundwater pressure, and surcharge loads
   ii. Longitudinal joint bursting load
   iii. Loads induced due to additional distortion
   iv. Other loads (for example, earthquake, fire and explosion, TBM load of upper tunnel to lower tunnel in case of stacked arrangement of tunnels, aerodynamic loads, mechanical and electrical loads, railway loads, temperature load, and loads during segmental ring erection)

In the strength design procedure, the required strength (U), also known as required design strength, is expressed in terms of factored loads such as the ones shown in Table 3.2 for presented governing load cases. Note that this table provides comprehensive factored load combinations for a specific case of tunnel segments. If different load factors are provided by the local codes, they should be used in place of the factors in this table. In this document, aforementioned load cases are divided into three categories: production and transient loads, construction loads, and service loads. The resulting axial forces, bending moments, and shear forces are used to design concrete and reinforcement.

3.3—Design approach

A common design approach for concrete tunnel segments starts with selecting an appropriate geometry, including thickness, width, and length of segments with respect to the size and loadings of the tunnel. Considering specified compressive strength (f_c') and type and amount of reinforcement, the design strength of segments is compared with required strength against all critical load cases. Methods of calculation for required strength against these load cases will be explained in the following chapters. The geometry, compressive strength, and reinforcement of segments should be specified to provide sufficient design strength against all load cases as well as satisfying all service conditions. The design procedure starts with initial considerations for a segmental ring system and geometry that is discussed in the following section and further checked against the demand of different loadings.

Table 3.2—Required strength (U) for governing load cases (ACI 544.7R)

Load case	Required strength (U)
Load Case 1: stripping (demolding)	$U = 1.4w$
Load Case 2: storage	$U = 1.4(w \pm F)$
Load Case 3: transportation	$U = 1.4(w \pm F)$
Load Case 4: handling	$U = 1.4w$
Load Case 5: thrust jack forces	$U = 1.0J$ (1.2 if maximum machine thrust is unknown)
Load Case 6: tail skin grouting	$U = 1.25(w \pm P_{gr})$
Load Case 7: secondary grouting	$U = 1.25(w \pm P_{gr})$
Load Case 8: earth pressure and groundwater load	$U = 1.25(w \pm WA_p) \pm 1.35(EH + EV) \pm 1.5P_0$
Load Case 9: longitudinal joint bursting	$U = 1.25(w \pm WA_p) \pm 1.35(EH + EV) \pm 1.5P_0$
Load Case 10: additional distortion	$U = 1.4M_{distortion}$

3.4—Segmental ring geometry and systems

Segmental tunnel linings installed in the rear of the TBM shield are generally in the shape of circular rings. The size of the ring is defined by the internal diameter, thickness, and length of the ring. Other important design considerations include ring systems, ring configurations in terms of number of segments that form a complete ring, geometries of individual segments, and geometry and tapering of key segments (Bakhshi and Nasri 2018b).

3.4.1 *Internal diameter of the bored tunnel*—The dimensions of the tunnel inner section should be determined considering the internal space required during the service, which depends on the intended use of the tunnel. For the railroad and subway tunnels, the inner dimensions of tunnels in a single-track case are generally governed by the train clearance envelope (clearance gauge), track structure, drainage trough, structure of the overhead catenary contact line stays, and emergency evacuation corridor (egress space). In a double track and twin tunnel cases, tunnel inner dimensions are additionally governed by distance between the centers of tracks and the cross passageway. The internal diameter of the tunnel is first set by obtaining a circle that satisfies these conditions. Then, the electrical equipment, water pipes, and other equipment are installed in the unoccupied space inside this circle. Sufficient ventilation space is generally provided if egress space and cross passageways are allocated (RTRI 2008), but this needs to be verified. For the road tunnels, the geometrical configuration of the tunnel cross section should satisfy the required horizontal and vertical traffic clearances; shoulders or sidewalks/curbs; barriers; fans and suitable spaces for ventilation, lights, traffic control system, and fire life safety systems including water supply pipes for firefighting, cabinets for hose reels, fire extinguishers, and emergency telephones. As shown in Fig. 3.4.1, the smallest tunnel encircling these clearances and elements are considered as the minimum internal tunnel diameter. The available spaces in a circular cross section can be used to house other required elements for road tunnels including tunnel drainage, tunnel utilities and power, signals and signs above roadway lanes, CCTV surveillance cameras, communication antenna and equipment, and monitoring equipment of noxious emissions and visibility (AASHTO DCRT-1). If the

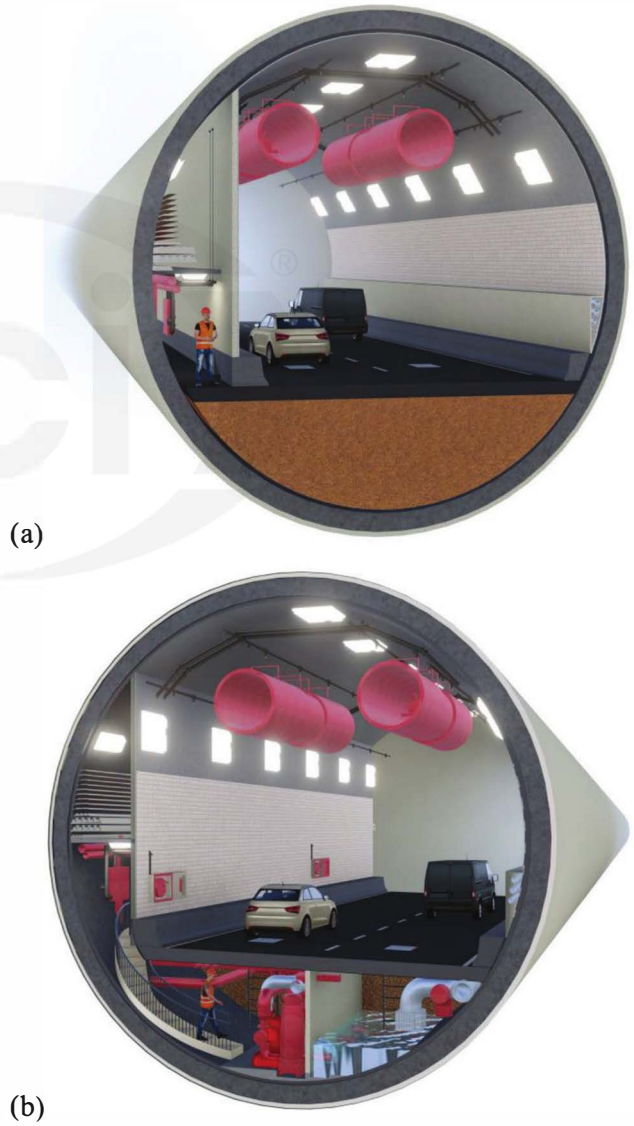

Fig. 3.4.1—Schematics of interior space of TBM-bored road tunnels: (a) typical section; and (b) section at low-point pump station.

space is not sufficient for all these elements, the tunnel needs to be enlarged accordingly. Note that for the spaceproofing of road and railway tunnels, it is crucial to consider impact of maximum super elevation of the tightest curve on the alignment on the rotation of clearance envelopes. In determining the ring internal diameter, sufficient construction tolerance should also be provided. DAUB:2013 recommends a radius tolerance of $R = \pm 4$ in. (100 mm) for TBM-bored tunnels. Therefore, the internal diameter of the tunnel needs to be made 8 in. (200 mm) greater than the required internal structural boundary. The internal size of the wastewater or combined sewer overflow tunnels is designed based on the storage volume and sometimes volumetric flow rate of design storm (for example, 25-year, 50-year, and 100-year) specified by local authorities and updated collection system modeling. The internal diameter of the water tunnel is sized based on the volumetric designed flow rate.

3.4.2 *Thickness of ring and outside diameter*—The thickness of segmental lining ring as a structural member is determined in accordance with the result of design calculation. The segment design is an iterative procedure that starts with an assumption of a reasonable thickness and is later optimized during detailed design calculation. Therefore, it is crucial to consider a reasonable thickness for segmental rings in the beginning of the design process. A review of more than 100 projects published in ACI 544.7R, AFTES:2005, Groeneweg (2007), and Blom (2002) shows that the ratio of internal tunnel diameter (ID) to the lining thickness falls in a specific range of 18 to 25 for tunnels with an ID of more than 18 ft (5.5 m), and 15 to 25 for tunnels with an ID of 13 to 18 ft (4 to 5.5 m). JSCE 2007 recommends that the ring thickness be less than 4 percent of the outer diameter of segmental ring, which translates into an ID to thickness ratio of 23. Most of tunnels are larger than 13 ft (4 m) in internal diameter and therefore it is suggested to consider one-twentieth of the ID as the initial lining thickness. For tunnels under 13 ft (4 m) in diameter, no correlation could be identified between the lining thickness and the tunnel diameter, which ranges between 5.9 and 11 in. (150 and 280 mm).

During the analysis and design stage, the capacity of the lining section with the selected thickness should be sufficient when transverse reinforcement ratio is less than 1 percent and close to the minimum reinforcement (AFTES:2005). The minimum segment wall thickness should satisfy the conditions imposed by the contact joints such as sufficient bearing surface area and sufficient space and clear distance for segment recesses. The minimum segment wall thickness should be compatible with the bearing surface area of TBM longitudinal thrust cylinders (AFTES:2005). To achieve a robust design, the segment thickness should be adequate to all requirements with an extra amount for unforeseen loads, particularly if sealing gaskets are installed. In addition to structural factors, the lining thickness is also designed based on durability, and DAUB:2013 recommends a minimum thickness of 12 in. (300 mm) for one-pass tunnel linings. Note that in combined sewer overflow tunnels, if a sacrificial layer was considered for design life of the tunnel (for example, 125 years), the sacrificed layer thickness should be added to required structural thickness.

The outer diameter of a tunnel is determined by adding the lining thickness to the inner dimension. The shield outer diameter is determined by adding the tail clearance and shield skin plate thickness to the tunnel outer diameter (RTRI 2008). Shield outer diameter also limits the minimum curve radius of the alignment. A review of more than 100 tunnel projects with different sizes (JSCE 2007) shows that when shield outer diameter is less than 20 ft (6 m), between 20 and 32 ft (6 and 10 m), and more than 40 ft (12 m), the minimum curve radius can be limited to 260 ft (80 m), 520 ft (160 m), and 990 ft (300 m), respectively. In practice, larger radii are being considered in projects and mentioned limits can be used as lower bound limits for the curve radius. It is noteworthy to mention that minimum curve radius limitation is a function of ring geometry (taper and ring width), overcut, shield design (articulated or not), and radial gap between segment and tail skin rather than just the shield outer diameter. All these parameters should be taken into account for determining minimum curve radius. In addition, curves can be both horizontal and vertical but usually horizontal curves are the tightest curves on tunnel alignments. For transportation tunnels, the minimum radii are generally governed by the policy documents published by the transportation agency, which include considerations of various safety-related factors such as the speed of vehicle, line of sight, length of curve, vehicle characteristics, and drainage considerations.

3.4.3 *Length of the ring*—Depending on the diameter, the ring length can range between 2.5 ft and 8 ft (0.75 and 2.50 m) (DAUB:2013). On one hand, it is desirable that the ring length be narrow for transportation and erection simplicity, easy construction of curved sections, and to reduce length of the shield tail. On the other hand, it is desirable for the ring length to be larger to reduce production cost, numbers of joints, total perimeter of segments, gasket length, and the number of bolt pockets where leakage can occur, as well as increasing the construction speed (JSCE 2007). Therefore, the ring length needs to be optimized for the efficiency of tunnel works. Analysis of data from more than 60 projects presented in JSCE 2007 demonstrates that although in some cases increasing the diameter results in an increased ring length, there is no consistent relationship between the ring length and outer diameter of the segmental lining. This is mainly because, for the smaller diameters, the available space for segment supply and handling defines the limitation of the ring length, whereas for larger diameter, segment weight and production are the limiting factors. The current practice is to use a ring length of 5 ft (1.5 m) for TBM tunnel diameters of 19 to 23 ft (6 to 7 m), and a ring length of 6 ft (1.8 m) for tunnels of 23 to 30 ft (7 to 9 m) diameter. When a TBM larger than 30 ft (9 m) is used for excavation, the most common ring length is 6.5 ft (2 m). Recent large-diameter projects have taken advantage of 7.2 ft (2.2 m) long rings by optimizing the segmental lining thickness. Depending on the project conditions, in many cases, weight limitations given

by transportation to the site on public roads are the main considerations.

3.4.4 *Segmental ring systems*—Parallel rings, parallel rings with corrective rings, right/left rings, and universal ring systems are among different systems used for tunnel segmental rings. Parallel ring systems, as shown in Fig. 3.4.4(a), comprising rings with parallel end faces and with circumferential faces perpendicular to the tunnel axis are not suitable for curved alignments. Practically all tunnel alignments have curves and, therefore, for directional corrections (even in case of curves with large radius), packers are the only solution that can be adopted to be placed in circumferential joints. Such a segmental ring system cannot always be properly sealed because the packing reduces the compression in the gasket. This system is not inherently suitable for curves. It is not suitable either for straight alignments without packers as rings can never be built perfectly straight; and methods to restore line and grade are always needed with this system. Parallel rings with corrective ring systems are similar to parallel ring systems, with corrective rings (up, down, left, right ring) replacing packers for directional corrections. With this system, the requirements for different types of formwork set is the main disadvantage.

The right/left ring is a type of ring that tapered in a way that when the key segment is above the springline, the ring turns in the right/left direction. The most common taper for this system is when the ring has a slightly longer length on the right/left side, respectively. Nonetheless, there are right/left systems with double taper. As shown in Fig. 3.4.4(b), right/left systems are often assembled from rings with one circumferential face perpendicular to the tunnel axis and the other one inclined to the tunnel axis. The difference between maximum and minimum ring length is called taper. Right/left rings have been also made of rings with tapers on both faces of the rings, with half of the required taper on each end face of the rings. The sequence of right-tapered and left-tapered rings produces a straight alignment or a tangent alignment whereas a sequence of right/right ring, as shown in Fig. 3.4.4(b), results in a curve to the right, and left/left rings produces a curve to the left with a minimum system radius. Upward and downward directional corrections are achieved through rotation of the tapered segment ring by 90 degrees (ÖVBB 2011). This ring system provides a proper sealing performance for an impermeable tunnel, with the only disadvantage being requiring different types of formwork set.

The universal ring system is a system in which the key segment can be located anywhere in the tunnel including below the springline. This system can turn the ring into any desired direction: up, down, left, right, and their combinations. The most conventional universal system is the one with the circumferential surface of the ring inclined to the tunnel axis on both sides. However, universal rings with one tapered side are also used. The required ring taper is divided in one or both circumferential ends of the universal rings. As shown in Fig. 3.4.4(c), all curves and directional corrections can be negotiated through the rotation of the segmental ring. The main advantage of this system is the requirement of only

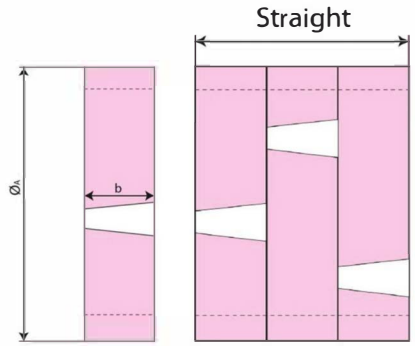

(a) Parallel rings

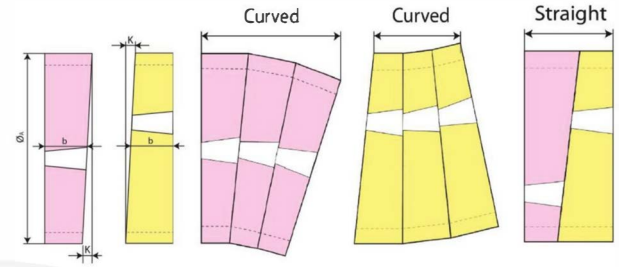

(b) Ring/left rings

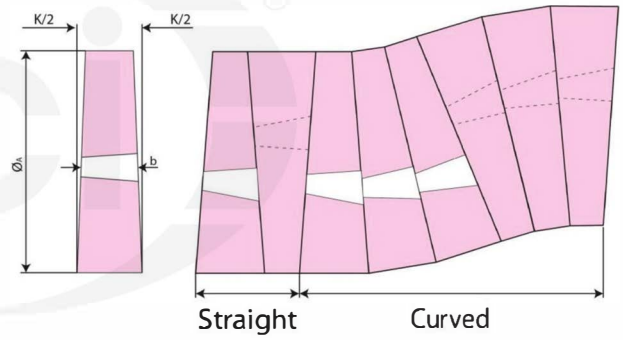

(c) Universal rings

Fig. 3.4.4—Different ring systems plan views and tapering and curve negotiation schematics: (a) parallel rings; (b) right/left tapered rings; and (c) universal rings.

one type of formwork set (ÖVBB 2011). The required ring taper (k) can be calculated with the following formula.

$$k = \frac{\phi_A \cdot b_m}{R} \tag{3.4.4}$$

where ϕ_A is outer diameter of the segment ring; b_m is the average ring length; and R is the minimum curve radius. Note that a correction curve drive that in the event of deviation returns the TBM back into the designed tunnel alignment should be taken into consideration. The correction curve radius should be at least 20 percent less than the smallest desired curve radius horizontally and vertically (DAUB:2013).

To have a straight drive using universal rings, it is necessary to turn each ring by 180 degrees in reference to the

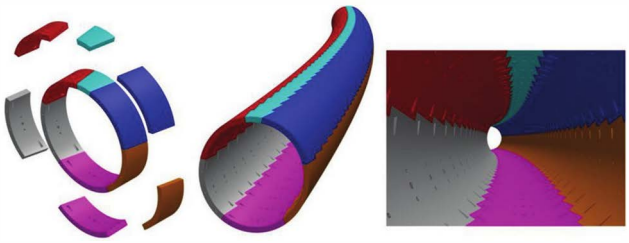

Fig. 3.4.5—Most common ring configuration (5+1) used for mid-size tunnels under 20 ft (6 m) diameter and virtual build of tunnel when negotiating the tightest curve.

previous one, having the key segment both on the top and the bottom or left and right. Taper can be provided alternatively on the right and left sides of the rings and therefore key segment can be placed on the left and right sidewalls to yield a straight drive. Using the right ring and the left ring, it is possible to always have the key segment on the top and, therefore, to be able to construct the ring from the bottom upward. Nonetheless, in recent years and using advanced software for guiding TBM, universal rings can negotiate the straight drives with keys above springlines through adjusting the drive error of less than a few millimeters in two or three rings.

3.4.5 *Ring configuration*—One of the main parameters for segmental lining design is the number of segments comprising a ring. Similar to the ring length, the shorter the curved length of each segment, the easier the transportation and erection process. Attention should be paid to the fact that ring length and curved segment length are not measured in the same plane. From the handling perspective, it is good to divide a ring to as many segments as possible. However, longer segments and less joints results in a much stiffer segmental ring, reduced production cost, less hardware for segment connection, shorter gasket length, and fewer number of bolt pockets where leakage can occur. More importantly, the construction speed can increase significantly. Normally the space available in the backup to turn the segments is a major factor in setting limits for maximum length of segments. In very large diameter tunnels, however, the segment weight is a decisive factor in selection of maximum length of segments rather than the available space for handling segments inside TBM shields and in the backup gantries. The slenderness of the tunnel segment (λ), defined as the ratio between the breadth or curved length of segment along its centroid and its thickness, is a key parameter for segment length. Review of tunnel projects show that rings are divided into as many segments that yield a segment slenderness of 8 to 13, with fiber-reinforced concrete (FRC) segments around the lower boundary of this range. However, using the latest fiber technologies and high-strength concrete materials, FRC segments with slenderness ratios of 10 are frequently adopted. The latest developments show a record of successful use of FRC segment with slenderness of more than 10 and up to 12 to 13 in some recent projects (ACI 544.7R; Bakhshi and Nasri 2017a; Beño and Hilar 2013; Harding and Francis 2013; ITA Working Group 2 2016). In general, and for midsize tunnels, it is suggested to divide the ring into as many segments as necessary for a slenderness ratio of at least 10 to be obtained. Segment thickness depends on several factors that are mostly project-specific, such as related design criteria and load cases, resulting in slenderness values outside of the mentioned ranges in some specific cases.

A review of various tunnel projects (Bakhshi and Nasri 2018b) shows that for tunnels with a diameter of 20 ft (6 m) and below, a ring division into six segments is typical. Often, an even number of segments with an odd number of ordinary segments and one key segment are preferred. This type of design is more compatible with configurations of TBM thrust jack forces pushing on the segments. The most common configuration is five ordinary segments and one smaller key segment, also known as 5+1 ring (Fig. 3.4.5). A 4+2 configuration with four ordinary segments and two key segments alternating above and below the springline is also a common configuration. In tunnels under 13 ft (4 m) in diameter, the ring can be easily divided into a fewer number of segments but a division of rings into six segments is still more common. Other than the 5+1 and 4+2 configurations for a six-segment ring, other configurations are sometimes adopted: a 3+2+1 configuration with three ordinary segments (each covering 72 degrees on tunnel perimeter), two counter key segments (each covering 56.5 degrees), and one key segment (covering 31 degrees); or a 6 configuration with all six segments having the same size (each covering 60 degrees on tunnel perimeter) as every other segment can be the key segment in a trapezoidal shape. Usually these configurations are used when the key segment turns out to be too small in a 5+1 configuration. For tunnels of 26 to 36 ft (8 to 11 m) in diameter, a 7+1 configuration is the most common configuration and 6+2 configuration is also common. However, when tunnel diameter ranges between 20 and 26 ft (6 and 8 m), a 5+1 configuration may result in excessively long segments, and a 7+1 configuration in too short segments. In some cases, the size of key segments can be increased to reduce the size of ordinary segments, or a 6+1 ring can be adopted. Similar complexities are encountered when tunnel diameter is between 36 and 46 ft (11 and 14 m) as segmentation of a ring into an 8+1 configuration is not preferred. Special solutions are required, such as dividing the ring into eight segments (each covering 45 degrees on tunnel perimeter) with also dividing one of the ordinary segments into key and counter-key segments (covering 15 and 30 degrees). Using such configurations, excessively large key segments can be avoided, especially for such large diameter tunnel. At the same time, the configuration is compatible with TBM thrust jacking pattern of an eight-segment ring. For tunnels larger than 46 ft (14 m), a 9+1 configuration is the most common configuration with both small key and large key sizes. A 11+1 configuration has been also considered for this size of tunnel.

The common ring configurations explained previously are summarized in Table 3.4.5 according to the category of tunnel sizes. Note that presented ring configurations are the most common cases in practice and there will be segmental

Table 3.4.5—Most common ring configuration/segmentation for tunnel segmental lining systems

Range of tunnel diameter	Most common ring configuration/segmentation
Tunnel diameter < 20 ft (6 m)	5+1; 4+2; 3+2+1*
20 ft (6 m) < tunnel diameter < 26 ft (8 m)	6+1
26 ft (8 m) < tunnel diameter < 36 ft (11 m)	7+1; 6+2
36 ft (11 m) < tunnel diameter < 46 ft (14 m)	7+1 large key; 7+1+1†
46 ft (14 m) < tunnel diameter	9+1; 9+1 large key; 11+1

*This configuration consists of three ordinary segments, two slightly smaller counter key segments, and one small key segment.
†In this configuration, key can be one-third of ordinary segments and one of counter keys can be as small as two-thirds of ordinary segments.

lining configurations that fall outside of the presented configurations.

3.4.6 *Segment geometry*—Segment systems from the perspective of individual segment geometry can be divided into four main categories: hexagonal system, rectangular system, trapezoidal system, and rhomboidal system.

Hexagonal systems are assembled continuously from hexagonal elements, alternating bottom/top and left/right, with each element serving as a key segment by means of closing of a ring (Fig. 3.4.6a). The geometry of this system does not allow effective use of gaskets, and because it compromises the watertightness of the segments, it is not often used. If it is used, it allows very rapid advance rates. In hard rock tunnels without watertightness requirement, sometimes this system is adopted as part of a two-pass lining system and in combination with double-shield TBMs.

Rectangular systems are assembled in rings of rectangular or slightly tapered segments with a wedge-shaped key segment assembled from bottom to top, alternating between left and right (Fig. 3.4.6b). This system can provide proper sealing performance and has some advantages such as simple longitudinal joint geometry. However, staggered longitudinal joints are not always guaranteed and star or crucifix joints may be present that may cause leakage. One issue with this system is that it is difficult to place rectangular segments without impacting the gasket on the adjacent segment. This may also prevent use of fast-connecting dowels and enforce use of time-consuming bolt systems. The main reason is that unlike bolts that are fastened after complete segment insertion into the ring, dowels are preinserted into segments, which limits the segment approach path into a very narrow path and may cause more friction between gaskets of adjacent segments. This system is still in use for large-diameter tunnels where shear capacity of the dowel system connection between the circumferential joints may not be sufficient.

Trapezoidal systems are assembled from an even number of trapezoidal segments in a ring often with the same length at centerline, with half the segments as counter key segments (wider on the side of the previously placed ring) and the other half are key segments (narrower on the side of the previously placed ring). As shown in Fig. 3.4.6c, after installation of all counter key segments as the first part of the ring like an open-tooth shape, the second part is inserted in the gaps to form a complete ring. Advantages of this system are staggered longitudinal joints without encountering star joints and the fact that every other segment can be used as a key segment. The main disadvantage of this system is that the ring is not

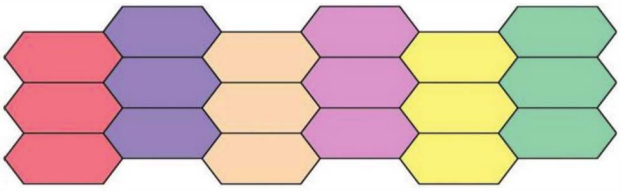

Fig. 3.4.6a—Hexagonal systems (ring developed plan view)

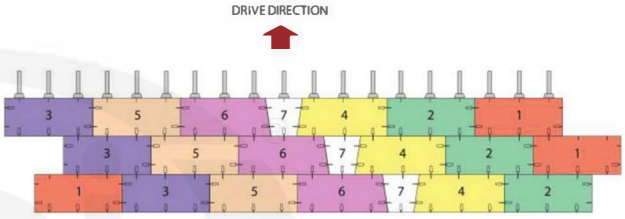

Fig. 3.4.6b—Rectangular systems developed plan view.

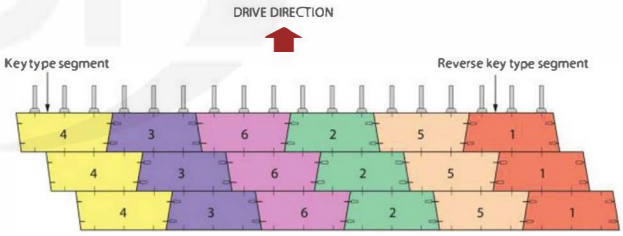

Fig. 3.4.6c—Trapezoidal systems developed plan.

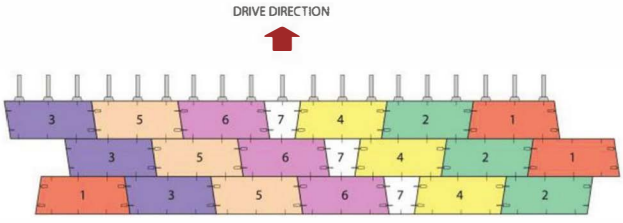

Fig. 3.4.6d—Rhomboidal or parallelogrammical and trapezoidal systems developed plan.

built continuously, which makes it difficult to place several key segments between the counter key segments.

Rhomboidal or parallelogrammical-trapezoidal systems are assembled from ordinary segments in the shape of parallelogram and a key and a counter key segment in the shape of trapezoid. As shown in Fig. 3.4.6d, the tunnel is built continuously ring by ring, and often from bottom to top. The assembly procedure starts with installing trap-

ezoidal reverse key segment and placing parallelogrammical segments next to the counter key first and then next to previous parallelogrammical segments alternating left and right. Ring assembly is completed with often smaller trapezoidal key segment. This system is now the most common system because of preventing crucifix joints and improved sealing performance, continuous ring build from bottom to top, and compatibility with dowel connection system. Note that angled segment joints provide another major advantage, which is avoiding early rubbing of the gaskets during segment insertion in the ring assembly phase, and facilitates use of fast connecting dowels in circumferential joints. Regardless of the shape of segments, the bolted connections are usually needed for longitudinal joints but not needed for circumferential joints in this configuration. In certain cases, longitudinal bolts are replaced by guiding rods, which will be explained in the following chapters.

3.4.7 *Key segment geometry*—The key segment is the last installed segment of a ring, always with a trapezoidal shape in plan view to provide an easy path for sliding into the ring. The key segment is often smaller than ordinary segments and is a proportion of ordinary segments such as one-third, two-thirds, or one-half, but it can also be of a different ratio with respect to ordinary segments. ITA WG2 and JSCE 2007 present two different key segment tapering geometries according to methods historically used for the ring assembly. One method that is not typically used is to insert the segments from the inside of the tunnel, in which the longitudinal side faces of the key segment are tapered in the direction of the tunnel radius. ITA WG2 provides a geometry formulation that is specified towards key segment insertion in the radial direction. The other method, which is common practice, is to insert the segments from the cut face side in the longitudinal direction of the tunnel in which the longitudinal side faces of the key segment are tapered in the longitudinal direction of the tunnel. Using this method, the key segment tapering is defined by the angle of the side faces with respect to joint centerline or longitudinal tunnel axis. Depending on designer and contractor experience, this tapering can be selected differently. A key segment taper angle of 8 to 12 degrees is recommended based on a review of recent projects. Note that when adopting a rhomboidal or parallelogrammical-trapezoidal system, the same joint angle for a key segment should be used for defining the geometry of other segments in the ring.

CHAPTER 4—DESIGN FOR PRODUCTION AND TRANSIENT STAGES

Production and transient loadings include the loading stages starting from the time of segment casting up to the time of the segment erection within the tunnel boring machine (TBM) shield. During these phases, the internal forces and stresses from stripping (demolding), storage, transportation, and handling are used for the design of precast concrete segments. Production and transient loads during these stages result in significant bending moment with no axial forces.

Figure 4a(a) shows the stripping (demolding) phase that is modeled by two cantilever beams loaded under their own self-weights (w). The design is performed with regard to the specified strengths when segments are stripped or demolded (that is, 6 hours after casting). As shown in Fig. 4a(b), the self-weight (w) is the only force acting on the segment and, therefore, the applied load factor in ultimate limit state (ULS) can be taken as 1.4 (ACI 544.7R).

Segment stripping (demolding) is followed by the segment storage phase in the storage yard at the precast plant where segments are stored to gain specified strength before transportation to the construction site. As shown in Fig. 4b(a), in the most common scheme, all segments comprising a full ring are piled up within one stack. Designers, in coordination with the segment manufacturers, provide the distance between the stack supports considering an eccentricity of e = 4 in. (100 mm) between the locations of the stack support for the bottom segment and the supports of above segments. This load case can be represented by a simply supported beam loaded under its self-weight as shown in Fig. 4b(b). The dead weight of segments positioned above (F) acts on the designed segment as a concentrated load in addition to its self-weight (w). Therefore, corresponding load combination can be considered as $1.4w + 1.4F$ (ACI 544.7R).

During the segment transportation phase, stored precast segments in the storage yard are transported to the construction site and TBM trailing gear. Segments may encounter dynamic shock loads during this phase and, as shown in Fig. 4b(a), half or all of the segments of each ring are transported on one dolly. Wood blocks provide supports for the segments. An eccentricity of 4 in. (100 mm) is recommended

(a)

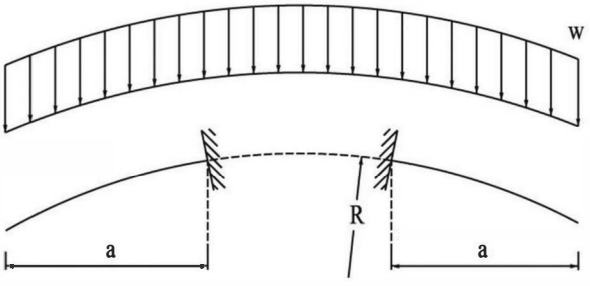

(b)

Fig. 4a—(a) Stripping (demolding) segments from forms; and (b) forces acting on segments.

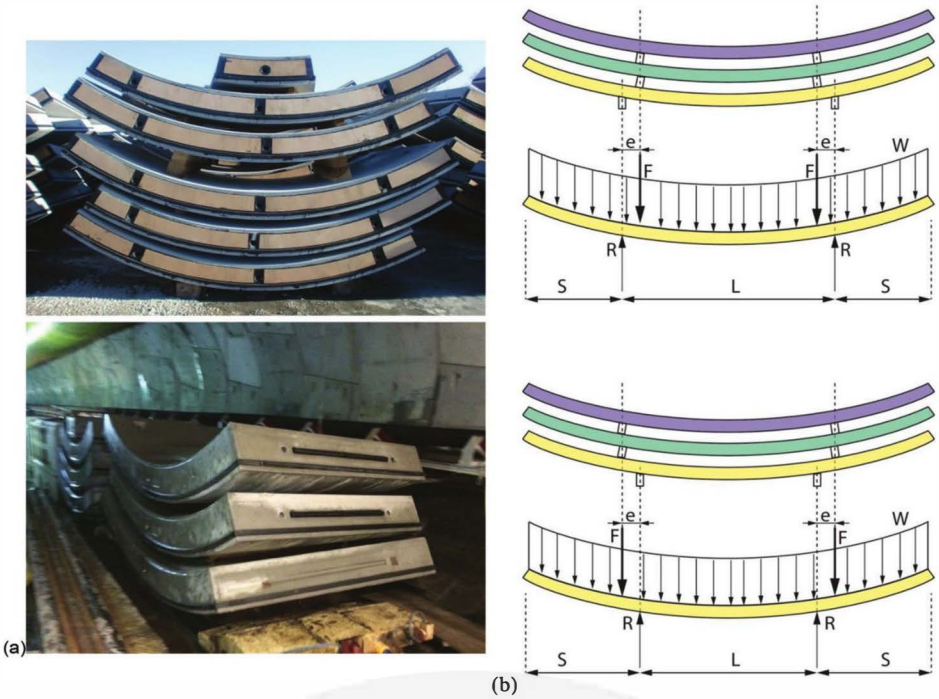

Fig. 4b—(a) Segments stacking for storage and transportation; and (b) schematics of forces acting on bottom segment.

Table 4—Summary of required design checks and factors for production and transient stages

Load case number	Phase	Dynamic impact factor	Maximum unfactored bending moment	Maximum unfactored shear force
1	Stripping (demolding)	—	$wa^2/2$	wa
2	Storage	—	$w(L^2/8 - S^2/2) + F_1e$ $w(S^2/2) + F_1e$	wS $wL/2 + F_1$
3	Transportation	2.0	$w(L^2/8 - S^2/2) + F_2e$ $w(S^2/2) + F_2e$	wS $wL/2 + F_2$
4	Handling (forklift)	2.0	$w(L^2/8 - S^2/2) + F_2e$ $w(S^2/2) + F_2e$	wS $wL/2 + F_2$
	Handling (other methods)		$wa^2/2$	wa

Note: F_1 is the self-weight of all segments completing a ring, excluding the bottom segment; F_2 is the self-weight of all segments carried by forklifts or placed in one carriage for transportation phase, excluding bottom segment.

for design. Note that the wood blocks should be installed nearly parallel to the segment axis. Similar to segment storage phase, simply supported beams represent the load case of transportation with dead weight of segments positioned above (F) and self-weight (w) as the acting loads on designed segment. In addition to load combination of $1.4w + 1.4F$ per ACI 544.7R, a dynamic impact factor of 2.0 is recommended to be applied to the F force for the transportation phase.

Segment handling inside the precast plant and from storage yard to trucks or rail cars are carried out by specially designed lifting devices such as vacuum lifters, forklifts, mechanical clamping, or a combination of them (Fig. 4c). For handling by vacuum lifters and mechanical clamping, the same analysis and design procedure used for segment stripping (demolding) should be followed. However, when segments are handled by forklifts as schematically shown in Fig. 4c(d), a loading scheme similar to segment stacking for storage and transportation (Fig. 4b(b)) should be adopted. In this case, the total eccentricity is equal to sum of spacing of forklift contact point from the wood blocks axis and the minimum design eccentricity of $e = 4$ in. (100 mm). A dead load factor of 1.4 in ULS and a dynamic impact factor of 2.0 are recommended for this load case (ACI 544.7R).

The maximum bending moment and shear forces developed during the aforementioned stages are used for design checks. In addition, as shown on Fig. 4c(e), pullout capacity of lifting inserts and concrete should be calculated. The plastic insert used to lift the segment from its center will be subject to the full self-weight of the segment under dynamic loading conditions. Nominal concrete breakout strength of a single bolt in tension, as shown in diagram of Fig. 4c(e), is calculated following concrete design codes such as ACI 318 and considering an appropriate strength reduction factor. The calculated capacity of concrete, as well as the pullout capacity of lifting inserts, should be greater than the

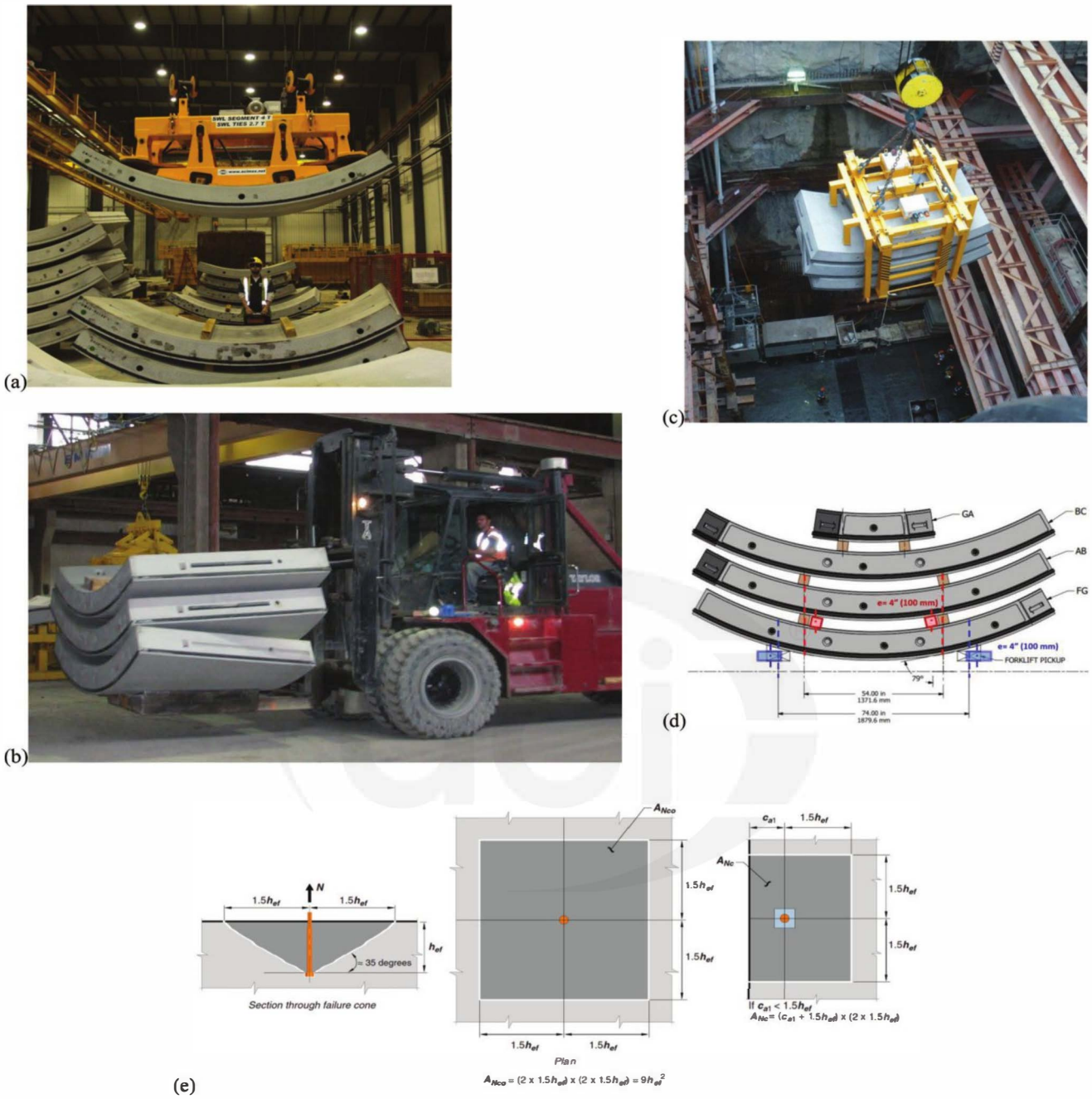

Fig. 4c—Segment handling: (a) using vacuum lifters; (b) forklifts; (c) mechanical clamping; (d) schematics of design eccentricities for segment handling with the forklift; and (e) diagram of pullout capacity of concrete during handling (ACI 318-19, Fig. R17.6.2.1).

demand, which is maximum pullout force applied on the lifting socket due to self-weight of segments and a dynamic impact factor.

Table 4 presents a summary of load cases; applied dynamic impact factors, if any; and maximum developed bending moments and shear forces for the various manufacturing, transportation, and handling stages. Precast concrete segments should be sufficiently reinforced to withstand developed bending moments due to these actions at an early age. Designers should follow structural codes and guides such as ACI 318 and ACI 544.7R for calculating the bending strength (M_n) and check the design strength versus developed bending moments and shear forces.

CHAPTER 5—DESIGN FOR CONSTRUCTION STAGES

Construction loads include the tunnel boring machine (TBM) jacking thrust loads on the circumferential ring joints and the pressures during the grouting operation exerted against the exterior of the completed rings. Precast concrete segments are designed to resist significant bursting and spalling tensile stresses that develop along the circumferential joints due to the advancing of the TBM. The segments

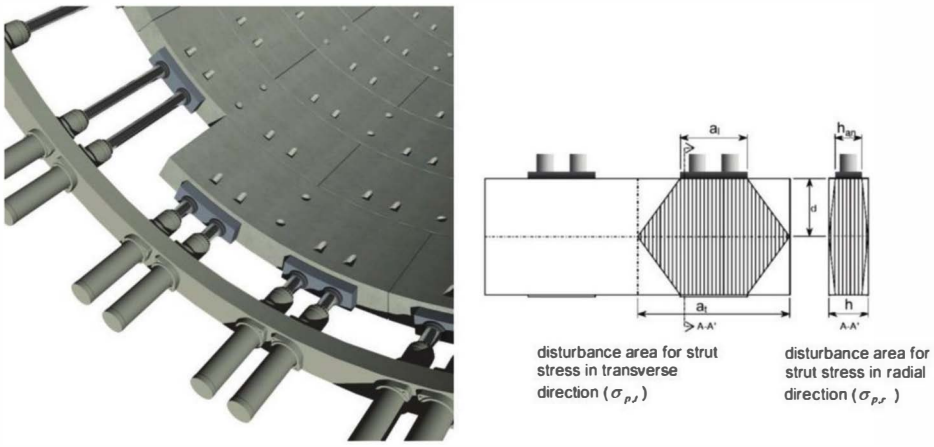

(a) *(b)*

Fig. 5.1—(a) Thrust jacks pushing on circumferential joints; and (b) schematics of a simplified disturbance area of strut under TBM jack shoes (Groeneweg 2007).

should also be able to resist the axial forces and bending moments that develop when the annular space between the segments and the ground is pressure-filled with grout. Included is the primary backfilling of the tail skin void and the secondary grouting that is needed in case a complete contact of the lining with the ground has not been achieved through the primary grouting.

5.1—Tunnel boring machine thrust jack forces

After assembly of a complete ring, the TBM advances by thrusting against the most recent assembled ring, as shown in Fig. 5.1(a). As part of this process, the TBM jacks bear against the jacking pads placed along the exposed circumferential joint. Schematics of a simplified disturbance area of strut under TBM jack shoes are presented in Fig. 5.1(b). High compression stresses develop under the jacking pads and result in the formation of significant bursting tensile stresses deep within the segment. Furthermore, spalling tensile forces also act between adjacent jack pads along the circumferential joint.

Different methods are used for estimating TBM thrust due to the various geologic materials that can be encountered. For tunnel excavation through rock, TBM thrust can be estimated by the summing forces required to advance the machine. These forces include the forces necessary for boring through the rock, countering the friction between the surface of the shield and the ground, and the hauling of trailing gears. Methods found in Fukui and Okubo (2003) and Rostami (2008) can be used to evaluate the rock thrust based on rock strength, tunnel diameter, and cutter characteristics (Bakhshi and Nasri 2013a). For soft ground tunneling applications, the method presented by JSCE 2007 can be used to calculate penetration resistance based on earth or slurry pressure that acts at the cutting face.

Once the required machine thrust has been estimated for the ground conditions, the average thrust force per jack pair is determined simply by dividing the required machine thrust by the number of jack pairs. On sharp curves, the machine thrust is higher on the convex side of the curve than on the concave side. The higher thrust should be accounted for in the design. A simple technique can be used to account for the increased loading on the convex side by doubling the jacking loads. The load factor for this case is taken to be 1.2, which is in agreement with suggested load factor in ACI 544.7R. Note that this factor is only considered when the machine characteristics are unknown, which is the case before the completion of the final design. Whenever the TBM's total thrust is available, maximum thrust jack forces are known and therefore cannot be exceeded. Accordingly, the corresponding load factor should be selected as 1.0. Furthermore, different analysis and design methods are available for this load case, including ACI 318 equations for bursting forces, DAUB:2013 formulas, Iyengar (1962) diagram, and two- and three-dimensional finite element simulations.

5.1.1 *Simplified equations*—For post-tensioned anchorage zones of prestressed concrete sections, structural concrete codes such as ACI 318 allow the use of simplified equations (Eq. (5.1.1a)) to determine the bursting force, T_{burst}, and the centroidal distance from the face of the section, d_{burst}. These simplified equations are used to obtain the forces and stresses developed in the circumferential joints due to TBM advancement. DAUB:2013 recommends similar equations (Eq. (5.1.1b)) specifically for the design of tunnel segments.

$$\text{ACI 318 } T_{burst} = 0.25P_{pu}\left(1-\frac{h_{anc}}{h}\right); d_{burst} = 0.5\left(h-2e_{anc}\right) \quad (5.1.1a)$$

DAUB:2013

$$T_{burst} = 0.25P_{pu}\left(1-\frac{h_{anc}}{h-2e_{anc}}\right); d_{burst} = 0.4\left(h-2e_{anc}\right) \quad (5.1.1b)$$

This load case and corresponding parameter are schematically shown in Fig. 5.1.1. If no specific value has been

provided for e_{anc}, then the eccentricity of the jacking forces is generally considered to be 1.2 in. (30 mm). Figure 5.1.1 and Eq. (5.1.1a) and (5.1.1b) represent the radial bursting stresses in the circumferential joints. These equations are also applicable to tangential bursting stresses developed in the circumferential joints.

Reinforcing bar or fiber reinforcement is designed to resist the bursting stresses developed by jacking forces. Equations (5.1.1c) and (5.1.1d) have been adopted to determine the required area (A_s) of reinforcing bars with a yield stress of f_y for a reinforced concrete (RC) segment.

$$T_{burst} = \phi f_y A_{s\_radial} \text{ for radial direction} \quad (5.1.1c)$$

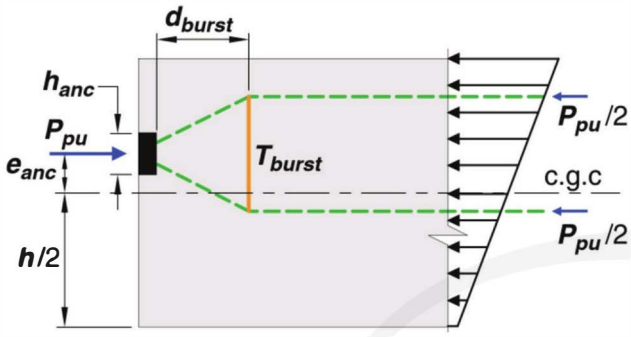

Fig. 5.1.1—Bursting tensile forces and corresponding parameters recommended by ACI 318.

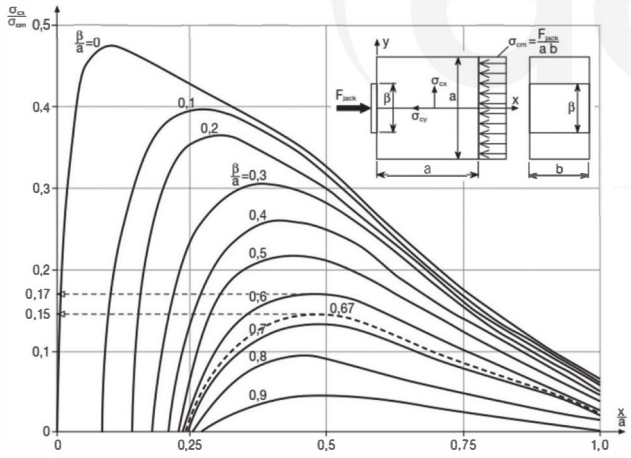

Fig. 5.1.2—Iyengar (1962) diagram for determining bursting tensile stresses.

$$T_{burst} = \phi f_y A_{s\_tangential} \text{ for tangential direction} \quad (5.1.1d)$$

High compressive stresses can be developed under the jacking pads due to the TBM thrust jacking forces. These compressive stresses, $\sigma_{c,j}$, can be estimated using Eq. (5.1.1e).

$$\sigma_{c,j} = \frac{P_{pu}}{A_j} = \frac{P_{pu}}{a_l h_{anc}} \quad (5.1.1e)$$

Because only part of the circumferential segment face is actually in contact with the pads, the allowable compressive stresses (f_c') can be factored to account for the strength of a partially pressurized surface. ACI 318 specifies the formula used for designing the bearing strength of concrete (Eq. (5.1.1f)) with a partially loaded segment face. DAUB:2013 recommends a similar formula for designing tunnel segment faces.

$$f_{c\bullet}' = 0.85 f_c' \sqrt{\frac{A_d}{A_j}} = 0.85 f_c' \sqrt{\frac{a_t (h - 2e_{anc})}{a_l h_{anc}}} \quad (5.1.1f)$$

5.1.2 *Iyengar diagram*—The analytical method of the Iyengar (1962) diagram has also been used for calculating the bursting tensile stresses for the design of tunnel segments (Groeneweg 2007). Similar to previous methods, the extent of load spreading and the resulting magnitude of tensile stresses depend on the dimensions of the loaded surfaces, β, and the final spreading surfaces, *a*, shown in Fig. 5.1.2. Using this approach, the bursting tensile stresses (σ_{cx}), which vary significantly from the face that TBM jacks bear against toward the centerline of segment, are determined as a fraction of the fully spread compressive stress ($\sigma_{cm} = F/ab$). Reinforcing bars are designed for the bursting tensile stresses shown in the diagram. Total bursting force can be obtained as the integration of stresses or the area under the curve, and required reinforcing bar area is determined by Eq. (5.1.1c) and (5.1.1d).

5.1.3 *Finite element method simulations*—As shown in Fig. 5.1.3a, in addition to the bursting stresses under the jacking pads, spalling stresses develop in the areas between the jacking pads and in the areas between the jacking pads and the end faces of segments due to the concentration of the jacking forces. Analytical design methods for spalling

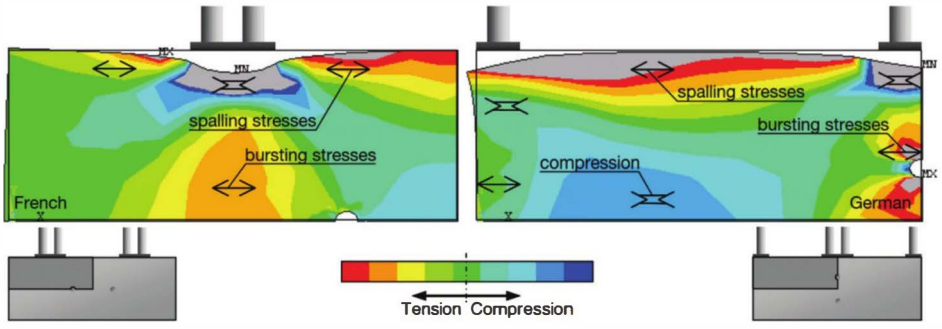

Fig. 5.1.3a—Spalling and bursting stresses in segment joints due to jack thrust forces (Groeneweg 2007).

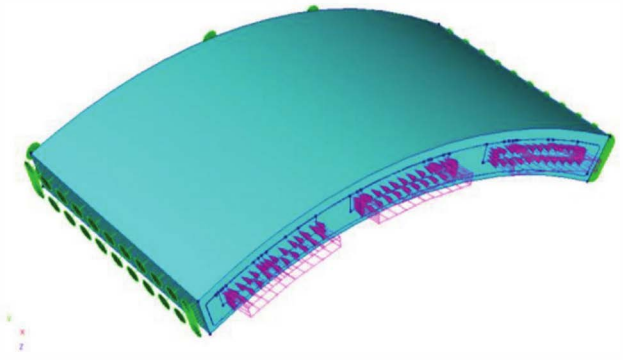

Fig. 5.1.3b—Three-dimensional FEM model for load case of TBM thrust jack forces.

stresses have not been provided in any of the previously reviewed approaches; however, analyzing the problem with a three-dimensional finite element method (FEM) is appropriate. While both linear elastic and nonlinear FEM simulations can be performed, the latter is considered suitable for the service design as nonlinear analyses capture the nonlinear response of the materials after cracking with respect to crack opening. As shown in Fig. 5.1.3b, this load case is simulated by modeling typical segments of two adjoining rings. The factored jacking forces are applied along the contact area between the jacking pads and the segment face. Recesses due to the gasket and stress relief grooves are modeled between two segments to simulate the transfer of force through a reduced cross section. With

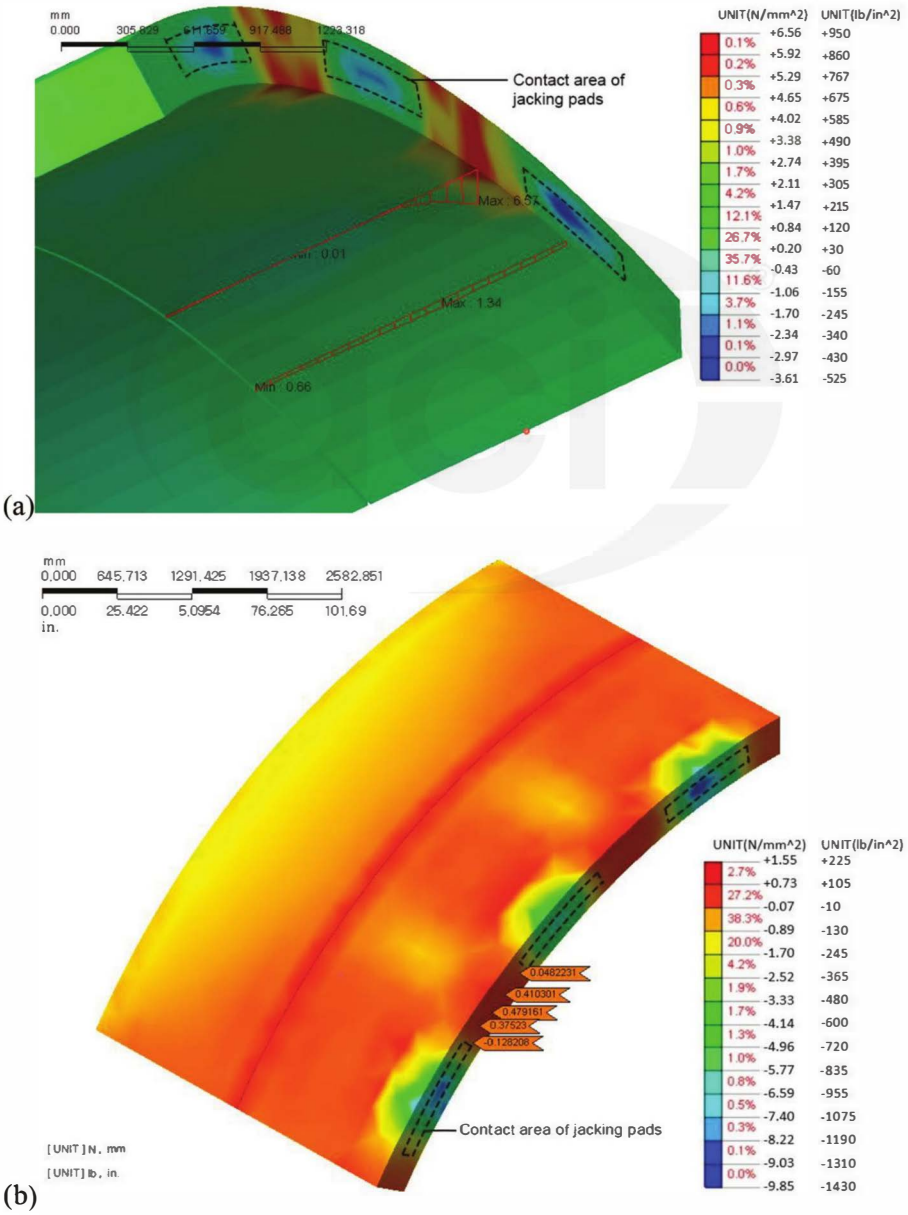

Fig. 5.1.3c—Example of bursting and spalling tensile stresses developed in segments due to TBM thrust jack forces (Bakhshi and Nasri 2013b, 2014d): (a) transverse stresses; and (b) radial stresses. (Note: Size of contact area of jacking pad is 7.8 x 30 in. [0.2 x 0.8 m]; segment thickness is 15.7 in. [0.4 m]).

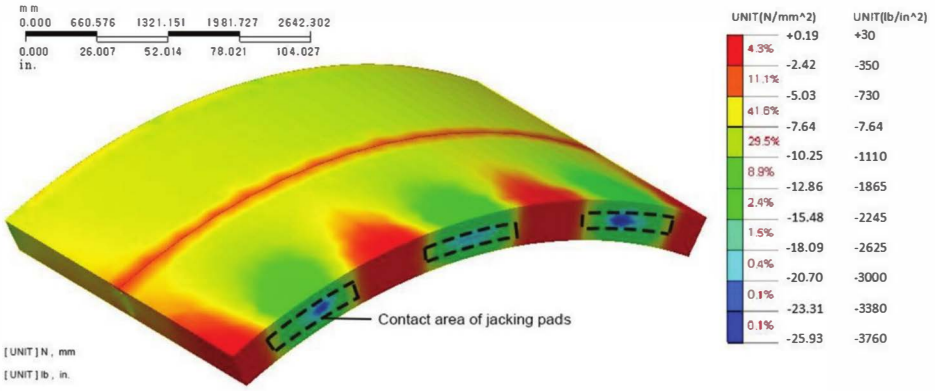

Fig. 5.1.3d—Typical compressive stresses developed in tunnel segments due to TBM thrust jack forces (Bakhshi and Nasri 2013b, 2014d). (Note: Size of contact area of jacking pad is 7.8 x 30 in. [0.2 x 0.8 m]; segment thickness is 15.7 in. [0.4 m]).

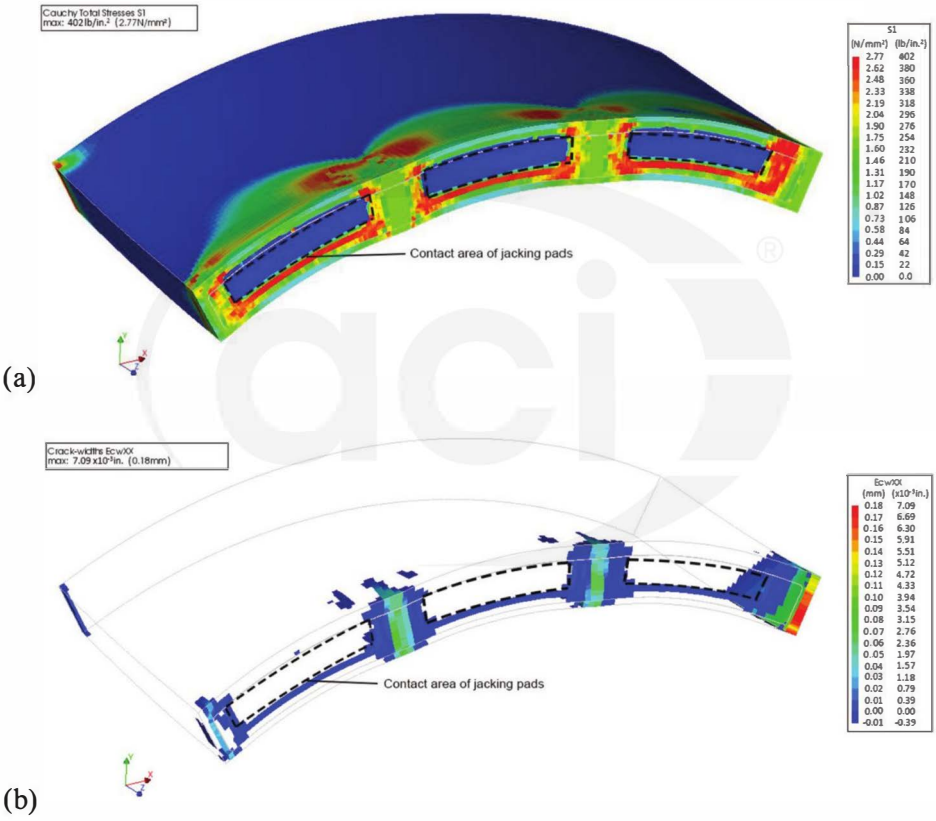

Fig. 5.1.3e—Example of a three-dimensional nonlinear FEM simulation for the load case of TBM thrust jack forces applied on fiber-reinforced concrete segment: (a) transverse tensile stresses; and (b) crack width dimension. Size of contact area of jacking pad is 6.8 x 24 in. (0.17 x 0.6 m) and segment thickness is 12 in. (0.3 m).

this approach, the translational degrees of freedom are fixed in all directions behind the previously installed segment. Figures 5.1.3c(a) and 5.1.3c(b) show typical results consist of the transverse and radial bursting stresses under the jack pad and the spalling stresses in the areas between the jacking pads as a result of an elastic FE analysis. Typical compressive stresses due to this load case are shown in Fig. 5.1.3d (Bakhshi and Nasri 2013b, 2014d).

Results from the three-dimensional FEM simulation indicate that spalling tensile stresses between the jack pads, and the jack pads and end faces, can be more significant than the transverse bursting tensile stresses under the jacking pads (Bakhshi and Nasri 2013b). Precast tunnel segments should be designed to withstand these high tensile stresses. Reinforcement bars are designed for the tensile forces determined by the integration of stresses through the tensile zone, similar to Iyengar (1962) diagram method. When segments are only reinforced with fibers, the spalling stresses are likely to exceed the tensile strength. Therefore, a three-dimensional nonlinear FEM simulation, such as the one shown in Fig. 5.1.3e, should be performed to validate limitation of the crack width dimensions to the allowable values set

forth by standards, guidelines, and project specifications or design criteria. In the example shown in Fig. 5.1.3e, tensile cracking strength of fiber-reinforced segments is 403 psi (2.77 MPa) and its post-cracking tensile strength is 233 psi (1.6 MPa). Figure 5.1.3e(a) shows the transverse tensile stresses, and Fig. 5.1.3e(b) shows the crack width dimension due to jacking force. As expected, cracks are observed at the regions with highest spalling stresses in the linear analysis—that is, between jacking pads, and jacking pad and edge of segment (Fig. 5.1.3c(a)). In this example, the size of contact area of jacking pad is 6.8 x 24 in. (0.17 x 0.6 m).

5.2—Tail skin back grouting pressure

Tunnel rings are assembled within the shield of the TBM. At this location, the excavated diameter of the tunnel is larger than the external diameter of the tunnel ring. As shown in Fig. 5.2a, a tail void is created between the ground and the tunnel lining. This load case is generated by back grouting or filling of the annular space using semi-liquid grouts under high pressure to control and restrict settlement at the ground surface as well as to ensure complete contact between the ring and the ground. Grouting material generally consists of sand, water, cement, and several additives such as bentonite or plasticizers. This material is not actually a liquid per se, but it does have very low shear yield strength of 0.003 to 0.015 psi (20 to 100 Pa), prior to its hardening. When grout flows, it can be continuously injected into the annular space behind the TBM by means of grout pipes routed through the tail skin.

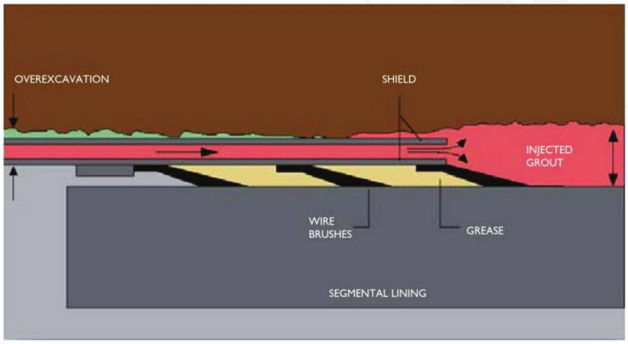

Fig. 5.2a—Backfilling of tail skin void (Guglielmetti et al. 2007).

To enter the annulus space created around the tunnel lining, the grout pressure needs to be greater than the water pressure surrounding the liner. The grout pressure should also typically be less than the overburden pressure to prevent pushoff of the soil, heave, hydrojacking, or all of these. Grouting models (Zhong et al. 2011) can be developed that predict the optimal grout pressure by considering the combined effects of groundwater level, plasticity of grout, rate of advancement of the TBM, and the filling rate of the tail void. Using Eq. (5.2a), the equivalent specific weight of the grout is determined by taking the equilibrium condition between the upward component of the total grout pressure, tunnel self-weight, and tangential component of the grout shear stresses (Groeneweg 2007). These forces are schematically shown in Fig. 5.2b.

$$\frac{\pi}{4} D_e^2 b \rho_{eq} = \pi D_e h b \rho_{concrete} + 2 D_e b \tau_{yield} \quad (5.2a)$$

The vertical gradient of the radial grout pressure between the crown and the invert of the tunnel is determined by Eq. (5.2b).

$$\Delta P_{g,\,invert} = \rho_{eq} \cdot D_e \quad (5.2b)$$

Note that AASHTO DCRT-1 specifies that 10 psi (69 kPa) above the groundwater pressure is the maximum permissible grouting pressure applied to the segmental ring. However, a maximum permissible grouting pressure of up to 22 psi (150 kPa) above the maximum groundwater pressure has been also considered (Ninić and Meschke 2017). For this load case, the lining is evaluated in a cross-sectional plane perpendicular to the longitudinal direction of the tunnel and modeled as a solid ring with a reduced flexural rigidity to account for the segment joints. Because the lining is surrounded completely by semi-liquid and fresh grout materials at this point, no interaction is taken into account between the ring and ground. As shown in Fig. 5.2b, the back-grouting load condition is modeled by applying radial pressure varying linearly from the minimum grout pressure at the crown to the maximum grout pressure located at the invert of the tunnel. The self-weight of the lining and the grouting pressure are the only loads applied to the tunnel lining at this stage of the analysis. For a load combination

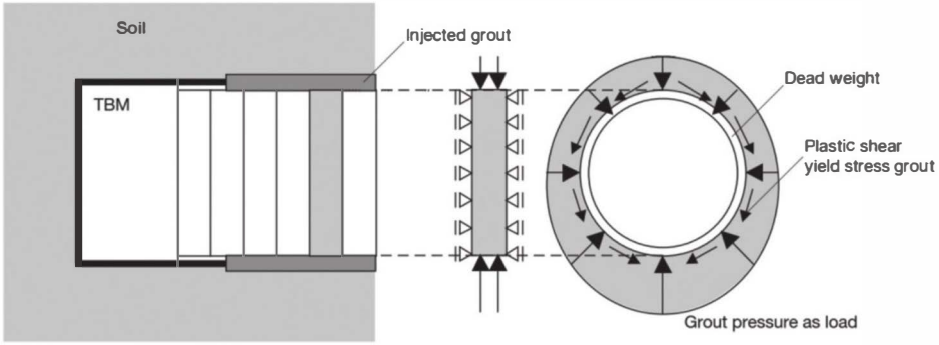

Fig. 5.2b—Forces and definitions for load case of tail void back-grouting (Groeneweg 2007).

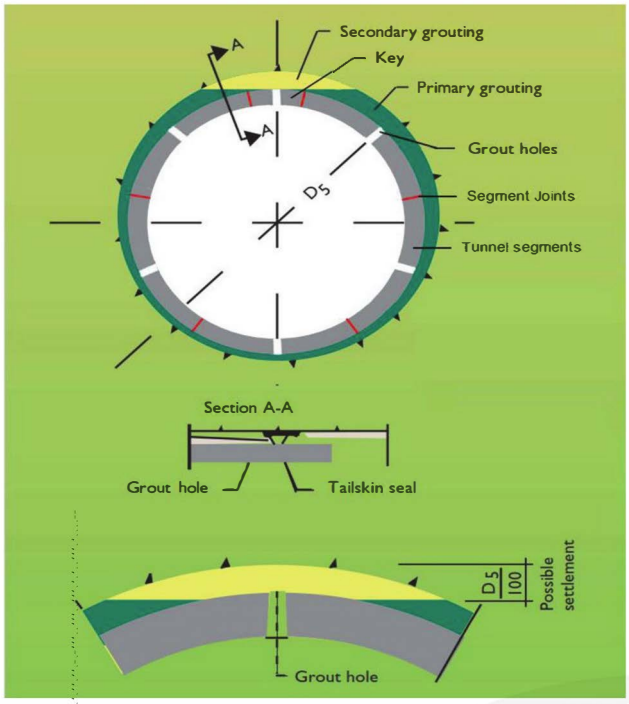

Fig. 5.3a—Secondary grouting through segment grout hole (Guglielmetti et al. 2007).

of self-weight and grout pressure, a load factor of 1.25 is suggested to both loads (ACI 544.7R). The analysis is performed using general structural analysis packages. As a result of this load case, it can be shown that significant axial forces and small bending moments can be developed in the tunnel segmental lining. Precast segments are designed for combined maximum bending moments and axial forces.

5.3—Localized back grouting (secondary grouting) pressure

Localized back grouting, also known as secondary or check grouting, is performed through holes that are manufactured into the segments. As shown in Fig. 5.3a, segments can be fitted with grout sockets that are screwed into position and remain closed with nonreturn valves and plastic covers during the ring installation process. Prior to the introduction of modern pressurized face machines, this grouting method was used to fill the annulus; however, the collapse of unstable ground into the annular space can generate significant settlements. As such, this method is now primarily used for secondary grouting in closed-face tunneling. To model the effects of secondary grouting, this load case consists of the forces applied to segments to verify whether the annular gap has been closed, which is similar to the tail skin back grouting method when only one of the grouting pipes is used. Following the ITA WG2 guidelines, this load case can be simulated using the force distribution shown in Fig. 5.3b. In this figure, secondary grouting pressure is applied on one-tenth of lining perimeter on the crown.

The lining for this load case is modeled in the cross-sectional plane perpendicular to the longitudinal direction of the tunnel using a solid ring with a reduced flexural rigidity

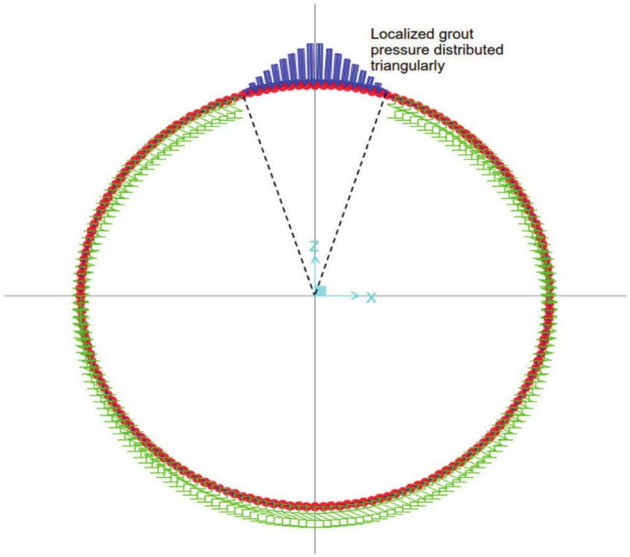

Fig. 5.3b—Modeling localized grouting pressure applied over one-tenth of the lining.

to represent the segment joints. Because secondary grouting occurs long after the primary grouting materials have cured, it can be assumed that tunnel lining is in full contact with the surrounding ground except in the local area where the secondary grouting is to be performed. To simulate the boundary condition for this case, the interaction between lining and surrounding ground or primary hardened grout can be modeled using radial springs with the segments supported radially. Linear translational springs have been used to represent this type of interaction. The method described by USACE EM 1110-2-2901 can be used, as an example, to determine the spring stiffness per unit of exterior tunnel surface. Using the same grout pressure on the crown as for the previous load case and with the radial spring stiffness, the bending moments and axial forces developed within the lining can be determined from the localized grouting operation. This loading case often results in small incremental axial forces with large bending moments. Precast segments are designed for this load case using axial force-bending moment interaction diagrams.

5.4—TBM backup load

TBM backup load is the self-weight of the backup equipment train behind the TBM shield, shown by schematics in Fig. 5.4a, applied as a concentrated variable load onto the segmental precast concrete lining. In general, TBM backup load may not be a critical or governing load case. However, in subsea and river crossing projects, to control buoyancy, an additional weight should be provided by the backup system inside the tunnel after ring installation and before installation of precast buoyancy unit. TBM drawings, such as Fig. 5.4b, show that this backup load is applied on specific locations in cross section on contact areas with tunnel lining intrados. In addition, longitudinal TBM drawings (Fig. 5.4b(b)) reveal that the backup load is applied longitudinally (with respect to the tunnel direction) on two wheels on each ring. For this load case, two-dimensional FEM analysis is often sufficient,

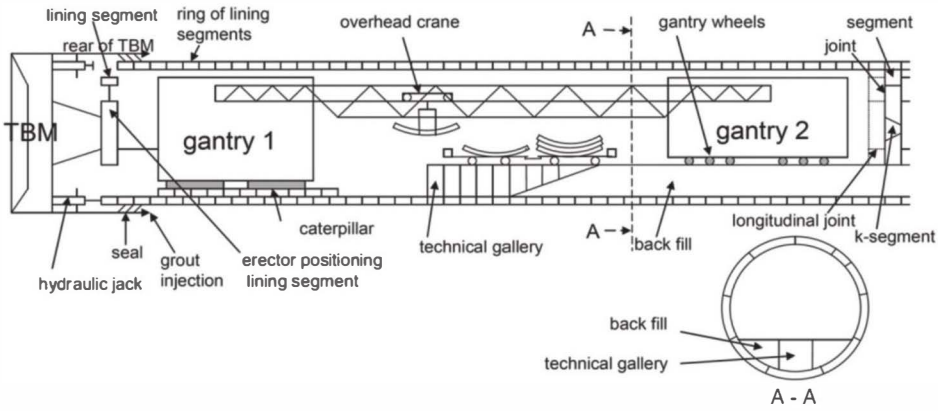

Fig. 5.4a—Schematics of TBM, backup train (gantries), and tunnel lining at the Groene Hart Tunnel as segmental lining is being erected inside the TBM (Talmon and Bezuijen 2011).

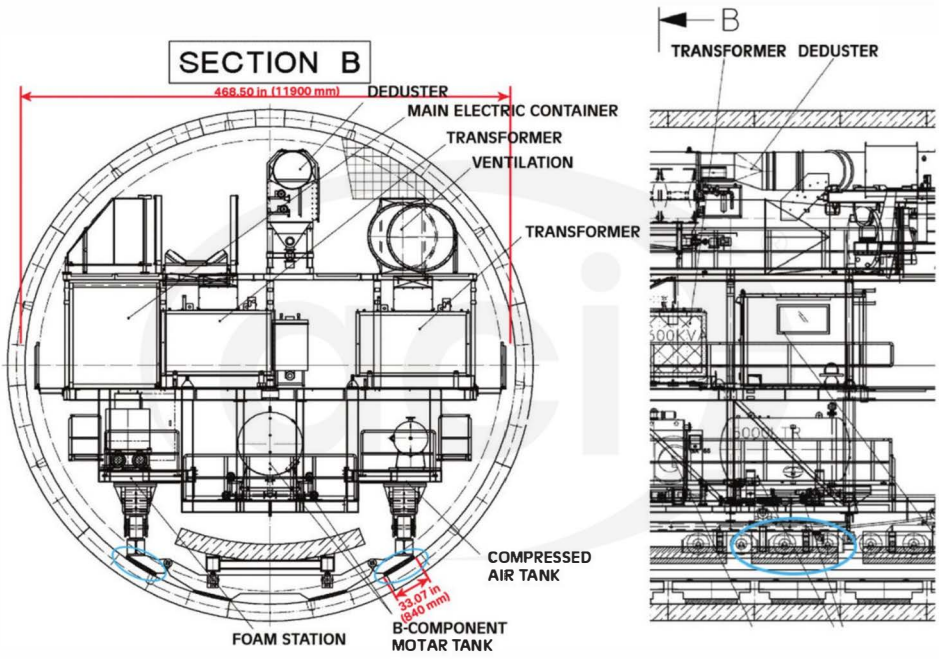

(a) (b)

Fig. 5.4b—Sections behind the shield through the heaviest part of backup train (gantries) where heaviest backup loads are applied on segmental ring before backfilling: (a) cross section; and (b) longitudinal section.

with the assumption that backup load is applied uniformly on this area. Typical analysis results including deformations, axial forces, bending moments, and shear forces are shown in Fig. 5.4c. Resulting factored bending moments and axial forces for all critical cases (for example, shallow cover and deep tunnel) are compared with axial force-bending moment interaction diagram of segmental lining. Results should confirm that precast concrete tunnel segments can withstand axial forces and bending moments induced by TBM backup load or otherwise design should be modified. Punching shear strength of the segmental lining should be also assessed following concrete design codes such as ACI 318 and BS EN 1992-1-1:2004.

For the TBM backup load consideration, the early stage strength (setting time) of the tail void grout and the TBM advance rate are also critical. The advance rate can be limited to the tail void grout strength needed for support of the first and second gantries.

CHAPTER 6—DESIGN FOR FINAL SERVICE STAGES

The final service stages are represented by the long-term loads imposed on the lining from the ground; groundwater; surcharges; and other factors, which generally are specific to the particular tunnel. Hoop force transfer along the longitudinal joints between segments, additional distortion, and other load cases specific to projects are also considered during this stage. Some common load cases specific to projects include earthquake, fire, explosion, adjacent tunnels, and longitudinal bending moments. For the most part, service loads

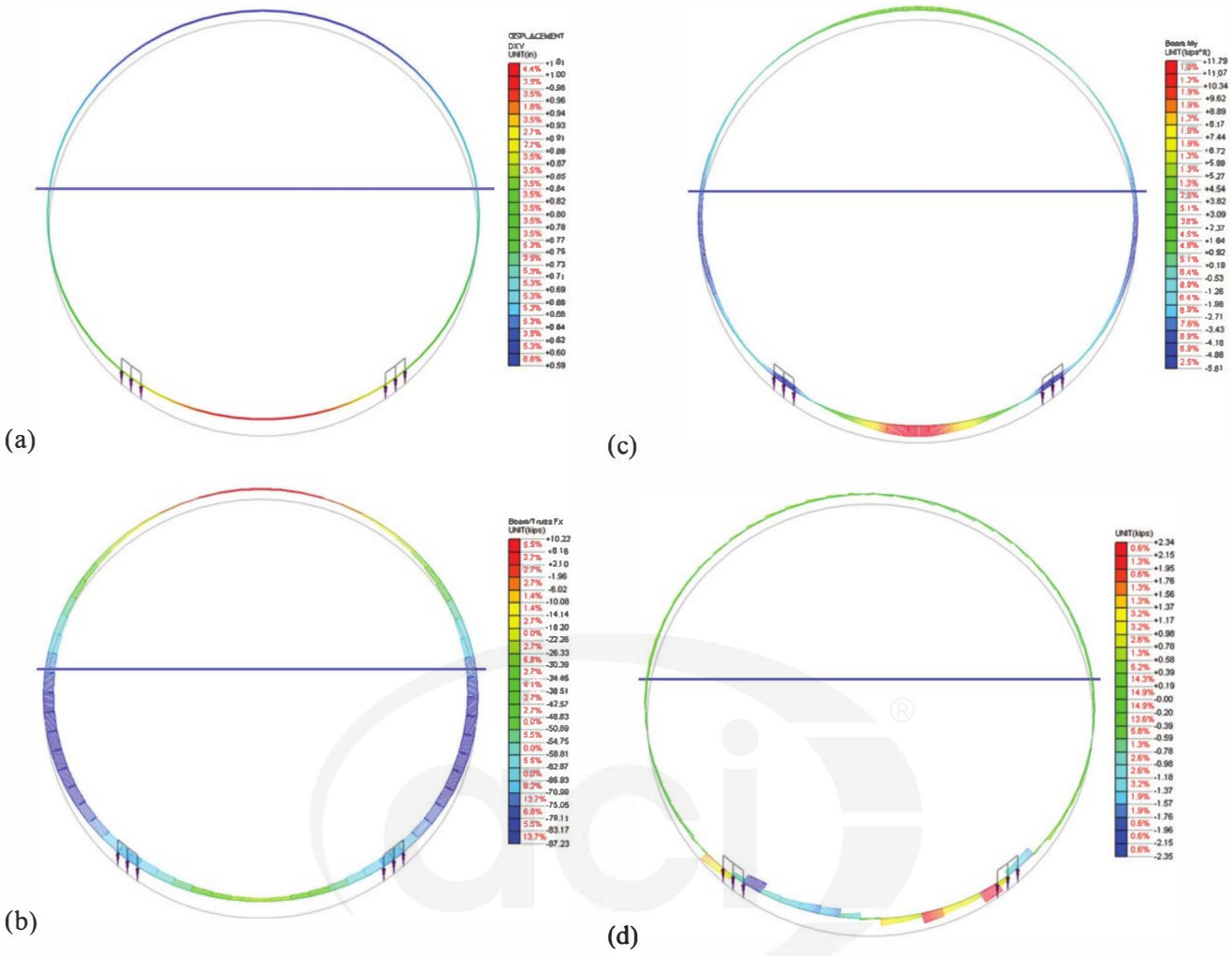

Fig. 5.4c—Typical results of FEM analysis for backup load case: (a) deformations; (b) axial forces; (c) bending moment; and (d) shear forces. (Note: Units are inches, kip, and ft-kip; multiply by 25.4, 4.45, and 1.36, respectively, for converting to mm, kN, and kN.m.)

Table 6.1—Load factor and load combination table for final service stages (AASHTO DCRT-1)

Load combination limit states	*w*, WA_P		*EH*, *EV*		*ES*	
	Maximum	Minimum	Maximum	Minimum	Maximum	Minimum
ULS	1.25	0.90	1.35	0.90	1.50	0.75
SLS	1.0		1.0		1.0	

generally result in axial forces and bending in the segmental lining. With the hoop force transfer in the longitudinal joints, significant bursting tensile stresses can be developed.

6.1—Earth pressure, groundwater, and surcharge loads

Precast concrete segments are used to withstand various loads from vertical and horizontal ground pressure, groundwater, self-weight, surcharge, and ground reaction loads. In accordance with load and resistance factor design (LRFD) principles and as explained in 3.1, 3.2, and 3.3, load factors and load combinations shown in Table 6.1 should be used to compute the ultimate limit state (ULS) and serviceability limit state (SLS).

Methods for analysis of segmental tunnel linings are presented in accordance with standards and guidelines from Europe, Asia, and America (Bakhshi and Nasri 2014a). The effect of ground, groundwater, and surcharge loads on segments is analyzed using elastic equations, beam-spring models, finite element methods (FEM), and discrete element methods (DEM). Other acceptable methods of analysis include Muir Wood's (1975) continuum model with discussion from Curtis et al. (1976), Duddeck and Erdmann's (1982) model, and an empirical method based on tunnel distortion ratios (Sinha 1989; Deere et al. 1969) that was originally developed by Peck (1969). The results of these analyses are used to specify the concrete strength and reinforcement. Reduction in bored tunnel segmental lining

moment of inertia also known as reduced flexural rigidity, where relevant, will be in accordance with Muir Wood's (1975) proposed method as presented in following equation.

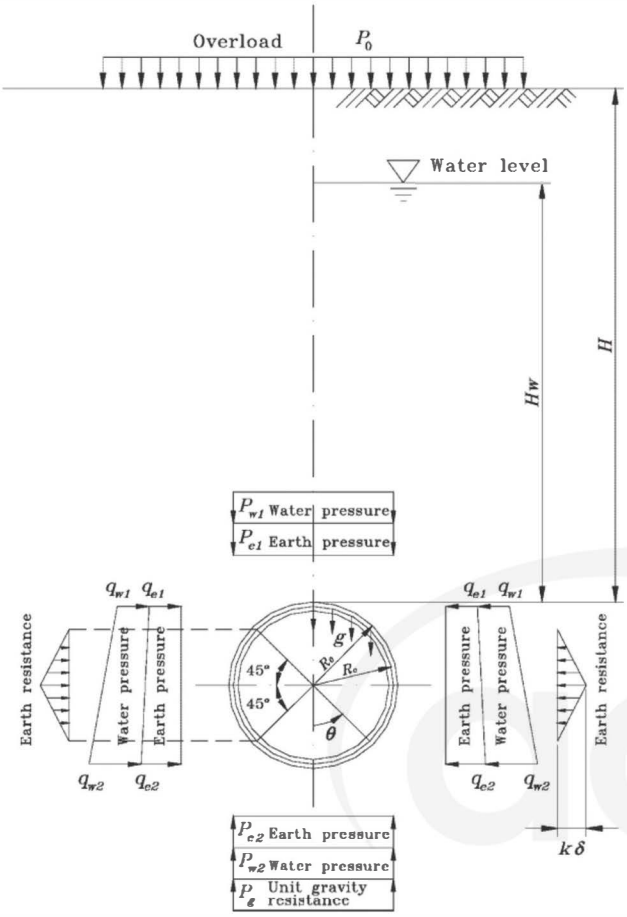

Fig. 6.1.1—Distribution of loads used in elastic equations method (JSCE 2007).

$$I_r = I_j + (4/n)^2 \times I \quad (6.1)$$

where I_j is moment of inertia at joint (taken as zero in the design); I is the moment of inertia for nominal lining thickness; and n is the number of segments per ring excluding key segment ($n \geq 4$).

6.1.1 *Elastic equation method*—The elastic equations method (ITA WG2; JSCE 2007) is a simple method for calculating member forces of circular tunnels. As shown in Fig. 6.1.1, the load distribution model consists of applying uniform vertical ground and groundwater pressures, a linearly varying lateral earth pressure, self-weight of the lining, and a triangularly distributed horizontal ground reaction between 45 and 135 degrees from the crown. Member forces are calculated using the elastic equations contained in Table 6.1.1 (JSCE 2007; ITA WG2). For this method, the segmental tunnel lining is modeled using a uniform reduced bending rigidity (Muir Wood 1975) that takes into account the effect of longitudinal joints between the segments. Subgrade reaction modulus (spring stiffness) formulations recommended by different guidelines are as follows

USACE EM 1110-2-2901:1997:

$$K_r = E_r/(R\,(1+\nu)) \quad k_t = 0.5k_r/(1+\nu) \quad (6.1.1a)$$

ÖVBB 2011 (Austrian):

$$K_r = E_s/R \quad k_t = 0$$

Groeneweg (2007):

$$K_r = E_s/R \quad k_t = 0$$

Table 6.1.1—Equations for calculation of member forces using elastic equation method (JSCE 2007; ITA WG2)

Load	Bending moment	Axial force	Shear force
Vertical load ($P = p_{e1} + p_{w1}$)	$(1 - 2S^2)PR_c^2/4$	S^2R_cP	$-SCR_cP$
Horizontal load ($Q = q_{e1} + q_{w1}$)	$(1 - 2C^2)QR_c^2/4$	C^2R_cQ	$-SCR_cQ$
Horizontal triangular load ($Q' = q_{e2} + q_{w2}$) ($Q - Q'$)	$(6 - 3C - 12C^2 + 4C^3)(Q - Q')R_c^2/48$	$(C + 8C^2 - 4C^3)(Q - Q')R_c/16s$	$(S + 8SC - 4SC^2)$ $(Q - Q')R_c/16$
Soil reaction ($P_k = k\delta_h$)	$0 \leq \theta \leq \pi/4$ $(0.2346 - 0.3536C)R_c^2k\delta_h$ $\pi/4 \leq \theta \leq \pi/2$ $(-0.3487 + 0.5S^2 + 0.2357C^3)R_c^2k\delta_h$	$0 \leq \theta \leq \pi/4$ $0.3536CR_ck\delta_h$ $\pi/4 \leq \theta \leq \pi/2$ $(-0.7071C + C^2 + 0.7071S^2C)$ $R_ck\delta_h$	$0 \leq \theta \leq \pi/4$ $0.3536CR_ck\delta_h$ $\pi/4 \leq \theta \leq \pi/2$ $(SC - 0.7071C^2S)$ $R_ck\delta_h$
Dead load ($P_g = \pi \cdot g$)	for: $0 \leq \theta \leq \pi/2$ $(3/8\pi - \theta S - 5/6C)R_c^2g$ for: $\pi/2 \leq \theta \leq \pi$ $(-\pi/8 + (\pi - \theta)S - 5/6C - 1/2\pi S^2)$ R_c^2g	for: $0 \leq \theta \leq \pi/2$ $(\theta S - 1/6C)R_cg$ for: $\pi/2 \leq \theta \leq \pi$ $(-\pi S + \theta S + \pi S^2 - 1/6C)R_c^2g$	for: $0 \leq \theta \leq \pi/2$ for: $\pi/2 \leq \theta \leq \pi$ $(-(\pi - \theta)C + \theta S + \pi SC - 1/6S)R_cg$
Horizontal deformation at springline (δ_h)	$\delta_h = \dfrac{(2P - Q - Q' + \pi g)R_c^4}{24(EI + 0.045k\mathbb{R}_c^4)}$		

Note: θ is angle from crown; $S = \sin\theta$; $S^2 = \sin^2\theta$; $S^3 = \sin^3\theta$; $C = \cos\theta$; $C^2 = \cos^2\theta$; $C^3 = \cos^3\theta$; EI is flexural rigidity in unit width.

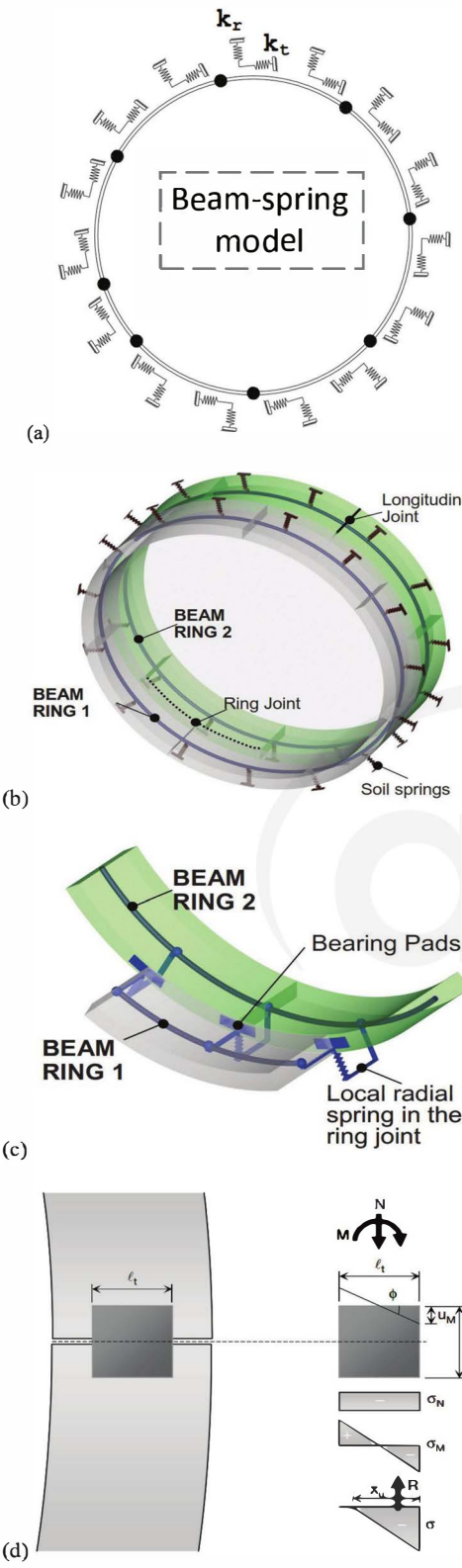

Fig. 6.1.2—(a) Demonstration of springs used for modeling of the interaction between ground and the lining; (b) double ring beam-spring model with radial springs simulating ground, and joint springs simulating longitudinal and circumferential joints; (c) scheme of ring joint (Plizzari and Tiberti 2009); and (d) presentation of parameters used in Janssen model for determining rotational spring stiffness.

JSCE 2007:

$$K_r = \text{NA} \qquad k_t = 1/3K_r$$

RTRI 2008:

$$K_r = \text{varies} \qquad k_t = \text{NA}$$

AFTES-WG7:

$$K_r = E_r/(R\,(1+\nu)) \qquad k_t = \text{NA}$$

DAUB:2005:

$$K_r = E_s/R \qquad k_t = 0$$

where E_s or oedometer stiffness has the following relationship with surrounding ground Young's modulus (Duddeck and Erdmann 1982)

$$E_s = \frac{(1-\nu)E_r}{(1-2\nu)(1+\nu)} \tag{6.1.1b}$$

For example, assuming $\nu = 0.25$, $E_s = 1.2E_r$.

6.1.2 *Beam-spring method*—Using the beam-spring (also known as bedded beam) method endorsed by AASHTO DCRT-1, JSCE 2007, and ÖVBB 2011, the lining can be modeled in the cross-sectional plane as a series of beam elements that span between the longitudinal joints of the segments. As shown in Fig. 6.1.2(a), the interaction between the ground and the lining is modeled in two-dimensional domain using translational springs in the radial and tangential directions. When modeling in three-dimensional domain, interaction of lining with the ground in longitudinal direction of the tunnel is also modeled by longitudinal springs accordingly. Because the lining and ground are represented by a series of beams and springs, this method is referred to as the beam-spring or bedded-beam method. In the U.S. tunnel industry, the stiffness of the springs is generally calculated using formulas recommended by USACE EM 1110-2-2901 (Eq. (6.1.1a)). Furthermore, various two-dimensional approaches are used to evaluate effects of the segment joints, including solid ring models with fully bending rigidity, solid ring models with reduced bending rigidity (Muir Wood 1975), ring models with multiple hinged joints, and ring models with rotational springs. However, two-dimensional models cannot be used to represent circumferential joints or staggered arrangement of segments between rings.

As shown in Fig. 6.1.2(b) and 6.1.2(c), a two-and-a-half-dimensional multiple-hinged segmented double-ring beam spring has been used to model the reduction of bending rigidity and the effects from a staggered geometry. This manipulation is achieved by modeling the segments as curved beams, flat longitudinal joints as rotational springs

or Janssen joints (Janssen 1983), and circumferential joints as shear springs. Under final service loads, the longitudinal joints may be open or closed.

$$\text{Closed joint: } \theta \le \frac{2N}{Ebl_t}$$

$$\text{Open joint: } \theta > \frac{2N}{Ebl_t}$$

The Janssen rotational spring stiffness (k_{jr}) is derived accordingly by following equations.

$$\text{Closed joint: } k_{jr} = \frac{bl_t^2 E}{12}$$

$$\text{Open joint: } k_{jr} = \frac{9bl_t EM\left(\frac{2M}{Nl_t} - 1\right)^2}{8N}$$

where b is the width of segment (contact area in longitudinal joint); E is the Young's modulus; l_t is the length of contact area between segments in longitudinal joints; N is the axial hoop force in segments; and θ is the rotation. Refer to Fig. 6.1.2(d) for presentation of parameters used in the Janssen model.

Two rings are used to evaluate the coupling effects; however, this method uses symmetry conditions to remove complex support conditions and only half of the segment width is considered from each adjacent ring for the longitudinal and circumferential joint zone of influence. Considering the self-weight of the lining, and distributing the ground, groundwater, and surcharge loads along the beam, member forces can be calculated using a conventional structural analysis package.

6.1.3 *Finite element method and discrete element method simulations*—In soft ground, loose rock, and partially homogeneous solid rock, ÖVBB 2011 and AFTES-WG7 recommend using FEM and finite difference method (FDM) to calculate the forces in the tunnel lining. The discrete element method (DEM), as shown in Fig. 6.1.3a, is generally considered more appropriate for tunnels in fractured rock. Recommended engineering properties for analysis of segmental lining in the rock formations includes properties of intact rock such as unit weight; modulus of elasticity; unconfined compressive strength (UCS); internal friction angle; tensile strength; and properties of discontinuities such as joint spacing, joint apparent dip direction, and joint apparent dip. Other required discontinuities parameters for a DEM modeling, as shown in Table 6.1.3 for a typical tunnel boring machine (TBM)-bored tunnel in rock, includes peak joint friction angle, peak joint cohesion, residual joint friction angle, residual joint cohesion, joint normal stiffness, joint shear stiffness, E_{ind}/E_{mass}, geological strength index (GSI), and M_i, which is a material constant for the intact rock based on Hoek-Brown failure criterion (Hoek and Brown 2018). In rock tunneling, a two-dimensional approach is generally sufficient for continuous linear structures that do not contain sudden changes in cross-sectional geometry or high concentrations of loadings. Three-dimensional techniques are generally used in soft ground tunneling due to three-dimensional arching effect and in cases with more complex geometry and loadings such as with crosscuts that intersect the main tunnel (ÖVBB 2011). As shown in Fig. 6.1.3b, FEM is used to model the ground surrounding the liner, where a continuum medium is discretized into smaller elements, which are connected along adjoining nodal points (Bakhshi and Nasri 2013c). The advantage of this method is to be able to model the ground deformations and the post-yielding behavior of the liner materials to include any redistribution of stress that results from deformation of the lining and excavation of the tunnel (ÖVBB 2011). FEM analysis techniques can also be used to represent nonuniform and anisotropic stresses such as when nonsymmetrical features are present in the ground. This can be the case when several different geologic forma-

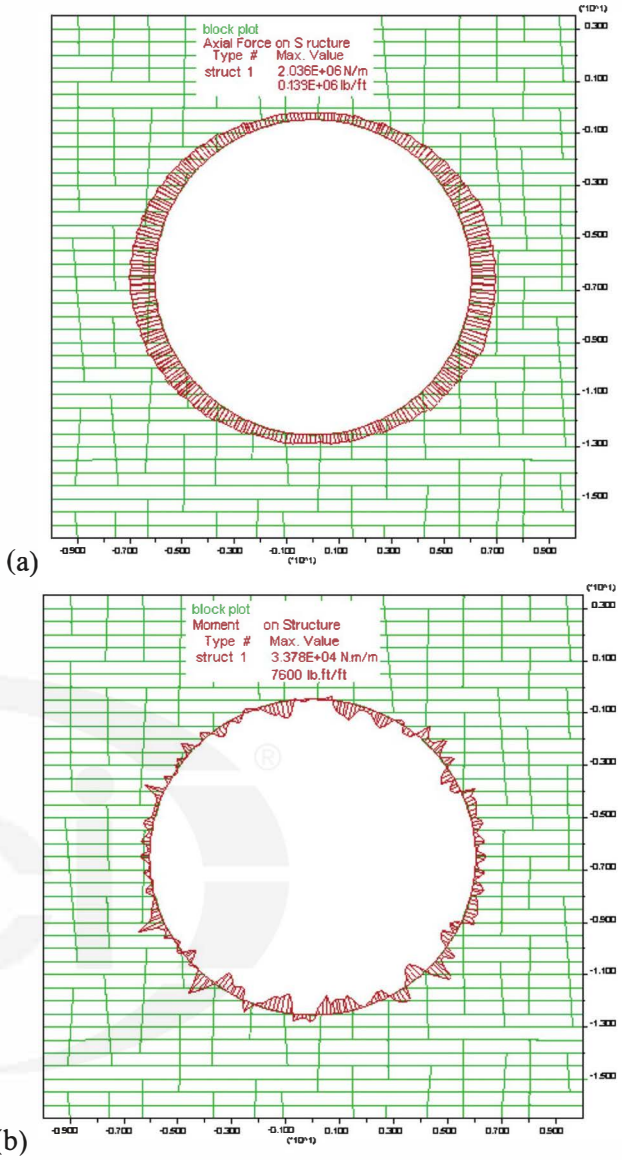

Fig. 6.1.3a—DEM model and developed internal forces along the lining perimeter as a result of DEM analysis on large-diameter tunnel excavation in fractured rock: (a) axial forces; and (b) bending moments.

Table 6.1.3—Example of geotechnical properties for rock formations in a tunnel project (Bakhshi and Nasri 2017a)

Reach		Intact Rock Properties					Properties of rock discontinuities									Joint Properties									
							Joint Set 1 - Bedding			Joint Set 2			Joint Set 3												
		Unit weight, lb/ft^3 (kN/m^3)	Modulus of elasticity, ×10^6 psi (GPa)	UCS, ksi (MPa)	Internal friction angle, degrees	Tensile strength, psi (MPa)	Joint spacing, in. (mm)	Joint apparent dip direction, degrees	Joint apparent dip, degrees	Joint spacing, in. (mm)	Joint apparent dip direction, degrees	Joint apparent dip, degrees	Joint spacing, in. (mm)	Joint Apparent Dip Direction, degrees	Joint apparent dip, degrees	Peak joint friction angle, degrees	Peak joint cohesion, psi (kPa)	Residual joint friction angle, degrees	Residual joint cohesion, psi m(kPa)	Joint normal stiffness, ksi/in. (MPa/m)	Joint shear stiffness, ksi/in. (MPa/m)	E_{mi}/E_{mass}	GSI	M_i, Hoek and Brown (2012)
1	Max	170 (26.7)	9 (62)	20 (138)	—	2600 (17.9)	—	60	30	—	315	85	—	270	90	36	70 (480)	31	60 (410)	—	—	—	—	5
	Min	160 (25.1)	1.6 (11)	5 (34.5)	—	40 (0.3)	—	135	5	—	245	65	—	255	75	17	0 (0)	15	0 (0)	—	—	—	—	9
	Average	165 (25.9)	4.7 (32.5)	12.5 (86)	45	940 (6.5)	10 (250)	97	15	59 (1500)	305	75	59 (1500)	263	82	30	35 (240)	26	16 (110)	232 (63)	91 (24.5)	3.1	60	7
2A	Max	181 (28.4)	11.5 (79)	44 (303.5)	—	3000 (20.7)	—	270	25	—	285	90	—	90	90	38	70 (480)	32	50 (345)	—	—	—	—	30
	Min	173 (27.2)	3.6 (25)	19 (131)	—	1200 (8.3)	—	90	0	—	270	65	—	105	80	22	0 (0)	15	0 (0)	—	—	—	—	20
	Average	178 (28.0)	9.6 (66)	30 (207)	50	2100 (14.5)	14 (360)	165	7	28.75 (730)	277	80	28.75 (730)	97	85	34	35 (240)	29	10 (70)	391 (106)	163 (44)	3.7	70	25
2B	Max	172 (27.0)	7.3 (50)	36 (248)	—	2700 (18.6)	—	120	30	—	285	90	—	90	90	36	70 (480)	31	60 (410)	—	—	—	—	15
	Min	164 (25.8)	1.4 (10)	19 (131)	—	900 (6.2)	—	60	0	—	270	65	—	105	80	17	0 (0)	15	0 (0)	—	—	—	—	5
	Average	167 (26.2)	5.2 (36)	26.5 (183)	45	1700 (11.7)	12 (300)	90	14	30.75 (780)	277	80	30.75 (780)	97	85	30	35 (240)	26	16 (110)	1100 (298.5)	413 (112)	1.8	72	10
2C	Max	185 (29.1)	12.9 (89)	50 (345)	—	3000 (20.7)	—	270	25	—	285	90	—	90	90	38	70 (480)	32	50 (345)	—	—	—	—	30
	Min	177 (27.8)	4.5 (31)	22 (151.5)	—	1500 (10.3)	—	90	0	—	270	65	—	105	80	22	0 (0)	15	0 (0)	—	—	—	—	20
	Average	180 (28.3)	13 (90)	34 (234.5)	50	2200 (15.2)	11 (280)	165	7	13.5 (340)	277	80	13.5 (340)	97	85	34	35 (240)	29	10 (70)	545 (148)	218 (59)	4.8	71	25
3A	Max	170 (26.7)	9 ,(62)	20 (138)	—	2600 (17.9)	—	30	35	—	255	79	—	275	50	36	70 (480)	31	60 (410)	—	—	—	—	9
	Min	160 (25.1)	1.6 (11)	5 (34.5)	—	40 (0.3)	—	120	5	—	290	50	—	295	30	17	0 (0)	15	0 (0)	—	—	—	—	5
	Average	165 (25.9)	4.7 (32.5)	12.5 (86)	45	940 (6.5)	12.5 (320)	75	22	15 (380)	275	62	15 (380)	285	35	30	35 (240)	26	16 (110)	329 (89.5)	138 (37.5)	3.6	58	7
3B	Max	170 (26.7)	9 ,(62)	20 (138)	—	2600 (17.9)	—	30	28	—	255	73	—	275	42	36	70 (480)	31	60 (410)	—	—	—	—	9
	Min	160 (25.1)	1.6 (11)	5 (34.5)	—	40 (0.3)	—	120	5	—	290	45	—	295	28	17	0 (0)	15	0 (0)	—	—	—	—	5
	Average	165 (25.9)	4.7 (32.5)	12.5 (86)	45	940 (6.5)	10.25 (260)	75	20	23 (580)	277	59	23 (580)	285	33	30	35 (240)	26	16 (110)	407 (110.5)	171 (46.5)	2.8	63	7

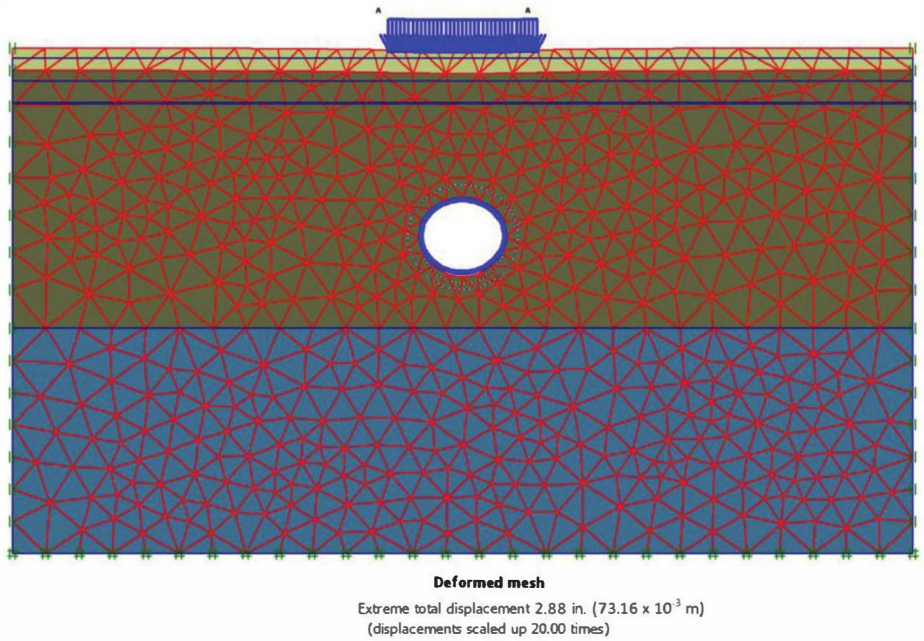

Fig. 6.1.3b—FEM simulation for a tunnel excavation in soft ground.

tions or external loads are present within close proximity of an existing structure (AFTES-WG7). Using FEM techniques, complex underground conditions, and tunnel characteristics can be analyzed with a degree of accuracy, and the large axial forces and bending moments developed in the segments can be reliably determined. Precast segments are designed using an axial force-bending moment diagram.

6.2—Longitudinal joint bursting load

Normal (hoop) forces developed in the section due to the permanent earth and groundwater pressures are transferred through a reduced cross-sectional area across the longitudinal joints where gaskets and stress relief grooves are present. Spalling is not a concern on longitudinal joints because that mode of failure is not applicable when longitudinal joints are fully in contact with adjacent elements, except to account for eccentricity of adjacent segments. Nonetheless, bursting tensile stresses can develop along the longitudinal joints similar to the TBM thrust jacking loads on the circumferential joints. The design is undertaken for the maximum ULS design compressive force. Simplified equations from ACI 318, DAUB:2013, Iyengar (1962), and two-dimensional (2-D) FEM simulations are the most common methods for carrying out the analysis and design of longitudinal joint bursting (Bakhshi and Nasri 2014b).

The simplified equation of ACI 318 for post-tensioned anchorage zones of prestressed concrete sections (Eq. (6.2a)) can be used for analyzing this load case, where P_{pu} is the maximum normal force from the permanent ground, groundwater, and surcharge loads, and e_{anc} is the maximum total eccentricity, consisting of the normal force eccentricity (M/N) and the eccentricity of the load transfer area.

ACI 318:

$$T_{burst} = 0.25P_{pu}\left(1-\frac{h_{anc}}{h}\right); d_{burst} = 0.5\left(h-2e_{anc}\right) \quad (6.2a)$$

Similar to ACI 318, simplified equations by DAUB:2013 (Eq. (5.1.1a)) are used for evaluating bursting stresses in the longitudinal joints. Nonetheless, DAUB:2013 presents more details about this specific load case using an approach that transfers force by means of a stress block, as shown in Fig. 6.2a. Additional reinforcement for spalling and secondary tensile stresses are placed when there are high eccentric normal forces ($e > d/6$) (DAUB:2013). Bursting, spalling, and secondary tensile stresses are calculated using the following equations.

$$F_{sd} = 0.25 \cdot N_{Ed} \cdot (1 - d_1/d_s) \quad (6.2b)$$

$$F_{sd,r} = N_{Ed} \cdot \left(\frac{e}{d}-\frac{1}{6}\right); F_{sd,2} = 0.3F_{sd,r} \quad (6.2c)$$

where the total eccentricity, e, consists of eccentricity from normal force, e_l, and the eccentricity of hinge joint, e_k. Therefore, $e = e_l + e_k = M/N + e_k$, $d_1 = d_k - 2e$, and $d_s = 2e' = d - 2e_l$. These parameters are shown in Fig. 6.2a.

Bursting tensile reinforcement is placed at a distance of $0.4d_s$ from the face of the segments; reinforcement for spalling and secondary tensile stresses, if necessary, are placed at $0.1d_s$ and $2/3d$ from the face of the segment, respectively (DAUB:2013). Simplified equations, which include Eq. (6.2b) and (6.2c), can be used for this load case to determine the compressive stress and the strength of the partially loaded surface.

Iyengar diagram methods (Fig. 5.1.2) and FEM simulations can be also used as an alternative approach to determine the stresses within the longitudinal joints. Bursting stresses at the vicinity of the longitudinal joints are analyzed for the case of maximum normal force. Two-dimensional FEM models can simulate the longitudinal joint using appro-

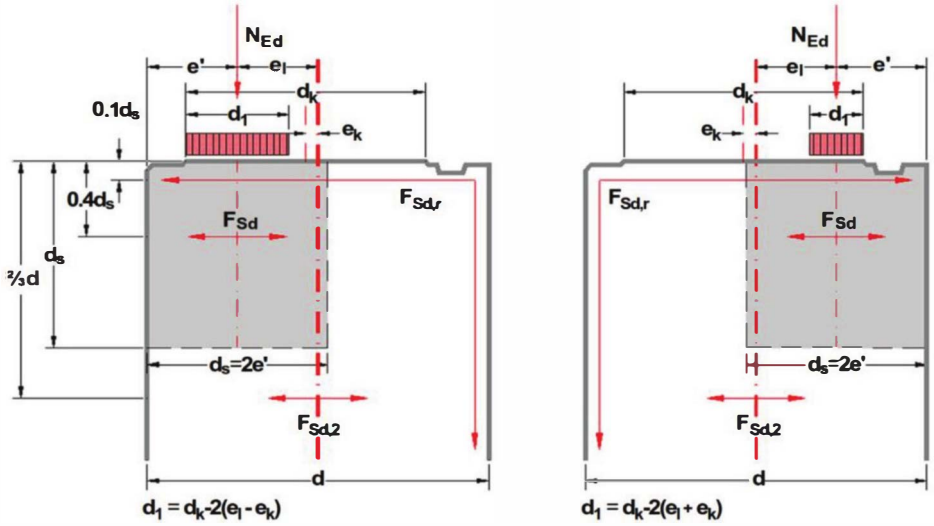

Fig. 6.2a—Force transfer recommended by DAUB:2013 in longitudinal joints using a stress block concept for case of hinge joint eccentricity in the same side as normal force eccentricity (left) and case of eccentricities on different sides of section centroid (right).

priately shaped ends to represent the recess of the gasket and the stress relief grooves (curvature of elements are neglected). Figure 6.2b shows generalized analytical results, including bursting tensile stresses and compressive stresses, in the area around longitudinal joints. Reinforcement is designed to take these bursting and compressive stresses, similar to the case for TBM thrust jacking loads.

In addition to the eccentricity of forces (*M*/*N*) and of the load transfer area (lips/steps), design for an additional eccentricity due to ovalization and misalignment during the ring erection are sometimes asked for in project's technical requirements. Such load case is referred to as ring ovalization due to out-of-round ring build or birdsmouthing. The design procedure includes an assumption that the ring is initially built in the shape of an ellipse, and that the chord length of the displaced segment, as shown in Fig. 6.2b(c), does not change. Note that in this figure, the x-axis and y-axis represent the dimension of the quarter of the segmental ring in the Cartesian coordinate system. Solid arc and dashed arc represent the shape of quarter of ring before and after ovalization, respectively. Specific out-of-round build allowance over diameter is considered (for example, 0.6 in. [15 mm]). Joint rotation and joint opening distance are calculated with total joint rotation causing birdsmouthing (*t* as in Fig. 6.2b(c)) and opening distance due to poor ring build (*d* as in Fig. 6.2b(c)) as the main parameters. Joint closure under minimum/maximum embedment loads on segment intrados and extrados are assessed by determining the load required to close the gap and comparison with the hoop force due to embedment loads. Depending on whether the joint remains open or closed, one of the two diagrams shown in Fig. 6.2b(d) is used for calculation of birdsmouthing eccentricity.

Note that although provided details are for flat joints as the most conventional joint shape, convex joint details are similar in terms of design approach with consideration of a line load instead of a distributed load at the joint locations.

6.3—Loads induced due to additional distortion

Segmental tunnel linings are designed to take an additional diametrical distortion in addition to the deflections caused by the effects of ground, groundwater, and surcharge loads, which were discussed in the previous load case. This additional distortion may occur during segment assembly under the self-weight of the segments due to construction-related events such as joint misalignment, yielding of joint connectors, or excessive grouting pressure. Furthermore, this distortion can result from ground movement caused by the construction of an adjacent tunnel. This additional distortion is the difference between the movement of the tunnel at the left and right springline or the crown and invert of the tunnel. Some local authorities such as LACMTA 2013 and LTA 2010 require the design to accommodate this additional distortion. The former specifies a minimum additional diametrical distortion of 0.5 percent of diameter due to imperfect lining erection and the latter specifies an additional distortion of ±5/8 in. (15 mm) on the diameter to allow for future development in the vicinity of the tunnel. The following formula introduced by Morgan (1961) is commonly used to calculate the additional distortional bending moment.

$$M_{distortional} = \frac{3EI\delta_d}{2r_0^2} \tag{6.3}$$

Using other approaches, the maximum distortion can be calculated based on the theory of elasticity or finite element methods (FEM). Note that during excavation in certain ground conditions such as clay materials, consolidation of underlying clay layers can result in additional distortion to be a function of time. In such cases, additional distortion should be considered and analyzed as a time-dependent phenomenon.

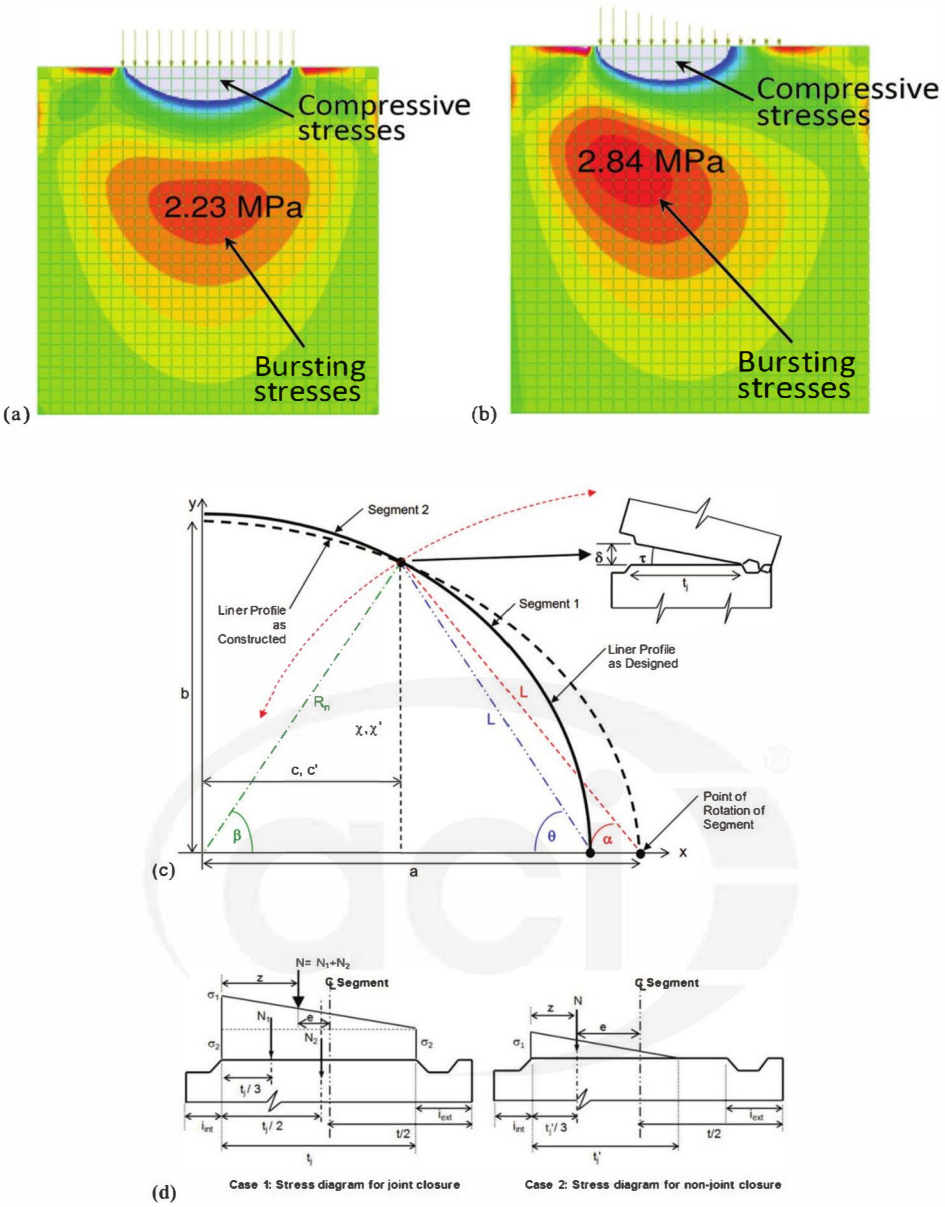

Fig. 6.2b—Developed bursting tensile stresses around longitudinal joints under hoop (normal) forces due to service loading condition and gasket pressure: (a) no eccentricity; (b) eccentric contact stresses (Francis and Mangione 2012); (c) ring ovalization due to out-of-round ring build; and (d) stress diagrams for joint closure (nonclosure). Note that in Fig. 6.2b(c), the x-axis and the y-axis represent dimensions of the quarter of the segmental ring in the Cartesian coordinate system while solid arc and dashed arc represent the shape of quarter of ring before and after ovalization, respectively.

6.4—Other loads

Other loads should also be considered based on ground condition; the tunnel function; and any special circumstances that may result in failure of the liner to include earthquake, fire, explosion, breakouts at cross passageways, portals, and shafts, as well as excessive longitudinal bending moments. For these extreme and special events, a load factor of 1 should be used for all loads including self-weight, ground pressure, groundwater pressure, surcharge, and earthquake loads (AASHTO DCRT-1).

Seismic design of tunnels to resist the maximum design earthquake (MDE) and operating design earthquake (ODE) is often performed using a ground deformation approach that includes ovaling, axial, and curvature deformations. For the ovaling analysis, LACMTA 2013 design criteria recommends that two approaches be used based on closed-form solutions and numerical modeling. LACMTA 2013 contains the criteria for determining the maximum axial forces and bending moments due to seismic ovaling deformation. Pseudo-dynamic time-history and dynamic time-history analyses are other alternatives. Furthermore, free-field deformation analysis provided by AASHTO DCRT-1 is often used for the longitudinal seismic response (axial and curvature deformations) of tunnels located within uniform geologic deposits. This approach is based on the calculation of combined axial and bending strains from the pres-

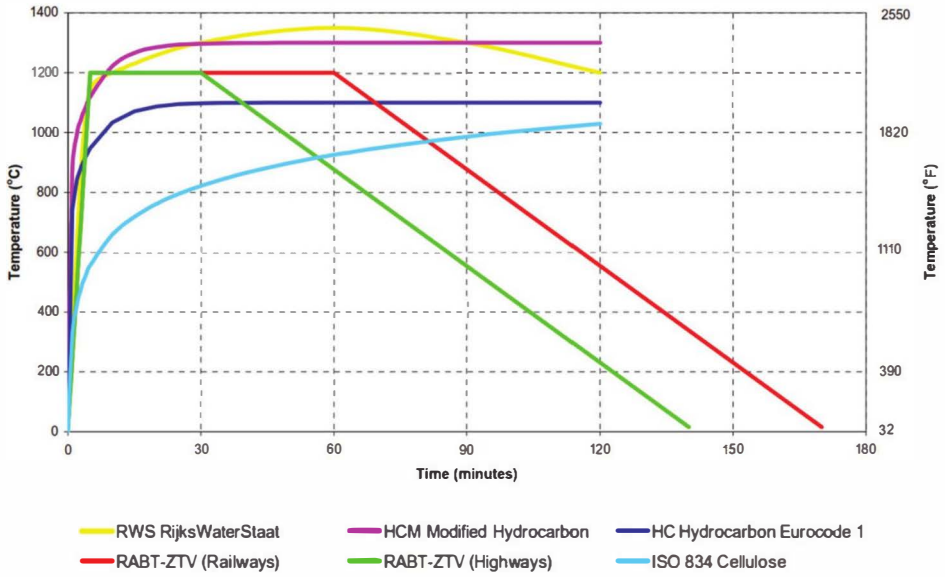

Fig. 6.4.1—Standard fire load curves.

sure waves (P-waves), shear waves (S-waves), and Rayleigh waves (R-waves). When tunnels run through highly variable geological conditions, a numerical modeling approach is preferred.

6.4.1 *Fire incident and explosion*—A load case specific to road and railway tunnels is tunnel fires. One of the decisive factors for the design of tunnel structures in the load case of fire is the heat release rate. Rates from 10 MW up to 200 MW have been proposed at different projects with the majority ranging around 100 MW. Another important factor is the duration of the design fire with values ranging from 30 minutes to 3 hours, sometimes with an added cooling phase. Both heat release rate and duration will depend on intended use of tunnel and project specific conditions such as the type of traffic (train, cars, heavy goods, or dangerous goods transport) and the required safety level (with stricter requirements in case of a possible impact on structures above the tunnel, or the risk of inundation) (Neun 2012). The actual time-temperature curve resulting from such a design fire that depends on the individual cross section and wind speeds inside the tunnel can be used for simulation of a temperature gradient between the intrados and extrados of the tunnel lining. However, because adequate computational fluid dynamics (CFD) modeling is very time-consuming and the results are not easily transferred to a structural model, it is common to use standard deterministic time-temperature curves for the projects (Neun 2012). Most common standard design fire curves for the structural design of tunnel structures as shown in Fig. 6.4.1 include RABT-ZTV (Railways) also known as EBA, RABT-ZTV (Highways) also known as ZTV, ISO 834 Cellulose, HC Hydrocarbon BS EN 1991-1-1, HCM Modified Hydrocarbon (HCinc) and Rijkswaterstaat also known as RWS (ITA WG6). The ISO 834 curve is recommended up to an expected fire heat release rate of 50 MW, above which the hydrocarbon curve (up to 100 MW) and thereafter the RWS curve (up to the stoichiometric limit) should be applied. When cooling phase is considered, RABT curves can be used. Once one of the standard design fire curves is selected (temperature versus time), it is applied on the tunnel intrados. The increase in lining temperature versus lining thickness is calculated and the resulting reduction in concrete and reinforcement properties (modulus and strength) is determined based on available data. This will determine the lining thickness loss during the fire. When applying nonlinear temperature gradients in basic structural analysis programs is not possible, an equivalent temperature load can be established that has the same impact on the equivalent section as the original temperature gradient has on the original section (Neun 2012). This can be followed by adopting a layered section analysis where the normal force (N) and bending moment (M) can be determined by integration/summation of the stresses in the individual layers.

Explosions, on the other hand, are simulated by increasing the internal radial pressure on the tunnel lining at the service condition by a representative value such as one atmosphere or 14.5 psi (1 bar) (Caan et al. 1998). This internal radial pressure in the direction opposite to ground and groundwater pressure results in reduced axial forces in the lining without significant change in the bending moments. Recently, an advanced and detailed design procedure for tunnels subjected to internal explosion and possibly preceded by fire accidents was developed (Colombo et al. 2015). Simplified finite element (FE) model and dynamic analyses were carried out to study the tunnel's response under internal blast loads in the form of pressure-impulse (p-i) diagrams and an ultimate limit state criterion based on eccentric flexural capacity (M-N interaction diagram) was generated. Also, a limit state criterion considering the fire-blast interaction was introduced through the modification of the M-N diagram. This procedure is suggested for an advanced blast-fire analysis.

6.4.2 *Breakout analysis and shear recovery systems*—Creating opening for cross passages and adit connections at TBM tunnel would result in permanent disruption to the structural response of segmental lining and change in effec-

Fig. 6.4.2a—Most common temporary steel bracing structures (support frames) in segmentally lined tunnels to mitigate ring ovalization resulting from opening and cross passage excavation. (Lee and Choi 2017).

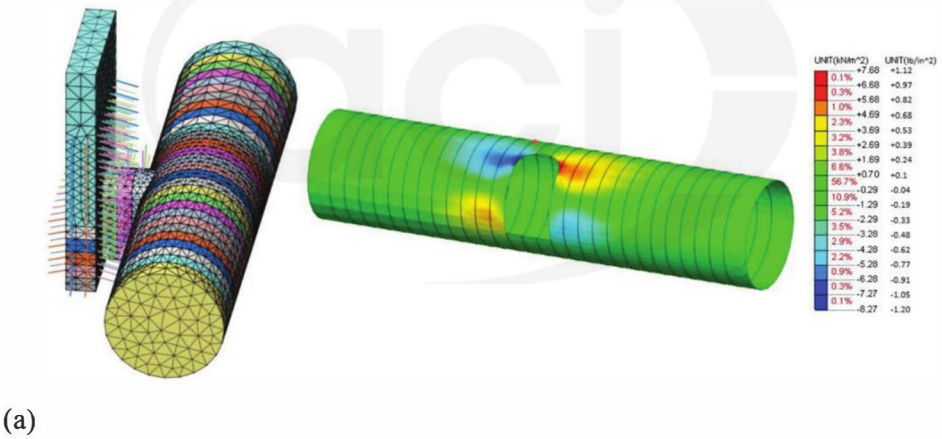

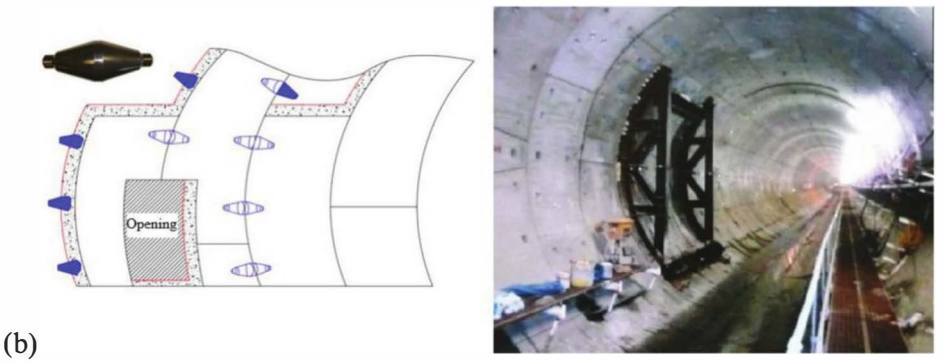

Fig. 6.4.2b—(a) Three-dimensional model for openings inside the segmentally lined tunnel and developed shear stresses as a result of the finite element analysis; and (b) shape and installation pattern of bicone shear dowels and temporary half-moon support frame around the opening.

tive stress of the ground in close proximity to segments where the cross passage is to be built. During excavation of the cross passage, there will be a temporary stage of reduced ground support to the tunnel lining. Temporary steel bracing is often installed inside the tunnel to provide support mitigating ring ovalization resulting from opening and cross passage excavation. The internal support will maintain the structural integrity of segments ensuring a safe design. As shown in Fig. 6.4.2a, steel lintel and sill beams, full-moon support frames, and half-moon support frames are among the most common temporary opening support systems (Lee and Choi 2017). Latest development includes use of shear recovery bicone systems in conjunction with temporary half-moon support frames that ease the problems with the creation of openings inside the segmentally lined tunnel by minimizing the amount of temporary work and minimizing interference with the TBM operations. Bicones, as shown in Fig. 6.4.2b, prevent any offset between the rings during ring assembly in the construction stage and absorb energy when the tunnel lining is partially suppressed for opening or when instantaneous and temporary stresses occur in exceptional instances. Bicones are designed to be used in the proximity of tunnel penetration areas such as cross passages, entrances, ventilation adits, and elevator adits. Although other methods such as anchors, steel connectors, and shear keys have been used in some specific cases for this purpose, bicones are the most technically advanced solution that are now being commonly used. Analysis is performed for the case of removal of several segmental rings with a maximum height equal to the opening size. A three-dimensional (3-D), nonlinear modeling approach using an FEM package is adopted to evaluate the impacts of excavation. Figure 6.4.2b shows typical geometry, developed meshes, and shear stresses around a penetration zone. Total shear force of a ring around the penetration area is calculated and compared to the shear strength of the bicones to determine the minimum number of bicones required for this action.

CHAPTER 7—DETAILED DESIGN CONSIDERATIONS

7.1—Concrete strength and reinforcement

Several recommendations are available on the compressive strength of precast concrete tunnel segments. AASHTO DCRT-1 recommends a compressive strength ranging from 5000 to 7000 psi (34 to 48 MPa) for one-pass lining systems. Japan's Railway Technical Research Institute (RTRI 2008) specifies segments' compressive strengths between 6000 and 7800 psi (42 and 54 MPa), whereas JSCE 2007 specifies a range of 6000 to 8700 psi (42 to 60 MPa). ÖVBB 2011 recommends 1700 and 5800 psi (12 and 40 MPa) as the minimum compressive strength for stripping (demolding) from the forms and at 28 days, respectively. DAUB:2013, referring to local German guideline ZTV-ING:2007, specifies a minimum stripping (demolding) strength of 2200 psi (15 MPa), and a 28-day strength between 5000 and 7200 psi (35 and 50 MPa). LTA 2010 specifies the minimum compressive strength for precast segments as 8700 psi (60 MPa), which is the highest requirement of all guidelines and standards. USACE EM 1110-2-2901 requires a concrete strength of 6000 psi (42 MPa) or higher for one-pass segmental linings. A summary of recommendations for compressive strength of precast concrete tunnel segments are presented in Table 7.1.

Precast concrete segments are reinforced with steel bar Grades 60, 75, or 80 (conforming to ASTM A615/A615M and ASTM A706/A706M), welded steel wire reinforcement Grades 70, 75, or 80 (conforming to ASTM A1064/A1064M), or steel fibers (conforming to ASTM A820/A820M). When reinforced with steel bars or welded wire mesh, reinforcement is often categorized to three different types: transverse reinforcement, which is the main reinforcement placed perpendicular to tunnel axis to resist forces and bending moments developed under final service load cases; longitudinal reinforcement in the direction of tunnel axis and perpendicular to transverse reinforcement, often designed as minimum temperature and shrinkage reinforcement; and joint reinforcement near segment and ring joints for resisting bursting and spalling stresses. A typical plan view of transverse and longitudinal bars in precast concrete tunnel segments is shown in Fig. 7.1a. No specifications or requirements can be found in tunnel guidelines for minimum bar size. However, a review of segmental tunnel projects reveals that transverse bar size ranges between No. 3 and No. 5 (ϕ10 and ϕ16). The general trend for recent projects built with even larger tunnel diameters has been the reduction of bar size to No. 3 (ϕ10) and using more bars in transverse direction by reducing bar spacing to below 3 in. (80 mm). In the longitudinal direction, reinforcing bar size ranges between No. 3 and No. 5 (ϕ6 and ϕ16) with more closely spaced bars in recent projects.

Typical sectional views of joint reinforcement in precast concrete tunnel segments are shown in Fig. 7.1b. Circumferential joint reinforcement includes transverse and radial

Table 7.1—Recommendations for compressive strength of precast tunnel segments

Authority	Compressive strength (stripping)	Compressive strength (28-day)
AASHTO DCRT-1	Not provided	5000 to 7000 psi (34 to 48 MPa)
RTRI 2008	Not provided	6000 to 8700 psi (42 to 60 MPa)
ÖVBB 2011	1700 psi (12 MPa) (minimum)	5800 psi (40 MPa) (minimum)
DAUB:2013 (referring to ZTV-ING:2007)	2200 psi (15 MPa)	5000 to 7300 psi (35 to 50 MPa)
LTA 2010	Not provided	8700 psi (60 MPa)
USACE EM 1110-2-2901	Not provided	6000 psi (42 MPa) (minimum)

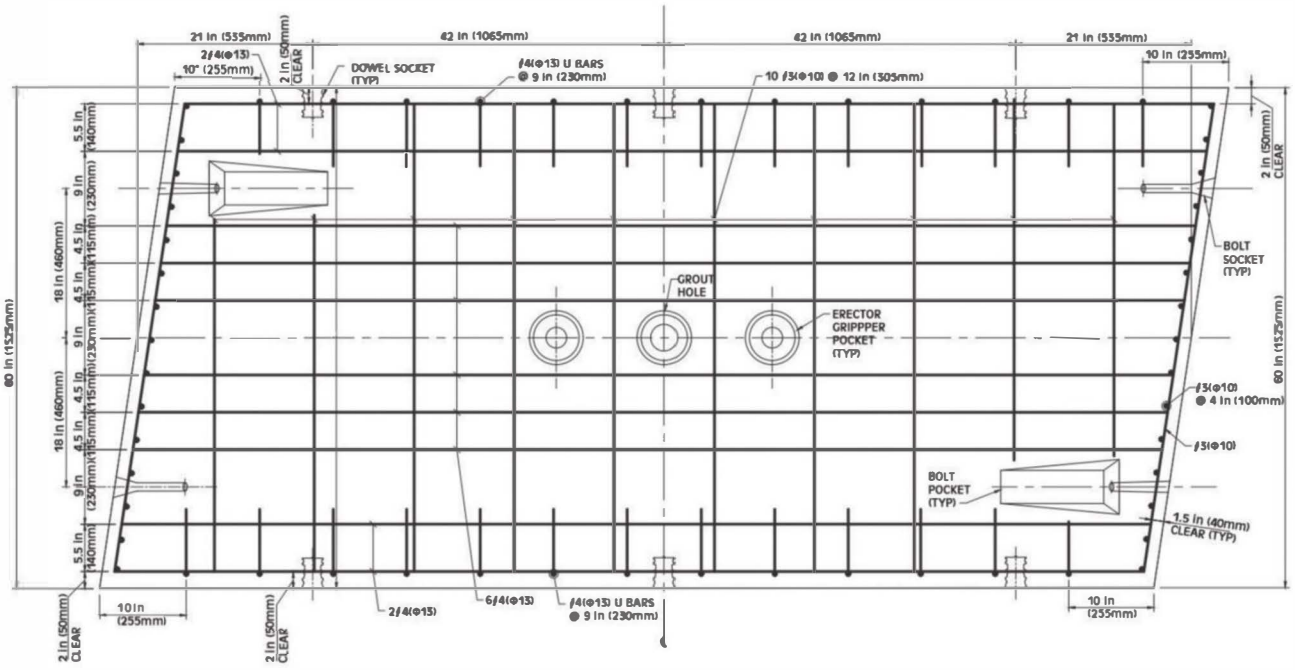

Fig. 7.1a—Typical plan view of transverse and longitudinal bars in precast concrete tunnel segments.

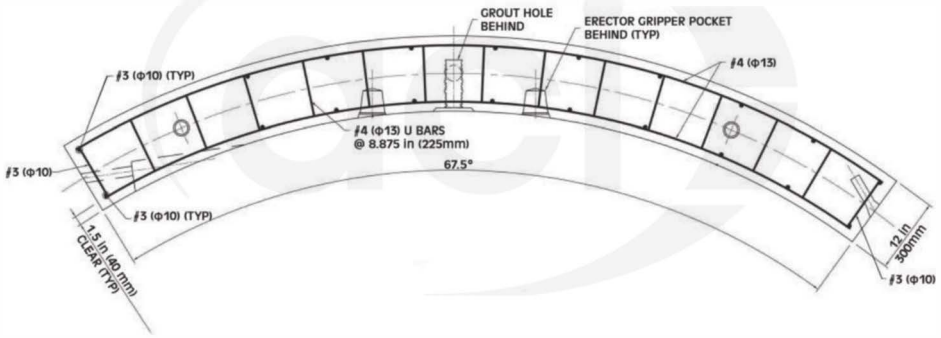

(a) circumferential joint

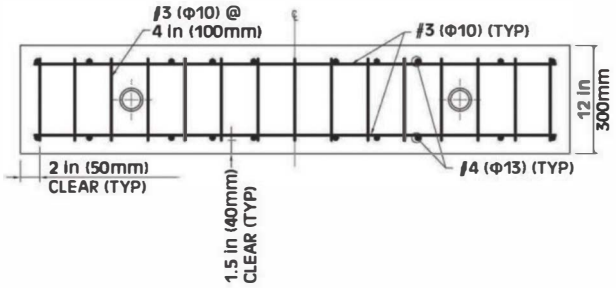

(b) longitudinal joint

Fig. 7.1b—Typical sectional views of joint reinforcement in precast tunnel segments: (a) circumferential joint; and (b) longitudinal joint.

Table 7.2—Minimum recommended concrete cover for reinforcing bars in reinforced concrete tunnel segments by national or international codes, guidelines, and recommendations

	ACI 318	AFTES:2005	DAUB:2013	JSCE 2007	NEN 6720:1995	ÖVBB 2011/BS EN 1992-1-1:2004
Minimum cover, in. (mm)	1-1/2 (38)	Intrados and extrados: 1.2 (30)	Intrados and extrados: 1.6 (40)	Noncorrosive environment: 1 (25)	1.4 (35)	1 to 1.8 (25 to 45) depending on exposure conditions
		Other zones: 0.8 (20)	Joint faces and near bolt pockets: 0.8 (20)	Corrosive environment: 1.4 (35)		

reinforcement. Transverse reinforcement in the circumferential joint is usually the same size as the main transverse reinforcing bars unless analysis shows that reinforcement is not sufficiently provided to resist stresses due to tunnel boring machine (TBM) thrust jack forces. Radial bars in circumferential joints in forms of ties or U-bars are either No. 3 or No. 4 (ϕ10 or ϕ13) bars designed either equally spaced or nonuniformly with more closely spaced bars around the tunnel boring machine (TBM) jack shoe locations. Longitudinal joint reinforcement in the radial direction are sometimes designed as ladder bars in addition to other forms (that is, ties and U-bars) due to the simplicity of welding ladder bars in a flat surface comparing to a curved face in the circumferential direction. Radial bars have been designed in longitudinal joints as No. 3 or No. 4 (ϕ10 or ϕ13). Longitudinal reinforcing bars in longitudinal joints are often of the same size as the general longitudinal reinforcement inside the segment.

7.1.1 *Early-age strength for stripping*—Depending on the production method, high early-age strengths may be required for the concrete (usually 6 to 8 hours) to resist early production and transient load cases. The design engineer should specify the required compressive strength at the time of segment stripping (demolding), which is usually between 2000 and 2500 psi (14 and 17 MPa). For fiber-reinforced concrete (FRC) precast segments, first-crack and residual flexural strength, as the basis of design, are specified in accordance with recommendations of ACI 544.7R-16, Chapter 4.

7.2—Concrete cover

DAUB:2013 recommends a minimum concrete cover of 1.6 in. (40 mm) on the surfaces of the tunnel segments. On the end faces of segments and in areas close to bolt pockets, the minimum concrete cover recommended by DAUB:2013 is 0.8 in. (20 mm). However, ACI 318 specifies a minimum concrete cover of 1-1/2 in. (38 mm) for precast concrete elements exposed to earth. ITA Working Group on General Approaches to the Design of Tunnels (1988) specifies a minimum 2 in. (50 mm) cover only for the cast-in-place concrete lining at its outer surface in contact with ground and groundwater. This specification does not apply to segmental lining, especially when a one-pass lining system is adopted. Among other codes, guidelines, and recommendations, AASHTO DCRT-1 does not specify a minimum concrete cover; JSCE 2007 specifies a minimum 1 in. (25 mm) concrete cover over reinforcement and a minimum 1.4 in. (35 mm) concrete cover in a corrosive environment for a one-pass segmental lining system; ÖVBB 2011 refers to BS EN 1992-1-1:2004, which specifies a minimum concrete cover of 1 to 1.8 in. (25 to 45 mm) depending on exposure conditions; AFTES:2005 specifies 1.2 in. (30 mm) as the minimum cover on the intrados and extrados faces and 0.8 in. (20 mm) concrete cover on other zones; and NEN 6720:1995 specifies 1.4 in. (35 mm) as the minimum concrete cover for precast elements. A summary of recommendations for minimum concrete cover over reinforcement are presented in Table 7.2.

7.3—Curing

Steam curing should be used as the primary curing method for the first 6 hours after concrete is placed into the forms. Immediately after segments have been cast, forms are placed in a sealed, vapor-tight enclosure to prevent escape of moisture and heat, but large enough to allow complete circulation of steam. Segments should not be removed from the forms until specified stripping (demolding) compressive strength is attained, determined by compressive cylinder test results. To avoid damages to early-age concrete micro-structure, as a common practice, enclosure ambient temperatures are kept below 100°F (38°C) for the first 2 hours of curing. After 2 hours of curing, enclosure temperature is maintained between 90 and 120°F (32 and 49°C) until specified curing strength is achieved. It is crucial to keep maximum temperature of the curing enclosure below 120°F (49°C) because this temperature is approximately equivalent to 150°F (65°C) internal concrete temperature, above which delayed ettringite formation (DEF) as a major durability factor can be generated in the presence of reactive aggregates. In addition, care should be taken to maintain rate of temperature change under 30°F (17°C) per hour. When specified strength is attained, segments are only allowed to cool slowly so as not to exceed the aforementioned rate of temperature change. Following primary steam curing, steam curing or moist curing methods can be adopted until 70 percent of the design strength is reached. Note that when using the moist curing method, segments should be placed in a special area where water is continuously sprayed or atomized.

7.4—Reinforcement spacing

There is no specific recommendation available in ACI 318 for reinforcement spacing in the precast tunnel segments. However, general spacing limits for reinforcement include minimum and maximum clear bar spacing of 1 and 18 in. (25 and 457 mm), respectively. DAUB:2013 provides a typical reinforcement spacing range of 4 to 6 in. (100 to 150 mm) for segmental tunnel linings and specifies a minimum clear spacing of 3.5 in. (90 mm). In the absence of any reinforcement spacing requirement by ITA Working Group on General Approaches to the Design of Tunnels (1988), AASHTO DCRT-1, and ÖVBB 2011, JSCE 2007 speci-

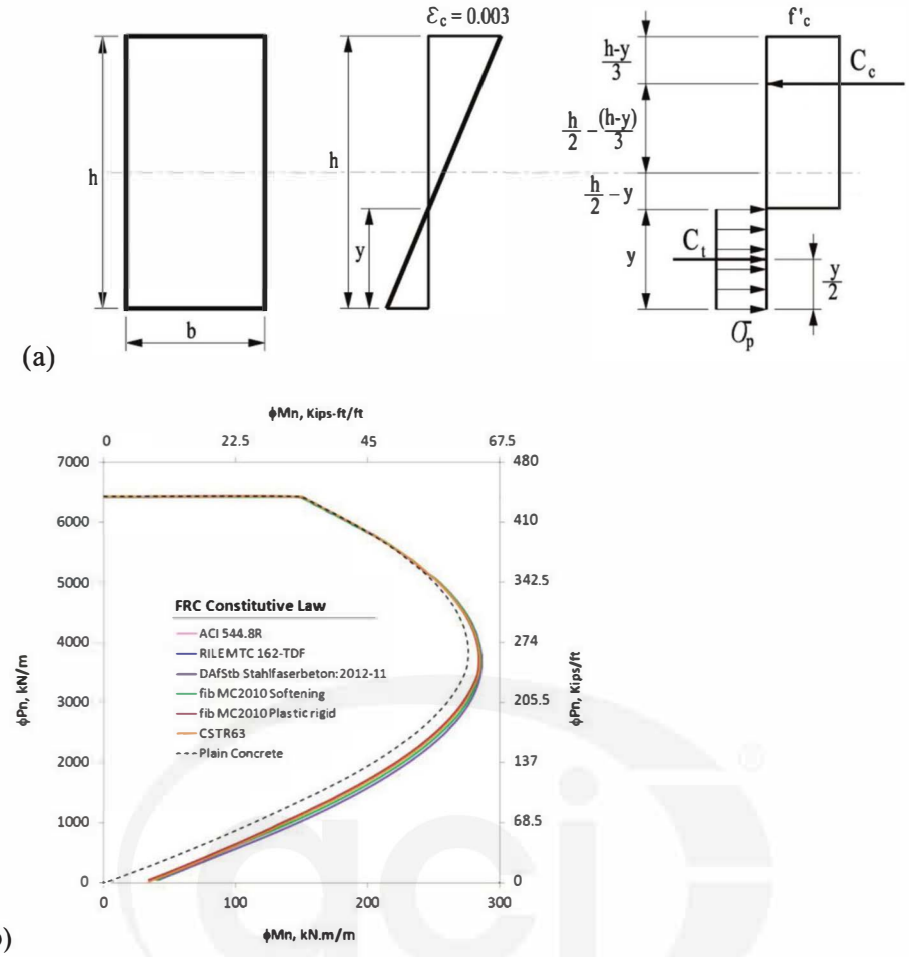

Fig. 7.5—(a) Strain and stress distributions through the section as part of it undergoes tension; and (b) effect of choice of constitutive law on the axial force-bending moment interaction diagrams as a key design tool (Bakhshi and Nasri 2014c).

fies a minimum bar spacing of 1.25 times the width of the maximum size of aggregates plus the diameter of the reinforcement. AFTES:2005, referring to Section 4.5 of BAEL 91 Révisé 99:2007, specifies the maximum spacing for reinforcing bars as the smaller of 8 in. (200 mm) and 1.5 times the segment thickness. NEN 6720:1995, on the other hand, specifies minimum bar spacing as the greater of 4/3 of the maximum size of aggregates, the largest bar diameter, or 1 in. (25 mm).

7.5—Fiber reinforcement

Fiber reinforcement has emerged as an alternative to traditional reinforcing bars and welded wire mesh reinforcement for precast concrete tunnel segments. Due to significantly improved post-cracking behavior and crack control characteristics, FRC segments offer advantages over traditionally reinforced concrete segments such as saving cost and reducing production time while developing a more robust product with improved handling and long-term durability (ACI 544.7R; *fib* Working Party 1.4.1 2017; ITA Working Group 2 2016).

Fiber-reinforced concrete technology has developed in recent years with the introduction of high-strength concrete, allowing the use of fibers as the sole reinforcement system for more challenging conditions on larger-diameter tunnel projects. In other cases, fiber and reinforcing bars have been used in conjunction to reinforce the tunnel segments (Yao et al. 2018a,b). Ladder bars at the longitudinal joint as well as bursting links at the circumferential joint may be significantly reduced by adding steel fibers. Tunnels with different sizes with internal diameters ranging between 7.2 and 39 ft (2.2 and 11.9 m) have been built using fiber reinforcement. Minimum and maximum thickness of the FRC precast segments in existing tunnels are 5.9 and 18 in. (0.15 and 0.46 m), respectively. These projects include water supply, waste water, gas pipeline, power cable, subway, railway, and road tunnels. Note that the FRC post-cracking nominal residual strengths are the most important parameters for design of FRC segments (ACI 544.7R; *fib* Working Party 1.4.1 2017; ITA Working Group 2 2016). ACI 544.7R and *fib* Working Party 1.4.1 2017 provide design procedures for FRC tunnel segments to withstand all the appropriate temporary and permanent load cases occurring during the production, construction, and design life of segmental tunnels, using specified post-crack residual tensile strength, s_p. Applying raw parameters from ASTM C1609/C1609M or BS EN 14651:2005+A1:2007 beam tests, such as f^D_{150} or $f_{R,3}$, requires caution to prevent overestimating the residual

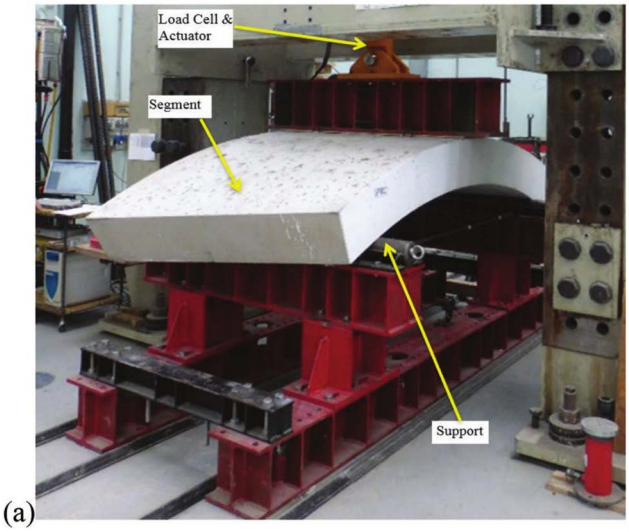

Fig. 8a—Bending test: (a) test setup; and (b) measurement instrumentation in two different views (Moccichino et al. 2010).

tensile strength when using elastic analysis (Bakhshi et al. 2014). A back-calculation procedure can be adopted to obtain specified residual tensile strength parameter s_p (Soranakom and Mobasher 2007). Alternatively, the post-crack flexural strength parameters determined in accordance with ASTM C1609/C1609M and BS EN 14651:2005+A1:2007 can be scaled by an adjustment factor ranging from 0.33 to 0.37 (Bakhshi et al. 2014; Mobasher et al. 2014; Vandewalle 2000; Barros et al. 2005; MC2010). As shown in Fig. 7.5(a),

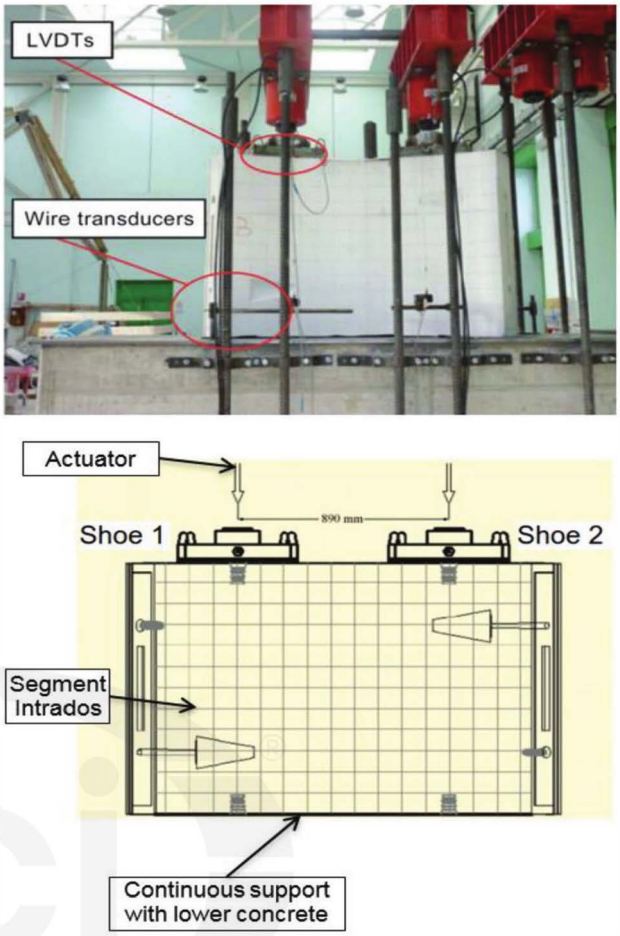

Fig. 8b—Point load test setup simulating TBM thrust jack force.

this strength parameter along with the specified compressive strength (f_c' or f_{cd}) are used to obtain strain and stress profiles through the section to construct the axial force-bending moment diagram that is the key design tool for segments. Although several different FRC constitutive laws (MC2010; DBV:2001; RILEM TC 162-TDF; CNR DT 204/2006; EHE-08) have been used for design of these elements, results of studies by Bakhshi and Nasri (2014c) shown in Fig. 7.5(b) reveal that the choice of constitutive laws does not have a significant effect on axial force-bending moment interaction diagrams and, therefore, the design outcome. Detailed design information on FRC segments can be found in ITA Working Group 2 (2016), *fib* Working Party 1.4.1 2017, and ACI 544.7R.

For FRC elements, following ACI 544.7R and *fib* Working Party 1.4.1 2017, appropriate strength reduction factors or material safety factors should be considered for flexure, compression, shear, and bearing actions of concrete segments. Such factors account for the uncertainty of post-crack tensile strength when calculating the design strength of FRC elements.

CHAPTER 8—TESTS AND PERFORMANCE EVALUATION

Performance testing or proof testing is approved by most structural codes. This is especially true for repetitive units, where large numbers are required to meet a particular purpose such as with the manufacturing of segments. Full-scale tests are often conducted to evaluate the design and performance of fiber-reinforced concrete (FRC) segments with slenderness ratio of 10 to 13. Nonstructural tests on precast concrete tunnel segments include ASTM E119, which helps to ensure the 4-hour fire resistance using standard time-temperature curves (Alder et al. 2010).

Bending and point load tests at full scale are conducted up to load levels much higher than the tunnel boring machine (TBM) nominal service load, and strength results are compared with the actions presented in Chapters 7 through 9. Bending tests, as shown in Fig. 8a, are performed to verify the design and performance of segments during the production stages of stripping (demolding), storage, transportation, and handling, as well as for unsymmetrical earth pressure at the service stage. Full-scale point load tests, as shown in Fig. 8b, simulate the TBM thrust jack forces on the segment cross section during the excavation process (Caratelli et al. 2012), as well as the force transfer through a reduced cross section in longitudinal joints. The cantilever load test, as shown in Fig. 8c, is another full-scale test that is used to investigate the circumferential joint strength under misaligned jacking loads (Poh et al. 2009). Concrete tunnel lining strength has also been evaluated by full-scale tests, such as those shown in Fig. 8d, to simulate dominant effects of axial forces, bending moments, and combined action of axial loads and bending moment (Mashimo et al. 2002). In this study, half of the circular tunnel lining was simulated for a tunnel with an outer diameter of 31.8 ft (9700 mm), a thickness of 12 in. (300 mm), and a height of 3.2 ft (1000 mm). Loads were applied on 17 locations every 10 degrees from the bottom with two jacks per each location, each 1 ft (300 mm) and 2.3 ft (700 mm) from the bottom of specimen. As shown in Fig. 8d, three types of loading were adopted. Type (a) represents a case that a load of loose rock/soil acts on the lining in the tunnel crown while rest of the lining is supported by the surrounding ground. To simulate this load case, loading was applied in all 17 locations to the lining with 34 jacks up to 4.5 kip/jack (20 kN/jack). Except for jacks applying loads on three locations in the crown that continued loading increase up to the failure, the remaining jacks maintained 4.5 kip/jack (20 kN/jack) axial force, simulating forces of springs as ground-structure interaction. As result of Load Type (a), axial force was the dominant internal force compared to the bending moment. On the other hand, Type (b) is for a case that beyond/behind a cavern, the load of loose rock/soil acts on the tunnel lining in the crown but ground does not provide support on a large part of the tunnel shoulder, and only a limited part of the lining is supported by the surrounding ground. Type (b) simulation was done by applying loads in nine locations, with four locations from the left as well as right bottom, and from one location at the crown. Loading was increased in the crown location after the axial force in

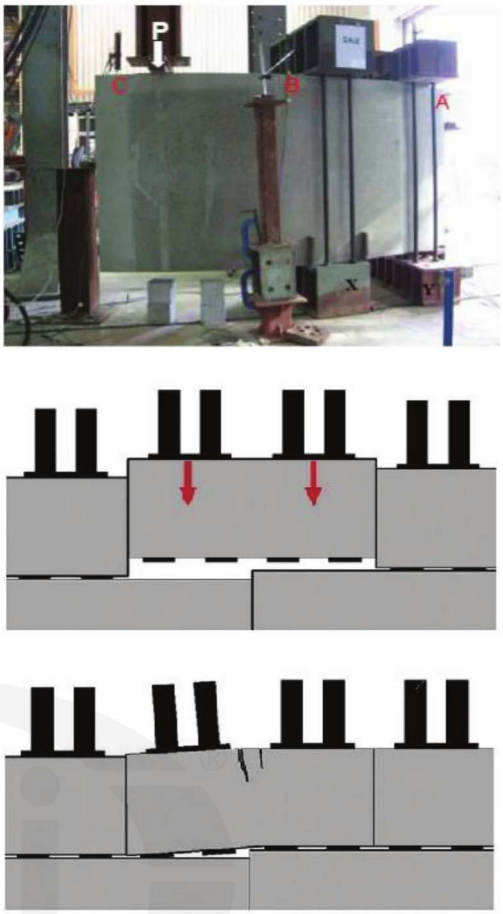

Fig. 8c—Cantilever load test setup and instrumentation (Poh et al. 2009).

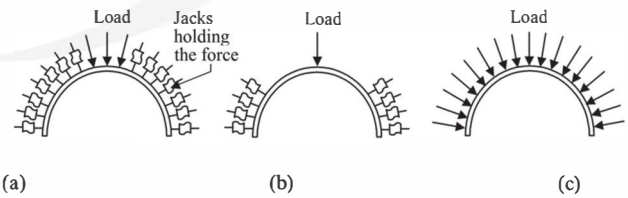

Fig. 8d—Full-scale loading cases on half of the circular lining simulating: (a) load of loose rock/soil acts on the lining in the tunnel crown while rest of the lining is supported by the surrounding ground; (b) beyond/behind a cavern, load of loose rock/soil acts on the lining in the crown but ground does not provide support on large part of tunnel shoulder and only limited part of lining is supported by the surrounding ground; and (c) ground is unfavorable and only acting against the lining in all direction without providing any support (Mashimo et al. 2002).

all other 16 jacks (two per location) reached and maintained 2.25 kip/jack (10 kN/jack) simulating loads of ground-structure interaction springs. As a result, bending moment in the tunnel shoulder was the dominant internal force in Type (b) loading compared to the axial force dominant effect in Load Type (a). Finally, Type (c) loading represents a case that ground is unfavorable and only acts as loading against the lining in all directions without providing any type of

support. For this simulation, loads in all 17 locations and 34 jacks (two per location) increase to failure. This load case combined the action of axial loads and bending moments. Experimental results include load-displacement curves at the crown measured by the load cell and linear variable differential transformer (LVDT) connected to the jack located at the crown.

CHAPTER 9—DESIGN FOR SERVICEABILITY LIMIT STATE

Conforming to the requirements of the load and resistance factor design (LRFD) method, the design engineer needs to design precast concrete tunnel segments for the serviceability limit states (SLS) (JSCE 2007). SLS are states beyond which specified service requirements for a tunnel are no longer met. The SLS in segmental tunnel lining systems correspond to excessive stresses, deflections, and cracking of concrete segments as well as excessive stresses and deformations of segment joints. These SLS may cause reduction of tunnel inner space due to excessive deflections, and durability and watertightness issues due to reinforcing bar corrosion and water leakage from segment cracks or enlarged gaps between segment joints (JSCE 2007; Mendez Lorenzo 1998; Çimentepe 2010). Figure 9 and Table 9 show a flowchart and design checks for verifying the SLS of tunnel segments. These states and particularly SLS of cracking are further discussed in this chapter.

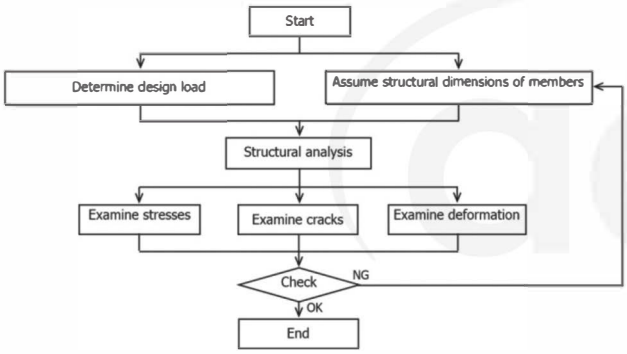

Fig. 9—Design flowchart for SLS (JSCE 2007).

Table 9—Design checks and limiting values for SLS of tunnel segments

SLS states	Location	Items to check	Limiting values
Stress	Segment section	Stress in concrete	Allowable compressive stress of concrete
		Stress in reinforcement	Allowable tensile stress of steel bars
	Segment joints	Stress in concrete	Allowable compressive stress of concrete
		Stress in connectors	Allowable stress of connecting bolts
Deformation	Segmental ring	Ring deformation	Allowable deformation
	Segment joints	Joint opening	Allowable gap between segments' joints
		Joint offset	Allowable offset between segments' joints
Cracking	Segment section	Flexural crack width	Allowable concrete crack width
		Shear force	Shear crack capacity

9.1—Verification for SLS in tunnel segments

The SLS design for the tunnel segments is performed considering different types and combination of loads acting on tunnel linings from the time of production through the final service stage. Different SLS conditions are explained and corresponding calculation methods and limiting values are presented according to international standards and guidelines.

As previously discussed, critical load cases for segment design include load cases of segment demolding, storage, transportation, and handling, while construction loads include tunnel boring machine (TBM) thrust jack forces, tail skin, and localized back grouting pressure. Final service loads include earth pressure; groundwater and surcharge loads; longitudinal joint bursting load; and special loads such as earthquake, fire, explosion, and loads induced due to additional distortion (ACI 544.7R). Design engineers can refer to Table 3.2 and use all possible SLS load combinations considering proper load factors which are often 1.0 for SLS loads.

9.2—Stress verification

Critical stresses in the segments at SLS are calculated for a combination of maximum bending moments and corresponding axial forces. Compressive stresses are limited in the structural codes to avoid microcracking that may lead to a reduction of durability. Maximum compressive stresses in both reinforced concrete (RC) and fiber-reinforced concrete (FRC) at SLS are limited to a restricted value of $0.4f_c'$ according to JSCE 2007, and $0.6f_c'$ according to BS EN 1992-1-1, AFTES-WG7, and MC2010. On the other hand, tensile stresses in the reinforcing bar are limited to f_y according to JSCE 2007 and to $0.8f_y$ according to BS EN 1992-1-1 and MC2010. AFTES-WG7 limits reinforcement tensile stresses to 34.8 ksi (240 MPa) for detrimental cracking and 29 ksi (200 MPa) for highly detrimental cracking.

Flexural stresses in the joints are calculated using maximum bending moments and corresponding axial forces at joints as results of analysis such as beam-spring modeling or finite element method (FEM) simulations. Developed stresses in the concrete at segment joints are limited to allowable compressive stress of concrete. Developed stresses and forces in the bolts are limited to allowable stress of connecting bolts reported by the manufacturer.

9.3—Deformation verification

Segment deformations are obtained directly as results of different models presented in Section 6.1 for load case of earth pressure; groundwater; and surcharge loads including elastic equation, beam-spring, and FEM and distinct element method. However, joint gap and joint offset are only obtained from models that simulate joints between segments and

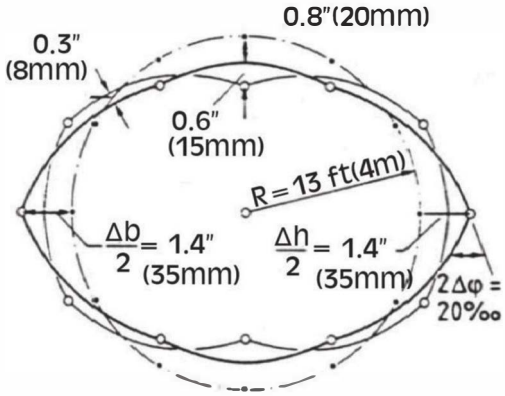

Fig. 9.3—Ring deformation criteria defined with respect to locations on a completely circular ring before taking any loads (ÖVBB 2011).

rings. For SLS verification, these deformations are limited to allowable values recommended by standards, guidelines, and often project specifications. ÖVBB 2011 recommends allowable deformations, shown in Fig. 9.3, for both segments and joints of tunnels with a diameter of up to 26 ft (8 m).

9.4—Cracking verification

Cracking in segments is a major cause for reduction in serviceability due to reduction of watertightness and reinforcement corrosion. In particular, cracking has a significant effect on the durability of the tunnel in an environment with frequent freezing-and-thawing cycles. Examination using appropriate methods should be carried out to ensure that cracking in segments does not impair the serviceability, durability, or intended purposes of the tunnel lining (Bakhshi and Nasri 2015a,b). Among possible cracks induced in segments under service loads are mainly the cracks due to bending moment and axial force. Cracking should be examined by ensuring that the flexural crack width is not greater than the allowable crack width. The flexural crack width calculation for RC and FRC segments is presented in the following.

9.4.1 *Flexural crack width in segments*—Crack width in tunnel segments due to bending moment and axial force is calculated using ACI 224.1R, JSCE 2007, and BS EN 1992-1-1:2004 formulas as shown in Eq. (9.4.1a) through (9.4.1c), respectively.

$$w = 0.076\beta f_s \sqrt[3]{d_c A} \times 10^{-3}$$

$$\text{and } w = 2\frac{f_s}{E_s}\beta\sqrt{d_c^{\,2} + \left(\frac{s}{2}\right)^2} \quad \text{(in.-lb)}$$

$$w = 0.011\beta f_s \sqrt[3]{d_c A} \times 10^{-3}$$

$$\text{and } w = 2\frac{f_s}{E_s}\beta\sqrt{d_c^{\,2} + \left(\frac{s}{2}\right)^2} \quad \text{(SI)} \qquad (9.4.1a)$$

$$w = s\left(\frac{f_s}{E_s} + \varepsilon'_{csd}\right);$$

$$s > 13.97\left(\frac{15}{0.006895 f'_c + 20} + 0.7\right)\cdot\frac{5(n+2)}{7n+8}\cdot \frac{(101.6 d_c + 17.78(s-\varphi))}{} \quad \text{(in.-lb)}$$

$$w = s\left(\frac{f_s}{E_s} + \varepsilon'_{csd}\right);$$

$$s > 0.55\left(\frac{15}{f'_c + 20} + 0.7\right)\cdot\frac{5(n+2)}{7n+8}\cdot \frac{(4\cdot d_c + 0.7\cdot(s-\varphi))}{} \quad \text{(SI)} \qquad (9.4.1b)$$

$$w = s_{r,max}\left(\frac{f_s - k_t\dfrac{f_{ct,eff}}{\left(\dfrac{A_s}{A}\right)}\left(1 + \dfrac{E_s}{E}\cdot\dfrac{A_s}{A}\right)}{E_s}\right) \geq s_{r,max}\left(0.6\frac{f_s}{E_s}\right) \qquad (9.4.1c)$$

MC2010, CNR DT 204/2006, RILEM TC 162-TDF, and DAfStB Stahlfaserbeton:2012-11 can be used to calculate the crack width in concrete sections reinforced by fibers with and without conventional reinforcement. The flexural crack width of FRC segments has been well presented in *fib* Working Party 1.4.1 (2017) by considering analytical sectional approaches as well as FEM.

9.4.2 *Maximum allowable crack width*—Cracking in tunnel segments is controlled by limiting the crack width to specific levels to prevent durability issues due to increased permeability, excessive water leaks, and reinforcement corrosion. The allowable crack widths are recommended by standards and guidelines considering the function, importance, service, life span, purpose, surrounding environment, and surrounding soil conditions of the tunnel (JSCE 2007). ACI 224.1R limits allowable cracks in structures exposed to the soil to 0.012 in. (0.30 mm). Similar to ACI 224.1R, BS EN 1992-1-1:2004 recommends an allowable crack width of 0.012 in. (0.30 mm) for RC members. In a more restricted manner, MC2010 limits the allowable crack width to 0.008 in. (0.2 mm) if leakage into the structure is to be limited to a small amount and only some surface staining is acceptable. Among references specific to tunnel segments are LTA 2010, DAUB:2013, and JSCE 2007 that specify the allowable crack width to 0.01 in. (0.30 mm), 0.007 in. (0.2 mm) with 0.006 in. (0.15 mm) when below the groundwater table, and $0.004d_c$, respectively, where d_c is the concrete cover over the reinforcing bar. As the most comprehensive guideline, ÖVBB 2011 specifies the allowable crack width in segments

Table 9.4.2—Allowable crack width for tunnel segments (ÖVBB 2011)

Requirement class	Designation	Application	Requirement	Allowable crack width
AT1	Largely dry	- One-pass lining with very tight waterproofing requirements - Portal areas	Impermeable	0.008 in. (0.20 mm)
AT2	Slightly moist	- One-pass lining for road and railway tunnels with normal waterproofing requirements (excluding portals)	Moist, no running water in tunnel	0.010 in. (0.25 mm)
AT3	Moist	- One-pass lining without waterproofing requirements - Two-pass lining systems	Water dripping from individual spots	0.012 in. (0.30 mm)
AT4	Wet	- One-pass lining without waterproofing requirements - Two-pass lining as drained system	Water running in some places	0.012 in. (0.30 mm)

based on the tunnel function and corresponding watertightness requirements, which is shown in Table 9.4.2.

9.4.3 *Verification of current crack width criteria*—Bakhshi and Nasri (2017b) provide an analytical methodology for prediction of water inflow into cracked concrete linings. The method is sensitive to all major physical factors and focuses on the mechanism of water flow through the cracks by introduction of formulas calibrated by several different experimental data. Best fits to experimental data were presented by introducing upper- and lower-bound factors to the water flow rate coefficient as an important factor for determining water inflow rate. Effect of different types of reinforcement, including conventional reinforcing bars or fiber reinforcement versus plain unreinforced concrete on controlling water inflow rate in cracked samples was introduced in a quantitative manner. To verify validity of current crack width criteria, water inflow rates corresponding to the allowable crack widths were calculated for a midsize tunnel. Results show that the crack width is not the only dominant factor impacting the water inflow rate. Water pressure head, segment thickness, length, and water temperature also have significant effects on the water infiltration into tunnels. Results also imply that, without consideration of autogenous healing, inflow rate may not be in agreement with the qualitative designations provided in codes and guidelines such as ÖVBB 2011 by setting fixed allowable crack width ranges. However, because autogenous healing in cracked concrete results in significant reduction of water inflow with time, further studies are needed to verify the validity of current crack width criteria. On the other hand, results of parametric studies and application to a case of a midsize tunnel show a significant impact of fiber reinforcement in controlling the initial water inflow. The proposed methodology indicates that in addition to the superior effect of fiber reinforcement in controlling the cracks under service load, compared to conventional reinforcement, fiber reinforcement also significantly improves the watertightness of cracked concrete lining most likely due to change in morphology of cracks. The proposed approach can be used to provide project-based allowable crack width for concrete tunnel lining based on parameters that are specific to the project, including the type of reinforcement.

CHAPTER 10—DESIGN OF SEGMENT GASKET

Watertightness of tunnels are often ensured during design and construction to prevent water infiltration and minimize

Fig. 10—Segment gaskets positioned near the lining extrados for joint watertightness.

maintenance and repair costs, maintain operational safety, and protect mechanical and electrical equipment inside tunnels. In a one-pass segmental lining system, which is the most commonly used system in tunnel boring machine (TBM)-bored tunnels, the watertightness of the tunnel should be guaranteed by the individual components of the support system—namely, precast concrete segments and segment gaskets placed between segments in the longitudinal and circumferential joints. As shown in Fig. 10, gaskets are positioned around the individual segment like a frame and primarily near the lining extrados to provide the joint tightness.

10.1—Gasket materials

Recommended materials for segment gaskets are ethylene propylene diene monomer (EPDM) rubber compounds that have replaced the formerly used chloroprene gaskets. EPDM compounds guarantee a life span of more than 100 years, and economically and technically are the most suitable material to withstand climate and groundwater with varying water composition. EPDM rubber compound is stable enough not to react with the environment or deteriorate in contact with other materials such as concrete; grease; injection materials; and ground and groundwater anions, cations, heavy metals, volatile, and semi-volatile organic compounds. EPDM elastomer resistance to some of the substances that may be found in some specific grounds, such as hydrocarbons, oils, and tar, are limited. However, in such cases, often due to low concentrations of these substances and the embedment of gaskets in the segment joints, EPDM elastomer gasket

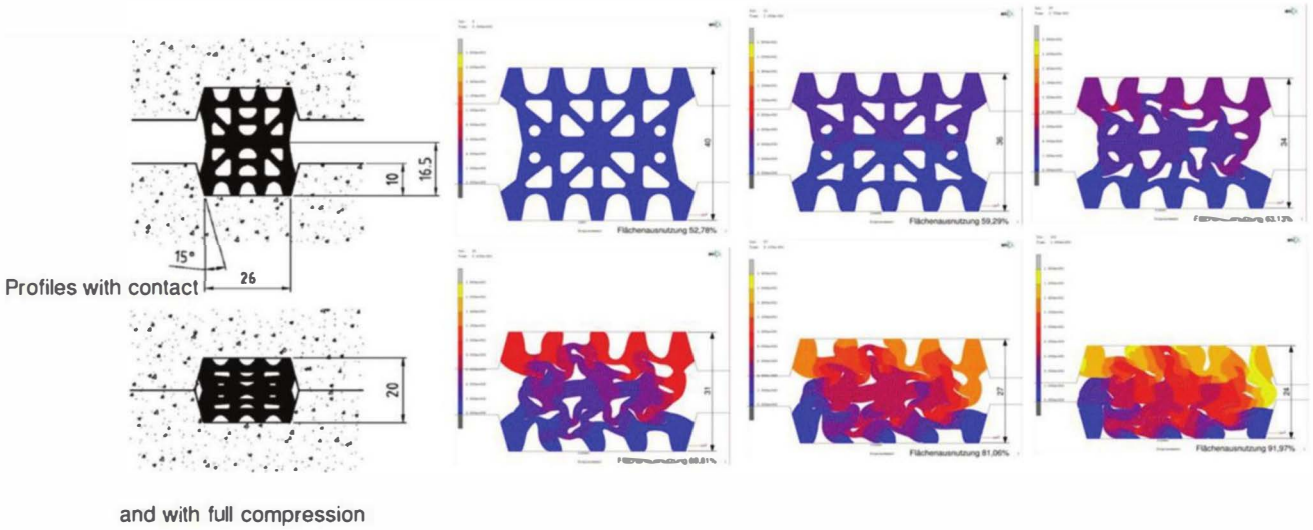

Fig. 10.2a—Watertightness between segments created through gasket compression.

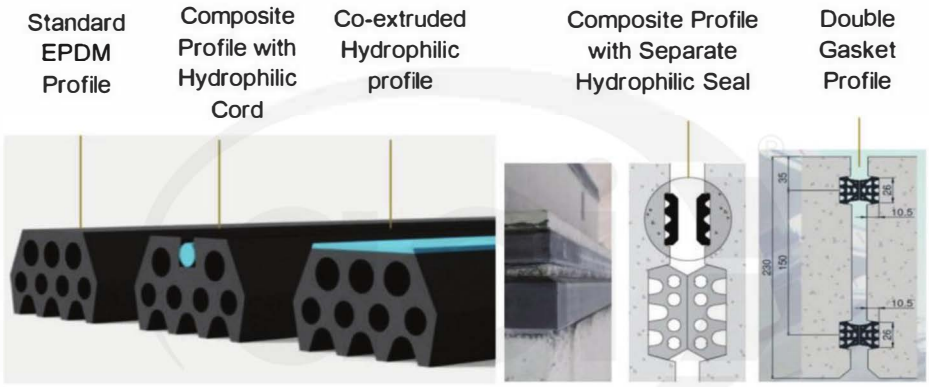

Fig. 10.2b—Standard, composite, and double-gasket solutions for projects with different watertightness requirements.

contact with such substances does not raise a significant concern. An alternative elastomer material, which in theory offers a better resistance to hydrocarbons, oils, and tar, would be a chloroprene rubber/styrene butadiene rubber (CR/SBR) compound. However, CR/SBR compounds offers much lower or no resistance to most other substances, especially acids; has serious application issues in groundwater with a pH value of 2; has a much weaker resistance to aging and weathering effects; has weaker behavior with regard to stress relaxation over a tunnel service life, which in turn has decisive influence on long-term waterproofing performance; and has a lower gas permeability. Therefore, EPDM elastomer is recommended as the most suitable material for segment gaskets. To provide the desired characteristics of a project, several material-specific requirements should be met for the gasket to perform as intended. One of these properties is hardness of the rubber compound. BS PAS 8810:2016 requires a maximum shore hardness of 75 according to ASTM D2240, whereas STUVAtec:2005 and AFTES:2005 recommendations call for a maximum hardness of 85. Other important properties include tensile strength and elongation according to ASTM D412 that are recommended to be greater than 1700 psi (12 MPa) and 300 percent, respectively.

The technical solutions that engineers need to implement to the design of segment gaskets and achieve the required watertightness depend on specific project circumstances. The important factors for design and application of tunnel sealing gaskets are water pressure, safety factor, size of tunnel and segments, gap and offset between segments, and tolerances.

10.2—Water pressure and gasket design

The most important parameter for design of gaskets is the maximum water pressure. Depending on the expected water pressure in the tunnel, different solutions and different gasket profiles are selected. The first gasket generation could only withstand a maximum water pressure of 3 bar. Today, with the advance of technology and limited offset between adjacent segments due to more accurate segment erection inside TBM, watertightness of up to 10 bar is often achievable with a standard monoextrusion EPDM gasket profile. As shown in Fig. 10.2a, watertightness between segments will be created through the compression of gaskets developed during the assembly process of the segments. For higher water pressure, two main solutions are available. The first solution includes a composite seal combining two different sealing technologies of EPDM compression gasket and a hydrophilic seal. As shown in Fig. 10.2b, this solution can

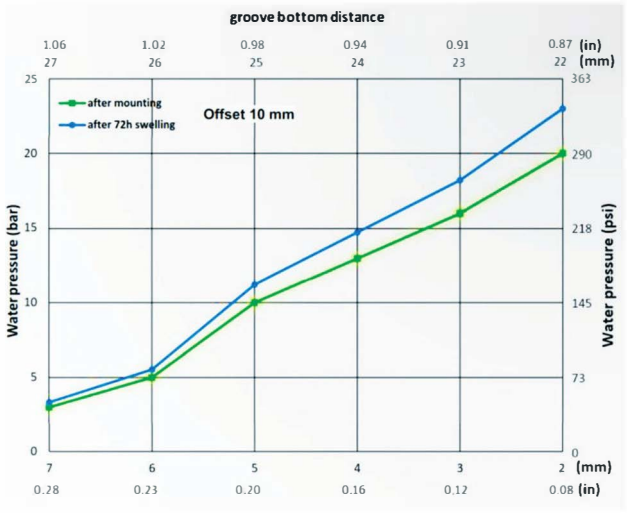

Fig. 10.2c—Effect of hydrophilic swelling cord on improving sealing performance of a composite EPDM gasket in terms of resisting higher water pressure after several days of immersion in water.

be provided by the application of coextruded gaskets with hydrophilic layer, composite profiles with hydrophilic cord, or designing a composite solution with separate hydrophilic seal next to the standard EPDM gasket.

Figure 10.2c shows effect of the hydrophilic insertion on improving sealing performance of a composite EPDM gasket in terms of resisting higher water pressure after several days of immersion in water. The hydrophilic cord swells under water pressure and can act as an extra backup of the EPDM profile. Note that tests with coextruded gaskets or hydrophilic swelling cord gaskets do not influence the test results in a short term, as the hydro-swelling takes longer than 24 hours to react. Approximately 50 percent of the swelling occurs within 7 days with nearly 100 percent of swelling occurring within 30 days. To measure the positive influence of hydro-swelling layers, long-term watertightness tests should be carried out.

A second solution includes two sealing gaskets—one near the extrados and one near the intrados of the segment, resulting in a higher waterproofing performance. When used in combination with a sealing profile connecting bars between the extrados and intrados gaskets, isolation chambers can be created that help confine any localizing leakages, thus permitting precise repairs by grout injection methods. A look at reference projects with double gaskets shows that in half of these projects, no connecting gasket bar was used. In projects with connecting gasket bar, except for one project, cross-connecting gasket bars were not vulcanized at the gasket manufacturing plant but were glued in place at the segment precast plant. Care should be taken to the fact that watertightness of a double-gasket system is defined by the higher capacity of the two gaskets, not by the sum of both gaskets' capacity (BS PAS 8810:2016).

10.3—Gasket relaxation and factor of safety

In addition to the expected height of the water pressure in the tunnel, the specifications should define the watertightness performance of a sealing gasket and thereby include a safety factor that takes rubber relaxation effects into account. To obtain long-term post-construction performance, it is crucial that the gasket profile and rubber compound uphold the designed reaction force to withstand the applied water pressure even years after its application. The majority of the relaxation occurs in the first months after installation. The relaxation can be tested with so-called accelerated aging tests using an accelerated procedure with elevated temperatures to get results within a reasonable timeframe (Fig. 10.3). Most of specifications ask for a minimum residual compressive stress of 60 percent after 100 years. This means a safety factor of 1.67 (1/0.60 = 1.67) is the minimum factor of safety for gasket profiles. Considering the relaxation effects of rubber and design life of most tunnels from 100 to 125 years, a safety factor of 2 is advisable to ensure that the gasket is able to withstand the design pressure in the long term. As the relaxation behavior of a sealing gasket is mainly influenced by the geometry of the profile, such aging tests should be carried out independently for every profile.

10.4—Tolerances and design for required gap/offset

The width of the gasket profile depends on the size of tunnel as segment thickness is a function of tunnel diameter. The following gasket profile widths are the current industry practice for different tunnel diameters.

a) Tunnel diameter < 13 ft (4 m) gasket width = 0.8 in. (20 mm)

b) 13 ft (4 m) < tunnel diameter < 23 ft (7 m) gasket width = 1 in. (26 mm)

c) 23 ft (7 m) < tunnel diameter < 36 ft (11 m) gasket width = 1.3 or 1.4 in. (33 or 36 mm)

d) 36 ft (11 m) < tunnel diameter gasket width = 1.4 or 1.7 in. (36 or 44 mm)

Note that in specific cases, a more conservative requirement (that is, a wider segment profile) may be requested by the owner. Gasket size is also related to erection tolerances that, in turn, depend on diameter of tunnel (segment size) and the connection system. Bolt and dowels are the two typical connection systems, and each allow for different gap and offset tolerances during the segment erection process. Gap openings and offsets are illustrated in Fig. 10.4a. A connection system with bolts usually allows offsets up to 0.6 in. (15 mm), which can be reduced to 0.2 in. (5 mm) with high-precision segment installation. Dowels, however, are the connection system with reduced tolerances. Note that reducing the tolerances has a considerable effect on the gasket system. First, the gasket needs to cover a smaller offset range and therefore a narrower gasket profile can be selected. Second, due to a reduction of gasket offset, the required gasket resistance pressure is reduced. In addition to smaller and therefore lower cost of gasket, other advantages of a sealing system with reduced tolerances include:

a) Reduction of TBM erector forces (up to approximately 50 percent)

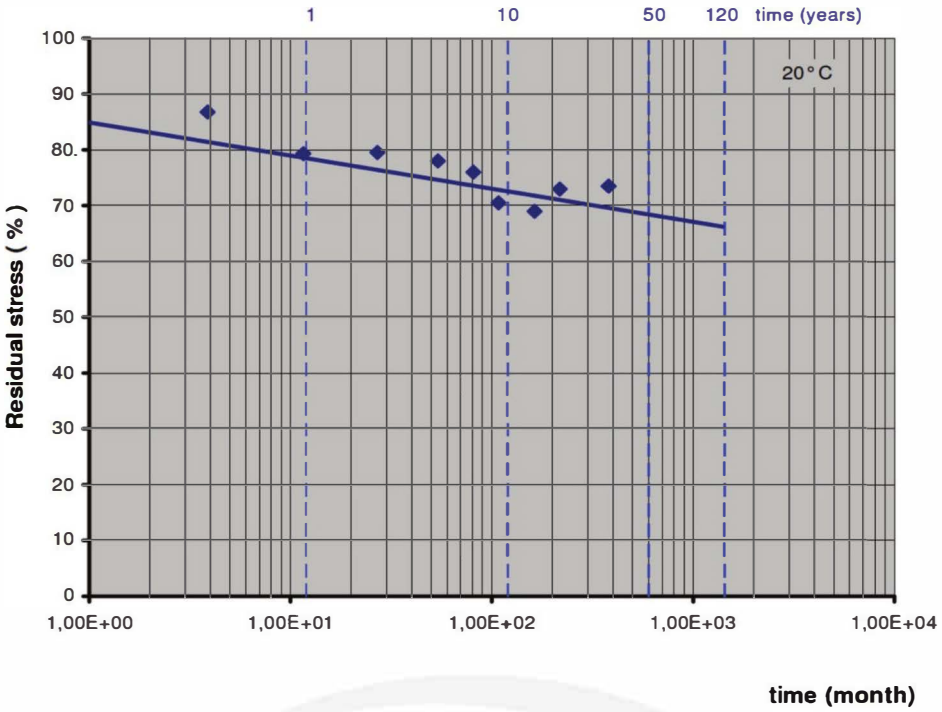

Fig. 10.3—Typical long-term relaxation test results according to ISO 11346:2004.

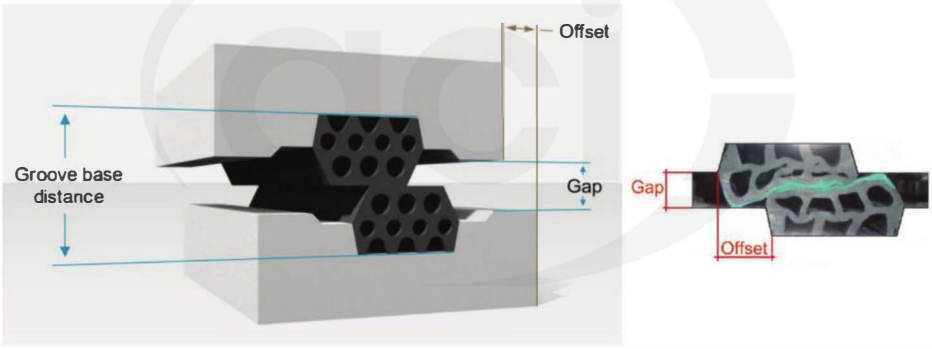

Fig. 10.4a—Illustration of gap opening and offset before and after compression.

b) Reduction of induced forces in connectors (up to approximately 50 percent) and in turn reduction in size of connection system

c) Reduction of designed space for connection and gasket systems

Most tunnel project specifications allow for 0.2 in. (5 mm) gap and 0.4 in. (10 mm) offset for segment gaskets. Dowels can easily provide this requirement. However, bolts are the predominant connection system in longitudinal joints. Contractors tend to change the joint conditions to a higher gap and especially higher offset values to avoid additional time and labor required for the very precise installation of connecting bolts. This, in turn, results in larger tolerances to be adopted for longitudinal joints. A review of 50 projects show that while the gap opening between segment gaskets ranges from 0.08 to 0.27 in. (2 to 7 mm), in 30 percent of these projects, the contractors selected to use a gap of more than 0.2 in. (5 mm). Also, with offsets between gaskets ranging from 0.2 to 0.8 in. (5 to 20 mm), in approximately 45 percent of these projects, contractors chose an offset of more than 0.4 in. (10 mm). Engineers are encouraged to consider possible larger gap (greater than 0.2 in. [5 mm]) and offset (greater than 0.4 in. [10 mm]) with potential higher cost savings due to faster erection and construction time than gasket materials itself.

Watertightness tests using gaskets can be performed on steel or concrete specimens. Working with concrete specimens is time-consuming and prone to failure. Therefore, only tests on steel specimens are currently carried out. Following STUVAtec:2005 recommendations, and as shown in Fig. 10.4b, the geometric situation is simulated on a T-joint in the laboratory whereby, as on the circumferential joint, a straight piece of sealing profile is pressed against the end of a longitudinal joint. Gaskets should guarantee the watertightness under all possible gaps and offsets. Therefore, it is necessary to run the watertightness test with different gaps and offsets. For every offset setting (0 to 0.8 in. [20 mm]), the test has to run through a range of different gaps. For every

gap, the water pressure is built up in steps of one bar and is held there for 5 minutes. In that manner, every setting should be tested until the profile shows leakage. The recording of all failure points leads to the required watertightness-gap diagram shown in Fig. 10.4c. Gasket-resisting pressure corresponding to designed gap and offset in the watertightness-gap diagram should be higher than the maximum factored working pressure of the project.

10.5—Gasket load-deflection

Gaskets, on one hand, should be able to withstand the water pressure long-term. Considering the relaxation effect, the gasket's compressive force, or reaction force, should be higher than the factored working pressure. On the other hand, if the reaction force is too high, a strong erection force should be provided to properly compress the segments. With a high compression force, there is a risk of cracking in the concrete groove that leads to a water penetration underneath the gaskets and causes durability and serviceability issues with the lining. In addition, connection systems are designed based on the initial reaction force of gaskets. Therefore, gasket short-term behavior should also be provided in terms of a load-deflection curve, which depends on the gasket material, the shape of gasket profile, and required gap and offset. As shown in Fig. 10.5(a), deflection is represented by the gap and because gasket reaction force is highest when there is no offset between gasket faces, this curve represents a response for the case of no offset. Connection systems are designed for maximum gasket load in this curve corresponding to zero gap. Connection systems can be designed in a less conservative approach for the maximum reaction force in the gaskets after short-term relaxation (within 5 minutes), as shown in Fig. 10.5(b). Note that 5 minutes is the minimum time for connectors to start acting against compressive force of gaskets and should be the absolute minimum time required for segment erection and TBM thrust jack force release.

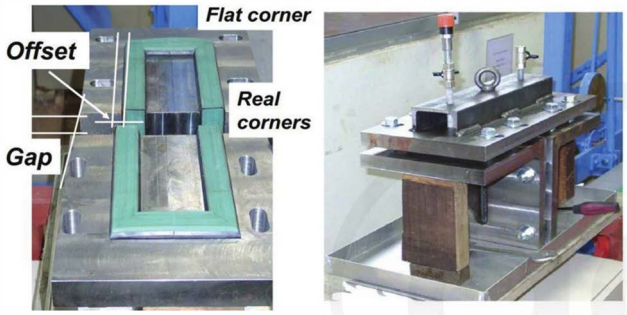

Fig. 10.4b—T-joint watertightness test setup for segment gaskets recommended by STUVAtec:2005.

10.6—Gasket groove design

The watertightness further depends on the groove geometry. Angle and groove depth should be in line with the chosen gasket. To avoid spalling of concrete, it is crucial that the net volume of the rubber can be housed within the groove when the tunnel segments are fully closed or gap is zero. To achieve that, the net profile volume (seen in a cross section) should be some percentage smaller than the groove cross section (the net profile should be approximately 90 percent of the groove cross section). In that way, even in cases of very high forces applied onto the segment joints (for example, TBM jacks), there is enough space for

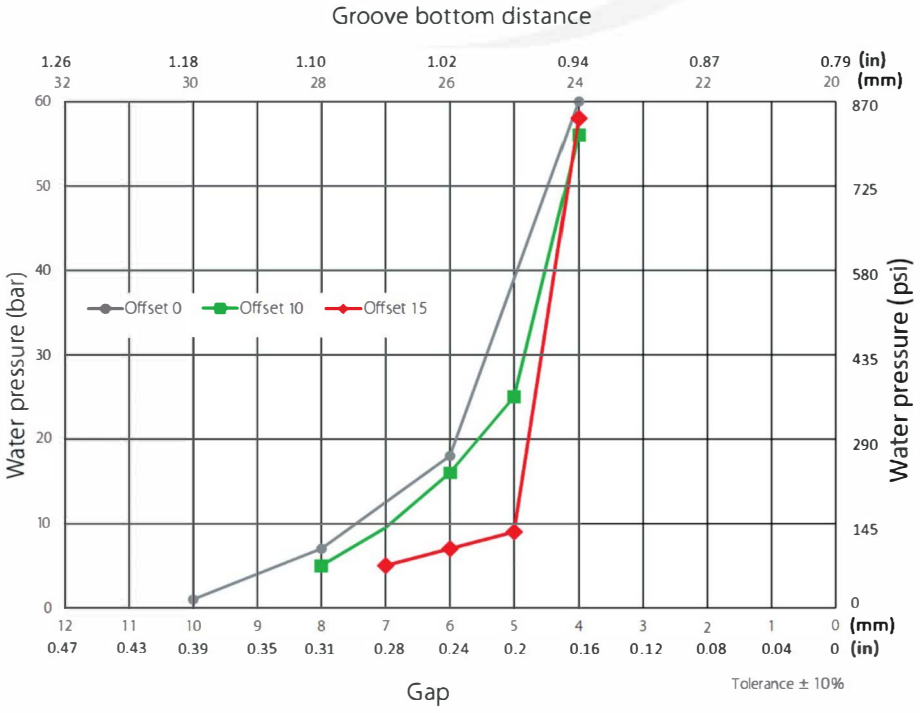

Fig. 10.4c—Typical watertightness-gap diagram.

the gasket to fit into the groove. However, practical experiences in tunnels with segments with narrow grooves and high TBM jack forces have shown that the concrete segment corners show cracks or concrete spalling even when the aforementioned criteria of the volume ratio is fulfilled. This is because EPDM rubber without voids is an incompressible material. When compressed, the applied force R will deform the gasket profile and close the hollow body. When reaching its full compression (no voids), the applied force, R, similar to hydrostatic pressure, will be evenly spread onto the groove flanks (p) and the groove bottom. Therefore, the spalling force (P_1 or P_2 in Fig. 10.6) on the flanks is directly depending on the groove depth. At the same time, this increase in lateral force can only partly be compensated by the slightly longer shear area that in the section is defined by the length of shear plane (a and b as shown in Fig. 10.6). The value of $a \approx b$ and this leads to the conclusion that the danger of spalling increases with a deeper gasket groove. With regards to concrete spalling, a flat profile design is more favorable than a stocky profile requiring a deeper groove. Another major conclusion is that the groove distance from outside edge of the segment (extrados) is also crucial to the spalling behavior. The closer the gasket is located to the segment extrados, the shorter the length of resisting shear plane (a or b in Fig. 10.6) and the higher is the risk of spalling. The real impact of the superimposed factors (for example, shear, torsion, and jack pressure) can only roughly be determined. A successful application without spalling also depends on the experience of the involved parties, especially on the skills of the worker guiding the TBM erector.

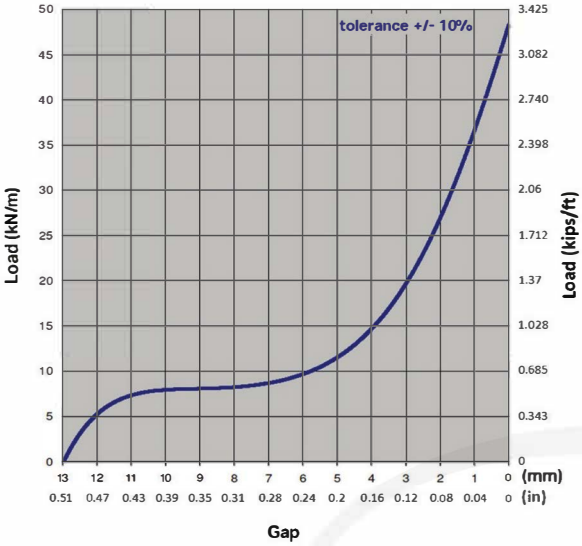

(a)

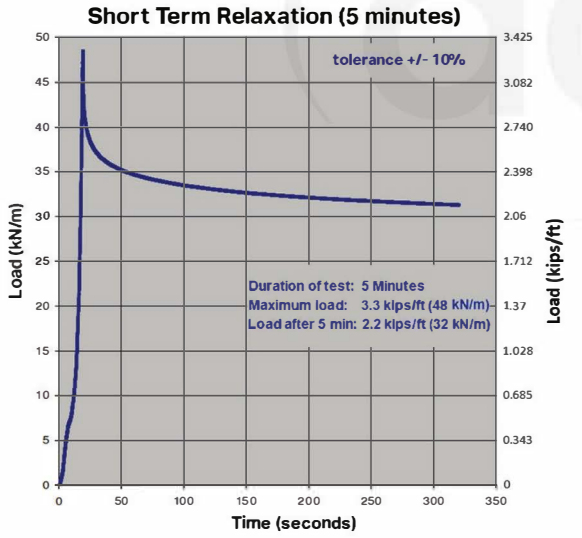

(b)

Fig. 10.5—(a) Typical gasket load-deflection or reaction force test results; and (b) typical short-term relaxation.

10.7—New development in gasket systems

Conventional gasket systems include the design of gasket grooves in the segment molds. After casting the segments, gaskets can be placed into the groove and glued with a contact adhesive and brush, or using a spray gun and a pneumatic pressing frame. In this gasket system, also referred to as glued gasket, gluing of gaskets is only carried out to ensure that they remain in their grooves during segment handling, storage, and erection. The main issue with this system is the low bond strength of glued gaskets to the segments to prevent the gasket from coming loose, especially during key segment installation. Recently, an alternative solution has been developed using anchored gaskets to meet high waterproofing requirements and provide higher bonding forces required to pull gasket off the segment. As shown in Fig. 10.7a, the gasket, which is equipped with special anchoring devices on the underside or footed legs, is directly embedded in concrete in the process of segment production. Thus, the seepage path of any water is prolonged and the gasket is held safely in place during installation (ÖVBB 2011). In addition to safer bond to segments, this gasket system has several other advantages over glued gasket systems.

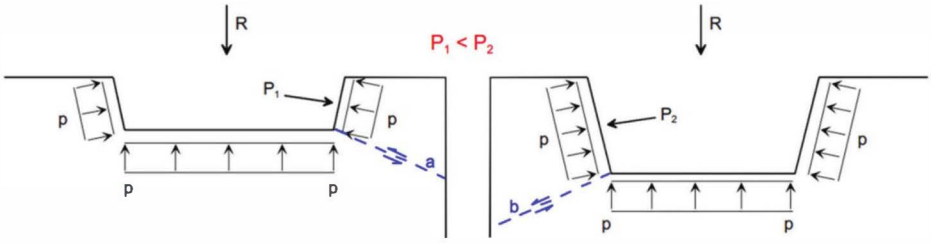

Fig. 10.6—Hydrostatic distribution of impact force R *in a gasket groove.*

a) Better waterproofing performance due to less failure on concrete groove side

b) No risk/problem of gasket falling off the segment during outside storage due to insufficient gluing, weathering, and frost during outside storage

c) Better working conditions and higher safety for segment production staff due to abolition of solvents that are used in all standard brands of tunnel gasket adhesives

d) Saving of costs for adhesives, gluing procedure, and equipment (for example, spraying gun, pressing frames, exhaust and ventilation systems, and disposal of empty adhesive tins)

For all types of gaskets, to avoid damage to the gasket through shearing at the groove base and to reduce the friction between segments during installation of segments, especially the key segment, covering or coating the gasket with a lubricant is recommended. Note that this is even more crucial when anchored gasket systems are adopted, as special anchorage system prevents debonding of gaskets and an excessive frictional force can be developed, which is directly transferred to concrete segments and may cause damage.

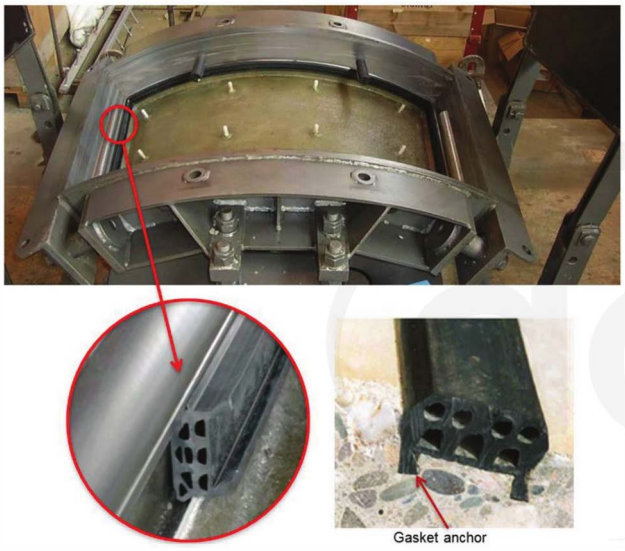

Fig. 10.7a—Anchored gaskets fixed into the concrete segment during segment production without using any gluing methods

Assembly procedure for anchored gaskets is shown in Fig. 10.7b. The anchored gasket frames are always designed with an excessive length of +0.5 percent. The installation procedure starts with inserting the gasket into the groove, beginning with the four corners first (Location 1 in Fig. 10.7b), and it continues with insertion of a gasket in the long side or circumferential joint side beginning from the middle (Location 2 in Fig. 10.7b) and then the remaining parts toward corners (Location 3 in Fig. 10.7b). Care should be taken that the gasket material is equably distributed along the groove and that the whole gasket profile along this long side is properly clipped in. Finally, the remaining gasket parts on the short side or longitudinal joint side are inserted in the mold, starting from the middle (Location 4 in Fig. 10.7b) and going towards the corners (Location 5 in Fig. 10.7b). For anchored gasket systems, as shown in Fig. 10.7b, the profile for each segment is always delivered as a continuous piece. Attention should be paid that the profile corners are precisely positioned, the anchored feet always point upward, and the sealing lips are positioned tightly alongside the steel counter surface.

Another major development is the design of the gaskets at the corners. Most of the manufacturers now provide prefabricated corner solutions with reduced stiffness of the corner element. This technology provides soft corners and reduces risk of spalling of concrete at the segment corners.

The most recent innovations and developments in gasket design is the use of new fiber anchored technology (Bakhshi and Nasri 2018a). The principal is the elimination of conventional anchored feet and application of plastic fibers as an anchoring element (Fig. 10.7c). This new technology offers additional pullout resistance comparing to conventional glued gasket system and in addition provides easier handling, improving the fixation in longitudinal direction;

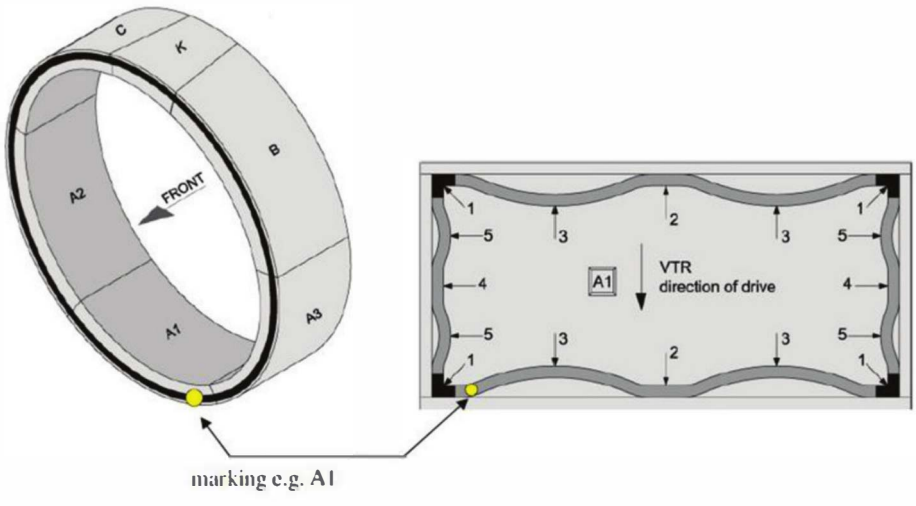

Fig. 10.7b—Assembly instruction for anchored gaskets with numbers representing installation point sequences in the mold.

Fig. 10.7c—Anchored segment gasket using fiber anchorage system.

reduced risk against spalling; no possibility of wrong installation (feet up or down); more economic packaging quantity; easier repair procedure because of perfect groove bottom (no holes from the feet); and no possibility for air entrapment in the anchorage area.

New repair concepts for post sealing of segment joints have been noted (Tintelnot et al. 2018). Leaking joints inside a segmentally lined tunnel is a well-known issue that is often caused by displacement of a gasket profile during installation of concrete segments. Another common reason is the lack or loss of compression force on gaskets due to an unprecedented increased gap between the segments' faces. Damaged concrete segments and cracked concrete edges due to eccentric forces during TBM jacking forces is also another major cause of leakage near joint sealing gaskets. This very recent repair method is based on direct drilling and injection through joint sealing gaskets (Kirschke et al. 2013). Four major steps for this repair method (shown in Fig. 10.7d) include:

a) Step 1: Pre-drilling ϕ9/16 in. (ϕ14 mm) to the gasket profile

b) Step 2: Drill and push injection needle through the entire gasket profile

c) Step 3: Injection using accelerated injection material

d) Step 4: Removal of extension tube; injection needle remains in the gasket

This repair method has several advantages over conventional methods of packer injection and built-in injection hose system. Main advantages of this repair system include efficient injection procedure with less time, material, and labor cost, less drilling work with no significant damages on concrete and steel reinforcement, and injection works only at leaking areas.

CHAPTER 11—CONNECTION DEVICES AND FASTENING SYSTEMS

11.1—Bolts, dowels, and guiding rods

The connections between segments within a ring and between rings can be divided into two categories: joint connections with bolts, or with dowels. In bolt-type connection, the segment is first placed in position and then the bolts are inserted and tightened. However, in dowel-type connections, the dowels are inserted into the segment during the assembly and are either mortise-inserted or dovetailed into the segment of the last assembled ring. Connections with bolts requires more effort in the construction of the mold because it is necessary to create pockets and grooves into which the bolts are inserted. It is also necessary to have more personnel in the tunnel to insert the bolts. This type of connection is traditionally associated with rectangular segments and is generally used both between rings and between segments, within a ring. The bolts are metallic while the embedded threads are generally plastic. Figure 11.1a shows the typical housing of a straight bolt. Attention should be paid to the following geometrical details:

a) Pockets should be large enough for head of the bolt and pneumatic wrench to be easily inserted

b) The slot side of the pocket should have a conicity of at least 1 degree

c) The bolt slot in the segment that houses the nut should have a compatible conicity

d) The bolt axis should pass through the center of the segment

e) The distance between the end part of the nut and the extrados of the segment should be sufficient

Joints with dowels require less work for the construction of the mold and less workforce in the tunnel for the insertion into segments. The dowels and sockets are made of plastic and sometimes have the core in steel. Figure 11.1b(a) shows the typical housing of a dowel, which is placed on the axis at the middle point of the segment. Because of the kinematics of the assembling process, this type of connection is only used between the rings in circumferential joints. In most cases, the dowel connections are used with rhomboidal and trapezoidal segments to avoid early crawling of the gaskets during the segments-approach phase of the ring assembly.

In addition to dowels, guiding rods (Fig. 11.1b(b)) can be also used as movable centering device that provides, with guidance, centering during segment installation and locking functionality. Guiding rods absorb shear forces in the longitudinal joints (ÖVBB 2011). An advantage of using guiding rods is that, in the longitudinal joints, inserted longitudinal guiding rods can prevent the segments slipping away from each other during ring building (DAUB:2013). Usually guiding rods are adopted in conjunction with dowel connection systems.

11.2—Design of connection device for gasket pressure

The maximum groundwater pressure defines the design of the sealing gasket. Considering the relaxation effects of rubber, a safety factor of 2 is applied to the maximum working water pressure to ensure that the gasket can withstand the design pressure in the long term. This leads to the selection of a proper gasket profile. As discussed in Section 10.5, maximum instantaneous reaction force in the gaskets from the gasket load-deflection curve or, in a less conservative approach, the maximum reaction force after short-term relaxation (within 5 minutes) should be considered during the design of connection systems. Figure 11.2 shows forces that are applied on dowels and bolts depend on the reaction force of specific type of gasket profile used in the project after accounting for short-term relaxation. Gasket reaction force in load-deflection curves is always presented as force per unit length of each specific gasket, and in units of kip ft (kN/m). Therefore, it is important to determine the corre-

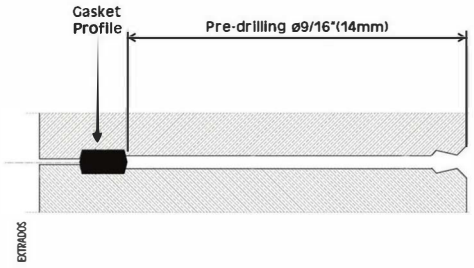

(a) Step 1: Pre-drill to edge of gasket profile

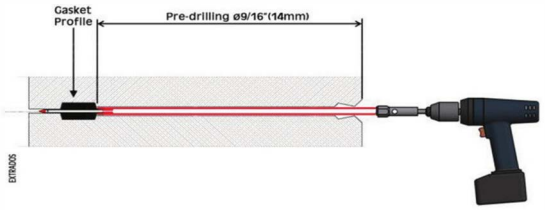

(b) Step 2: Drill and push injection needle through the entire gasket profile

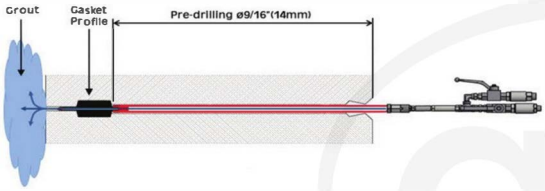

(c) Step 3: Injection using accelerated injection material

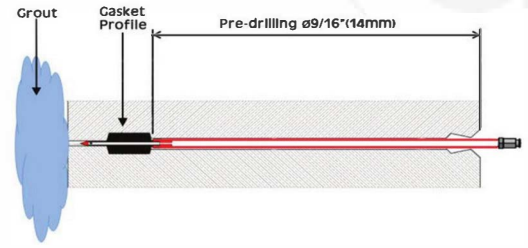

(d) Step 4: remove extension tube while injection needle remains in the joint gasket

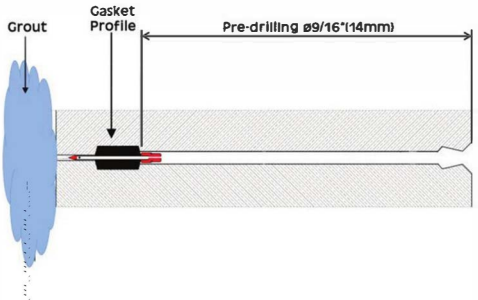

(e) Final condition after removing extension tube

Fig. 10.7d—Major steps of recently developed repair method for controlling groundwater inflow using injection through gaskets in leaking segmental tunnels (Kirschke et al. 2013).

sponding length of the gasket that is acting against each single dowel or bolts. For design of dowels, the total length of the gasket used in one segmental ring depends on the size and outer perimeter of the tunnel lining. Also, depending on the total number of dowels placed along the whole ring perimeter and considering a uniform gasket pressure distribution, a gasket length that pushes against one single dowel is determined. A safety factor of 1.25 should be considered for the dowel connection system, and the required pullout force should be obtained and used for the selection of dowel types. Bolts often in longitudinal joints are designed in a similar way, considering their inclined angle with centerline of the longitudinal joints (for example, 24 degrees in Fig. 11.1a and 11.2(a)). The length of the gasket in longitudinal joints is approximately equal to the ring length. Considering that often two bolts are designed in each longitudinal joint for the connection and that gasket pressure is uniformly distributed over the longitudinal joint, the force in each bolt due to gasket compression is calculated. A factor of safety of 1.25 is advisable and bolt connection systems should be selected or verified based on the system pullout force and tensile yield strength.

11.3—Latest developments in joint connection systems

Dowels are a relatively new hardware system in circumferential joints replacing conventional bolts. Advantages are faster installation and prevention of offset between the rings. Sometimes in large-diameter tunnel applications, the shear capacity of dowels is insufficient. To overcome this issue, new dowel systems have been introduced with the same basis as the current dowel system, but with new plastic materials that have a higher resistance and to void variations due to humidity and reduce the displacement as much as possible. As shown in Fig. 11.3, another modification includes integration of a screwable socket on one side of the bolt to reduce the installation tolerance and provide the workers with a smoother assembly process. Pullout resistance and shear capacity of 56 kip (250 kN) has been guaranteed with this latest system, as well as very low displacements during pullout and bending resistance of 9 kip (40 kN).

11.4—Fastening systems to segments

Fastening other systems to the precast segments are important parts of every bored tunnel lining system. They are used for fixing system components of the railway overhead catenary systems and fixing mechanical and electrical equipment. Other applications of fastening systems include fixing and supporting intermediate slabs, cross-passageway connecting doors, and platform screen doors.

Anchorage failures in tunnels are rare, but when they happen, consequences can be very costly and tragic. In general, these fasteners can be divided into two main categories of post-installed and cast-in-place systems. Post-installed anchors as traditional systems have several disadvantages over newly developed cast-in-place fastening systems. Requirements for providing anchorage zones by dimple grids, drilling procedure followed by dust and noise

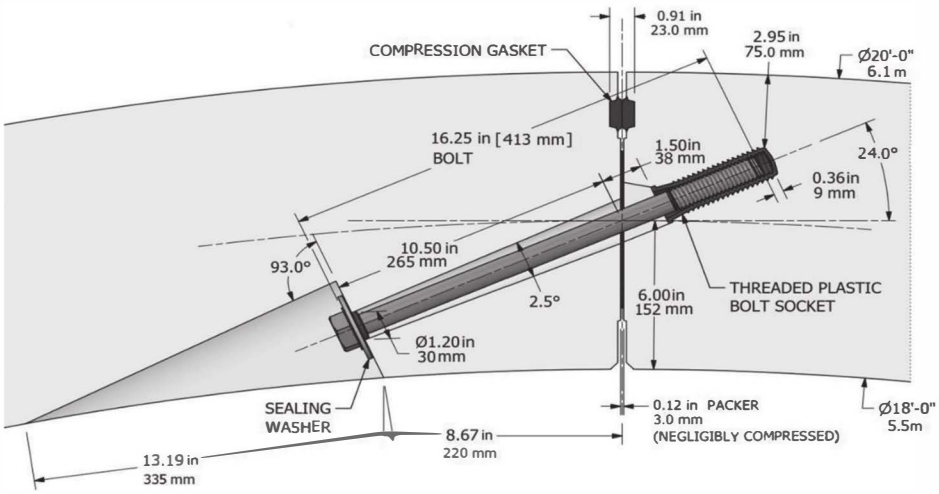

Fig. 11.1a—Typical detail of bolt connection in longitudinal joints.

generated during installation, and temperature dependency of the adhesive anchor and higher risk of anchorage failures make this system less favorable.

Additional efforts and power tools are needed when installing anchors in high-strength concrete. Most importantly, drilling may damage concrete, reinforcement, or segment gaskets with negative impacts on structural behavior, sealing performance, corrosion protection, and long-term durability. Some of the major issues with traditional post-installed anchor systems are shown in Fig. 11.4a.

Post-installed straight or curved anchor channels, as an alternative to direct anchor fastening systems, can provide some advantages regarding anchor adjustability and flexibility in future changes. With anchor channels, subsequent installation or anchorage of further components is always possible. This is important for repair and rehabilitation projects where expansion or upgrade of utility equipment and production facilities are required. However, the main issue of drilling and installation quality still remains. To overcome this problem, a solution has been developed by embedding anchor channels into segments without drilling and via connection bolts. Figure 11.4b shows this solution for 3200 ft (1 km) long Diabolo railway line twin tunnels with a 24 ft (7.3 m) internal diameter and 7+1 segmental ring configuration as described in 3.4.5. As shown in Fig. 11.4b, installation of curved anchor channels was done with mounting plates at the back of post-installed anchor channels and through the bolt connection system in circumferential joints. This fastening system has been used for anchoring all utilities and mechanical and electrical equipment in this tunnel. Such a system can provide over 6.7 kip (30 kN) service point load capacity every 12 in. (300 mm).

Segmental lining systems take advantage of dowel connections in circumferential joints and, therefore, circumferential pockets designed in segments for fastening bolts are often not available. Solutions such as in Fig. 11.4b cannot be always guaranteed with anchor channel systems and, despite all its advantages, the anchorage issue and drilling remain as a primary drawback. In the wake of providing a universal solution, the fastening technology shifted toward use of

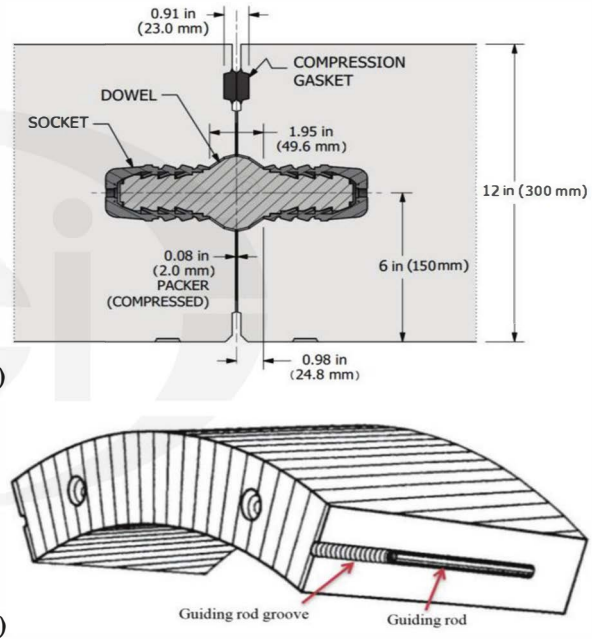

Fig. 11.1b—(a) Typical dowel connection in circumferential joints; and (b) location of guiding rod groove and guiding rod (ÖVBB 2011).

cast-in channel systems with mechanical interlock principle. Cast-in systems, as shown in Fig. 11.4c, are basically anchor channels with welded anchors (preferably I-anchors) that are placed in segment forms before casting concrete in the segment manufacturing plant. Such systems provide efficient, flexible, and safe methods of fastening without drilling and negative impact on precast segment quality. Adjustable fixing, flexibility in changes during construction and service life (replacements, extensions), use for temporary installations during construction, reliable planning by an accurate knowledge of assembly times, reduction of construction and installation time, and higher site productivity with reduced labor are among the advantages of this system.

Cast-in-place systems also have lower maintenance cost, lead to much easier quality control both in precast plants and

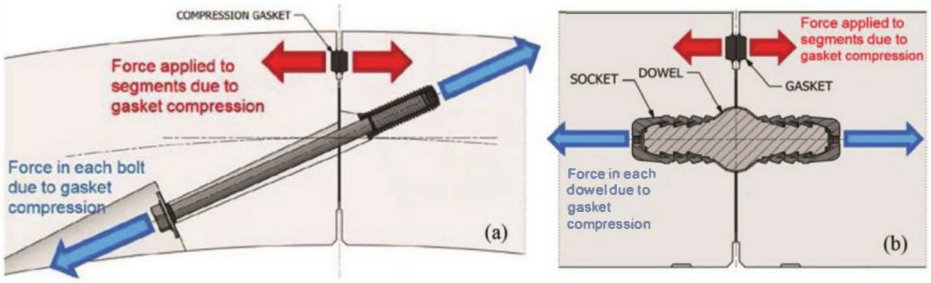

Fig. 11.2—Schematics of forces developed in segment connection devices due to gasket reaction force: (a) bolt; and (b) dowel.

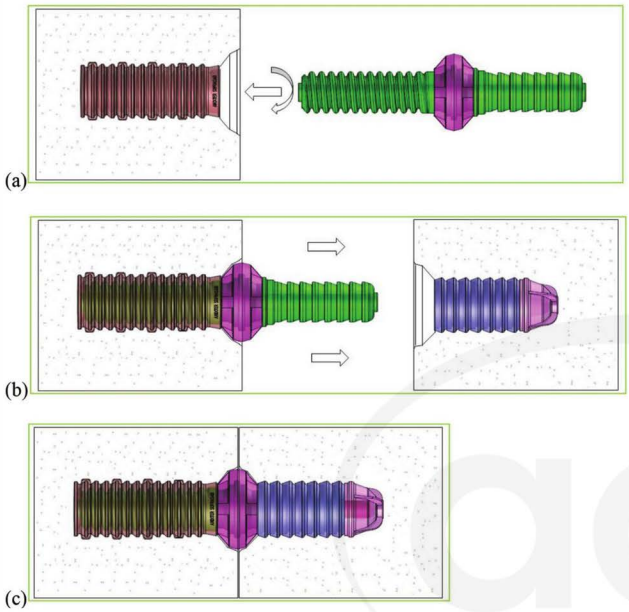

Fig. 11.3—New dowel connection system with pullout resistance of over 56 kip (250 kN). Twisting moment and axial force shown in the right side of the axis with thread in: (a) represent forces needed to apply by hand to insert main dowel piece (in green and purple color) before segment getting pushed with the TBM erector toward the previously installed segments with embedded sockets as shown in (b); and (c) represents the final position in the ring.

before ring assembly, and provide greater point load properties. Note that preliminary planning efforts are needed for all cast-in channel systems, namely preparation of installation drawings for segmental lining, as well as effects on ring construction logistics that need to be closely coordinated with the contractor and tunnel boring machine (TBM) operation team.

One of the most suitable applications of cast-in channels is in railway tunnel and especially high-speed rail tunnels. This is because of requirements for anchoring many electrification components to the tunnel lining, such as catenary support points, catenary wire anchoring, wheel tensioners, anchor points (locations where additional supports for catenary or ancillary wires such as signal and communication cables could be mounted inside the tunnel), and line feeders (Fig. 11.4d).

In addition, in these tunnels, resistance to fatigue as a dynamic type of load is a key requirement that cannot be

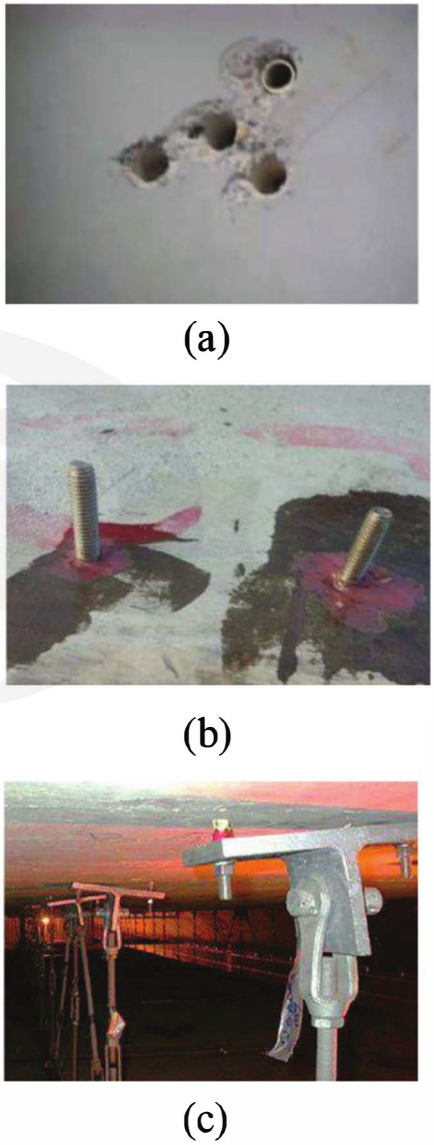

Fig. 11.4a—Major issues with post-installed anchors: (a) drilling; (b) installation quality; and (c) fixing failure.

easily met by post-installed anchors. Finne tunnel, 4.3 miles (7 km) long, twin tunnel tubes, 31.5 ft (9.6 m) diameter high-speed railway line from Erfurt to Leipzig (Germany), is one such example. Figure 11.4e shows all stages of building a cast-in fastening system for this tunnel from design to final service.

To provide protection against fresh concrete penetrating the anchor channels, a filling strip is provided that can be removed once installed so that the anchor channel rails, together with hook bolts, can be installed. Such integrated fastening systems can be employed for the temporary assembly of supply and transport lines, walkways, or working platforms while the tunnel is being driven. Similar systems have been used for subway tunnels such as the 15.5 mile (25 km) long, 5+1 segmental ring configuration (3.4.5) Shenzhen Subway Line 9. In this tunnel, due to requirements for anchoring in eight different locations all around the tunnel perimeter, a full-ring cast-in channel integrated system was adopted for power rail fixing, safety walkway fixation, and support of cables and mechanical and electrical equipment. Also, utility tunnels such as the 5.3 mile (8.5 km) long, 10 ft (3 m) diameter, Berlin Bewag tunnel with 5+1 ring configuration have taken advantage of the cast-in channel systems to house underground high-voltage cable networks.

Cast-in fastening systems provide similar opportunities for road tunnels with light fixtures, signal facilities, ventilation, and exhaust air ducts. Figure 11.4f shows another major opportunity for modern fastening systems in road and rail tunnels for supporting plenum slabs. Tension rod systems are quick and reliable mounting systems and favorable solutions when there is a high demand for loading capacity and high demand on corrosion and fire protection.

Fig. 11.4b—Post-installed fastening system without drilling and through curved channels anchored into segments using connection bolts and mounting plates at the back.

CHAPTER 12—TOLERANCES, MEASUREMENT, AND DIMENSIONAL CONTROL

Tolerances are the allowable deviations of actual dimensions of segmental lining either as individual components or as a system from their design dimensions. Deviations from the nominal geometry can be accepted when they do not result in lining damages and do not negatively impact the intended function and service of the tunnel. It is important to achieve the highest possible level of accuracy during the production and installation of segments; however, tolerances should not be unjustifiably tight to drive costs up through exaggerated demands in terms of accuracy. Accordingly, the design engineer should examine and specify tolerances on a project-specific basis and consider them in all relevant stages of segment design and analysis.

The allowable deviations of individual segment dimensions from the design dimension just after production are production tolerances. Construction tolerances, which include installation tolerances of segmental ring inside tunnel boring machines (TBMs), and subsequent deformations of the ring during and after TBM advances, need to be considered separately from the production tolerances. Therefore, segmental lining tolerances are often broken down into two main categories of production tolerances and construction tolerances.

12.1—Production tolerances

Considering production tolerances, a distinction should be made between formwork tolerances and segment tolerances. Tolerances of formwork used for segment produc-

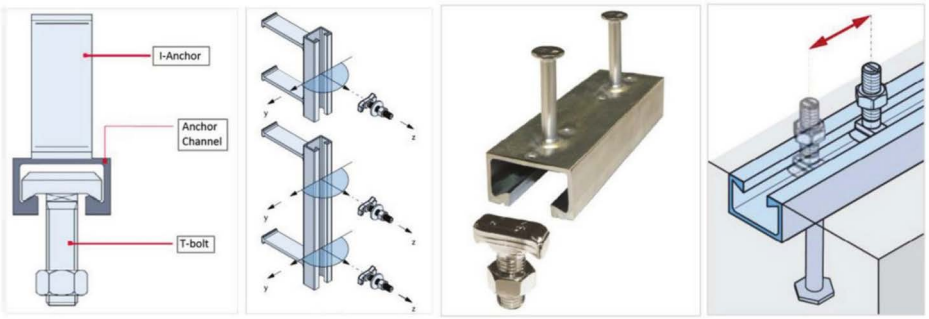

Fig. 11.4c—Cast-in fastening system for segments including channels with welded anchors and bolts (shown are flat channels, but curved anchor channels are similar).

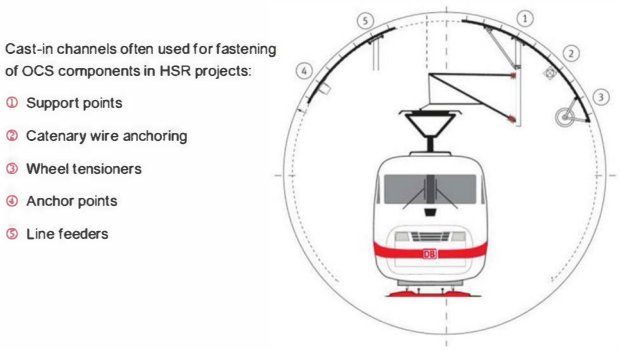

Fig. 11.4d—Schematics of electrification components to be anchored to tunnel lining in a high-speed rail line.

tion and the segment itself after production should be set tight to guarantee required production tolerances. Due to direct impact of formwork precision on segment tolerances, high-precision formwork is necessary for the precast tunnel segment production. Nonetheless, production tolerances for the formwork should be set to allow effects of temperature and deformation on formwork during segment production as well as formwork wear and tear. ÖVBB 2011 specifies ±0.004 to ±0.012 in. (±0.1 to ±0.3 mm) as the range of tolerances for high-precision steel forms for the reference dimensions shown in Fig. 12.1 at an ambient temperature of 64°F ± 4 (18°C ± 2). The range of ÖVBB 2011 tolerances for formwork, with the exception of width and side flatness dimensions, however, seems to be extremely tight. Figure 12.1 shows typical formwork tolerances for midsize tunnels.

While tolerances of produced segments before storage, transportation, and installation inside TBMs should not be too different from the formwork, the transportation and installation tolerances need to be less tight than those for formwork to take into account effects of temperature, shrinkage, creep, and segment self-weight. Effects of concrete creep is negligible, and segment tolerances are often controlled by storage and transportation. Therefore, guidelines such as ÖVBB 2011 define segment production tolerances as a summation of formwork tolerances and allowable deformations due to temperature (in the range of –22 to 113°F [–30 to +45°C]) and shrinkage (considering a relative humidity of 70 percent for determination of shrinkage value). Table 12.1a shows a comparison between formwork and segment tolerances for reference dimensions shown in Fig. 12.1. Note that most reference segment dimensions are measured on the inside of the segments due to full-face contact with high-precision forms. A comparison between these values shows that segment production tolerances are 1.1 to 5.5 times greater than the formwork tolerances, depending on the nature of measured reference dimension.

Specifying formwork tolerances may be helpful for dimensional control in the preproduction phase. Nonetheless, current practice is to specify segment dimension tolerances in contract drawings and specifications and control them directly during segment production in the precast plant. The dimensional tolerances for segments depend mainly on functions and serviceability requirements of tunnels, as well as size of the tunnel segmental ring. Different guidelines provide different ranges of segment tolerances. As shown in Table 12.1b, JSCE 2007, Ril 853:2011, ZTV-ING:2007, and DAUB:2013 provide segment tolerances for all tunnels, rail tunnels, road tunnels, and tunnels of different sizes, respectively. Production tolerances specified by DAUB:2013 in Table 12.1b are for all types of tunnels with segmental rings with internal diameter of smaller than 26 ft (8 m) or larger than 36 ft (11 m). DAUB:2013 recommends a linear interpolation of tolerances provided for tunnels within these two size categories and considering a roundup to 0.004 in. (1/10 mm) when needed. Reference segment dimensions in Table 12.1b are often divided into four major categories of linear segment dimensions; angular deviations and flatness of joints (or sides); dimensions of gasket, connectors, and accessories; and closed-ring dimensions. Note that closed-ring dimension tolerances are system tolerances that need to be controlled using the test rings erected horizontally in the precast plant. This type of tolerance is a production type of tolerance and different from construction tolerances that will be discussed in following sections. Among nearly 20 tolerances described in Table 12.1b, four major dimensional tolerances often emerge as the most critical and need special attention. These four tolerances include segment width, longitudinal joint taper/conicity deviation, segment circumferential (arch) length, and gasket groove (Handke 2012). Segment width inaccuracies may cause severe damage in the form of wide longitudinal cracks whereas excessive longitudinal joint conicity deviations impact the intensity of the forces transferred between segments in the longitudinal joints with implications on concrete cracking due to compression or, more importantly, spalling if additional reinforcement is not considered in the longitudinal joints. Circumferential length (arc) and gasket groove tolerances may have a major impact on the sealing performance of gaskets in the form of excessive gap or offset.

Differences between specified tolerances for each reference dimension presented in Table 12.1b are relatively small, with DAUB:2013 specifying the tightest and most complete set of tolerances. These tolerances are in good agreement with most of project specifications with the exception of warping tolerances, which seem to be less tight than most project specifications. Some project specifications do not allow for any use of segments that have been produced outside the tolerance requirements. DAUB:2013, on the other hand, allows these segments to be used but only in areas with low projected tunneling forces, provided gasket performance is not compromised and calculation demonstrates sufficiency of reinforcement in the joints and in deep-beam analysis in the event of exceeding joint distortion and segment width specified tolerances.

12.2—Measurement and dimensional control

A proper quality control system is essential to minimize the fabrication of defective segments and produce high-precision segments with tolerances within the limits imposed by contract documents. Segments, like any other concrete element, are subject to temperature, shrinkage, and creep

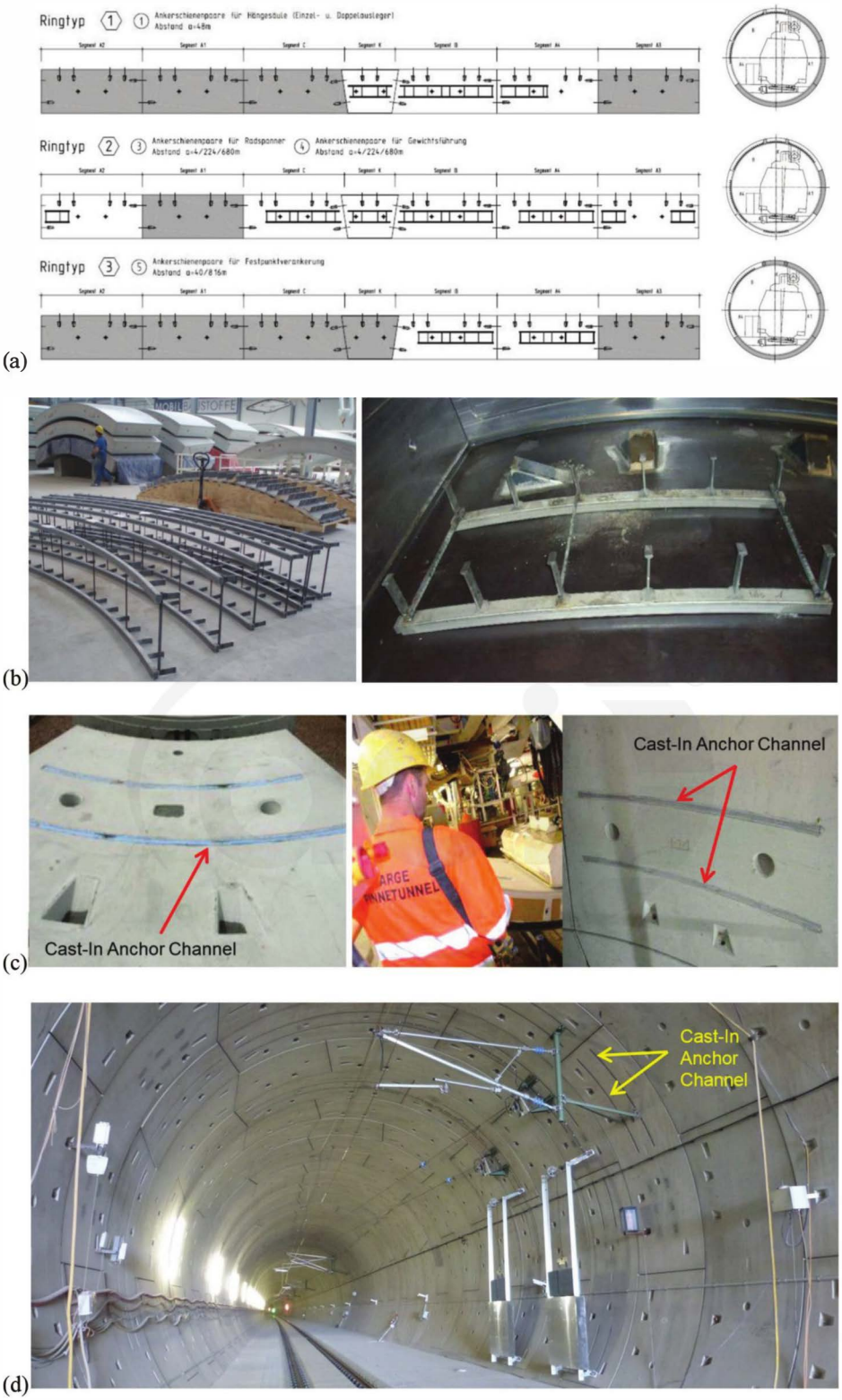

Fig. 11.4e—Curved cast-in channels as the most favorable fastening system in railway and high-speed rail tunnels: (a) installation drawings for segmental lining layout; (b) cast-in channels delivered in pairs to precast segment plant, laid and assembled in segment formwork; (c) handling and storage of segments with integrated fasteners in precast yard using vacuum erector; and (d) tunnel after fit-out and shortly before trial run.

Fig. 11.4f—Modern fastening systems with tension rods for supporting intermediate slab in Dobrovsky tunnel, Czech Republic.

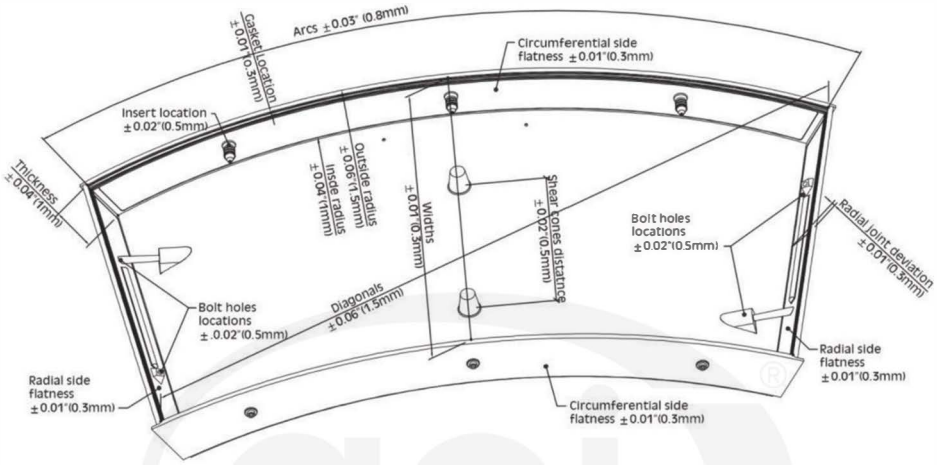

Fig. 12.1—Typical segment formwork tolerances for midsize tunnel projects.

Table 12.1a—Comparison between formwork tolerances and segment tolerances in typical segments for use in midsize tunnel projects

Reference dimensions	Formwork tolerances, in. (mm)	Segment tolerances, in. (mm)
Width	1/84 (±0.3)	1/16 (±1.6)
Thickness	1/25 (±1)	1/8 (±3.2)
Circumferential length (arc)	1/32 (±0.8)	1/16 (±1.6)
Inside radius	1/25 (±1)	1/16 (±1.6)
Outside radius	1/17 (±1.5)	1/4 (±6.3)
Diagonals	1/17 (±1.5)	1/16 (±1.6)
Warping	1/17 (±1.5)	1/12 (±2)
Longitudinal/radial joint deviation	1/42 (±0.2)	1/32 (±0.8)
Sides flatness	1/84 (±0.3)	1/32 (±0.8)
Location of gasket groove axis	1/84 (±0.3)	1/32 (±0.8)
Dowel insert location	1/50 (±0.5)	1/32 (±0.8)
Bolt hole location	1/50 (±0.5)	1/32 (±0.8)
Shear cones/erector pocket location	1/50 (±0.5)	1/16 (±1.6)

deformations after casting. Therefore, dimensional control measurements should take place after segments gained full maturity in approximately 28 days to avoid these early-age deformation deviations. However, this monitoring method is not suitable, as it would significantly reduce the productivity of the segment manufacturing process. Nonetheless, during production and storage phases, temperature, relative humidity, and other ambient conditions are maintained relatively constant in the plant; therefore, any dimensional deviation due to temperature or shrinkage can be neglected. Accordingly, the geometry at one specific phase of the production should be measured and controlled—that is, after segment stripping (demolding). It is important that all segment measurements be taken at the same time.

The measurement program should be implemented on the individual segments as well as segmental systems in the form of test rings. The most traditional method is manual measurement by means of steel templates, which are readjusted repeatedly in the course of quality control. Additionally, micron rods, caliper squares, precision measuring tapes, and measurement arms are used (ÖVBB 2011). However, conventional instruments such as micron rods or templates lack the global geometrical certification for an object. The measurement systems using theodolite and photogrammetry are among other alternative methods that lack the necessary speed and accuracy (within a few tenths of a millimeter) needed for regular quality control. Three-dimensional (3-D) industrial measurements prevail as the only accurate measuring method that can meet such high demands at a rate required for a high-speed quality control/quality assurance program. As shown in Fig. 12.2a, 3-D measurements using a laser interferometer system enables the accurate digitization of surfaces by direct polar coordinate measurement.

Table 12.1b—Production segment tolerances specified by guidelines and standards (Bakhshi and Nasri 2018e)

	Apply to which type of tunnel	All, in. (mm)	Railway, in. (mm)	Roadway, in. (mm)	Different sizes, in. (mm)	
Type of tolerance	Reference for dimensions	JSCE 2007	Ril 853:2011	ZTV-ING:2007	DAUB:2013 ID < 26 ft (8 m)	DAUB:2013 ID < 36 ft (11 m)
Linear segment dimensions	Width	±0.04 (±1)	±0.02 (±0.5)	±0.024 (±0.6)	±0.02 (±0.5)	±0.03 (±0.7)
	Thickness	+0.2, −0.04 (+5, −1)	±0.12 (±3)	±0.12 (±3)	±0.12 (±3)	±0.16 (±4)
	Circumferential length (arc)	±0.04 (±1)	±0.024 (±0.6)	—	±0.024 m(±0.6)	±0.027 (±0.7)
	Inside radius	—	±0.06 (±1.5)	±0.06 (±1.5)	±0.06 (±1.5)	±1 (±2.5)
	Outside radius	—	—	±0.08 (±2)	—	—
	Diagonals	—	—	—	±0.04 (±1)	±0.08 (±2)
	Warping (vertical spacing of fourth segment corner from plane formed by other three corners)	—	—	—	±0.2* (±5)	± 0.32* (±8)
Joints angular deviations and flatness	Longitudinal joint deviation	—	±0.0 12 (±0.3) [±0.04 degrees†]	±0.012 (±0.3)	±0.012 (±0.3)	±0.02 (±0.5)
	Longitudinal joint taper/ conicity deviation	—	±0.02 (±0.5) [±0.01 degrees†]	±0.02 (±0.5)	±0.02 (±0.5)	±0.03 (±0.7)
	Longitudinal/circumferential joint flatness	—	±0.02 (±0.5)	±0.02 (±0.5)	±0.012 (±0.3)	±0.02 (±0.5)
Gasket, connec-tors, and accessories dimensions	Location of gasket groove axis	—	±0.04 (±1)	±0.06 (±1.5)	±0.04 (±1)	±0.04 (±1)
	Sealing groove width/depth	—	+0.008 (+0.2), −0	±0.008 (±0.2)	±0.008 (±0.2)	±0.008 (±0.2)
	Bolt hole/dowel insert location	±0.04 (±1)	±0.04† (±1)	—	±0.04 (±1)	±0.04 (±1)
	Shear cones/erector pocket location	—	±0.08† (±2)	—	±0.08 (±2)	±0.08 (±2)
Closed-ring dimensions	Outer diameter	±0.3 (±7) (6.5 ft [2 m] < ID < 13 ft [4 m]) ±0.4 (±10) (13 ft [4 m] < ID < 20 ft [6 m]) ±0.6 (±15) (20 ft [6 m] < ID < 26 ft [8 m]) ±0.8 (±20) (26 ft [8 m] < ID < 40 ft [12 m])	±0.4 (±10)	—	±0.4 (±10)	±0.6 (±15)
	Inner diameter	—	±0.4 (±10)	—	±0.4 (±10)	±0.6 (±15)
	Outer circumference (to be measured in three planes)	—	±1.2 (±30)	—	±1.2 (±30)	±1.2 (±45)
	Assembly misalignment	±0.3 (±7) (6.5 ft [2 m] < ID < 13 ft [4 m]) ±0.4 (±10) (13 ft [4 m] < ID < 20 ft [6 m]) ±0.4 (±10) (20 ft [6 m] < ID < 26 ft [8 m]) ±0.6 (±15) (26 ft [8 m] < ID < 40 ft [12 m])	±0.4 (±10)	—	—	—

*Warping tolerances specified by DAUB:2013 seem to be less tight than most of reviewed project specifications.

†Only available in DS 853:1993.

Measurement of a single spherical retro-reflective prism enables the skilled operator to comprehensively measure the full profile of the object to be measured, with over 20 segments per shift being achievable (Clarke-Hackston et al. 2006). In addition to measurements taken from a single standpoint, the laser tracker should be relocated to a second standpoint, preferably near the other end of the segment (as shown in Fig. 12.2a(b)) to perform a complete measurement of form or segment dimensions. Figure 12.2b shows the output of spatial analyzer 3-D graphical software platform used for running a laser tracker that provides tolerances,

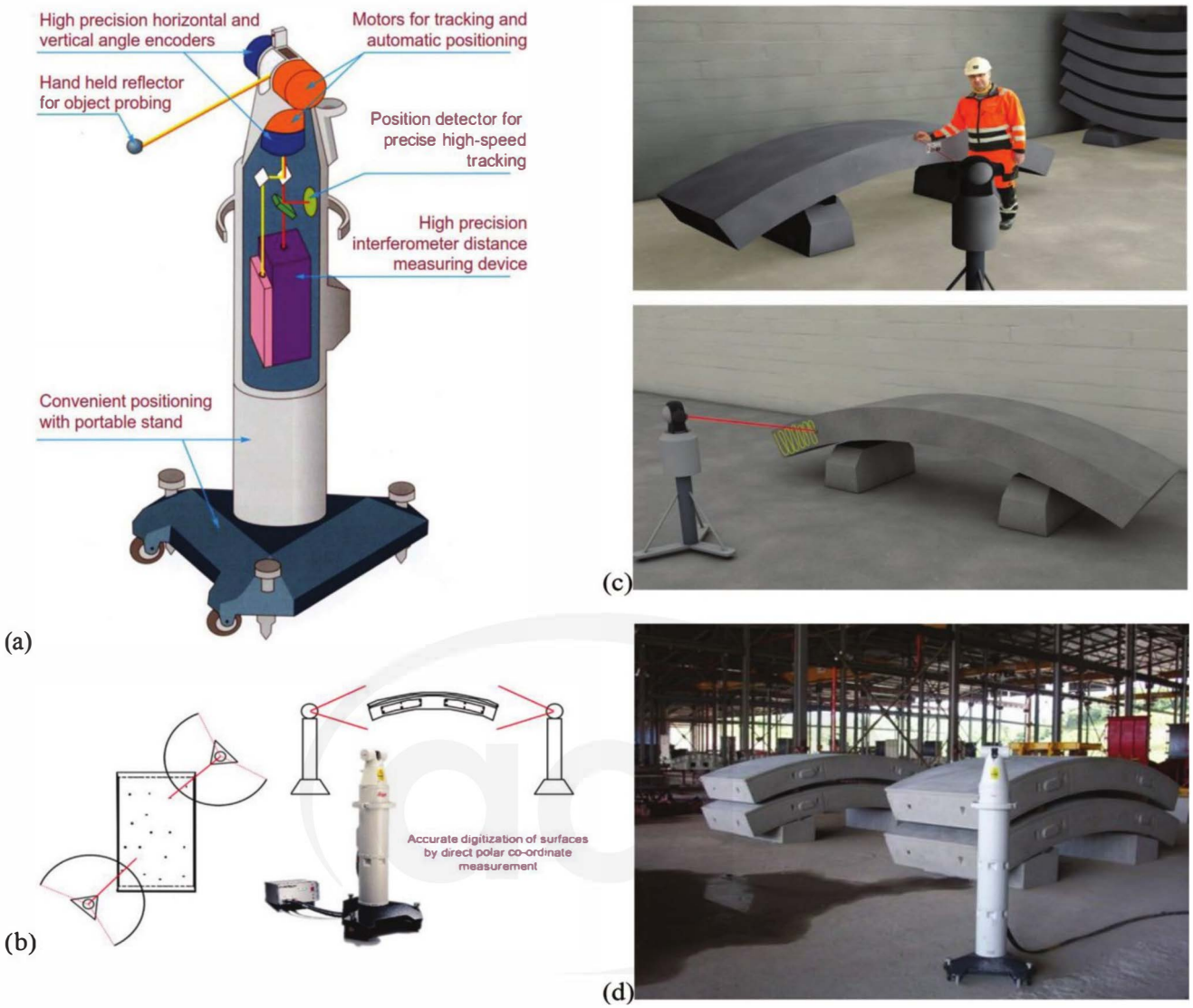

Fig. 12.2a—Three-dimensional measurement: (a) laser interferometer schematic; (b) laser tracker system; (c) instrument location for mold; and (d) stacked segments for rapid measurement.

best-fit of external surfaces, and derivation of all relevant intersection measurements.

12.3—Test ring and dimensional control frequency

Dimensional control occurs in preproduction and during the production. In the preproduction phase, dimension control is carried out on formwork or segments to measure tolerances of reference dimensions, and on the test rings, as shown on Fig. 12.3a, for controlling system tolerances. Although some project specifications require building test ring systems of three rings on top of each other in the preproduction phase, this seems to be unnecessary, especially considering unavoidable permutations. One of the original goals of test rings decades ago was to check for alignment of bolting and general ring assembly, including segment-to-segment and ring-to-ring connections. With 3-D computer-aided design (CAD) of forms, the risk of bolting or assembly location errors within the forms, which were possible with manual drafting 25 years ago, are, for all practical purposes, eradicated. As the test ring system, the recommendation is to build a single ring or a double ring with the bottom test ring to be measured completely. All guidelines that ask for segmental systems demonstration in the closed ring recommend test rings without the elastomer gasket in place to avoid recovery forces.

As shown on Table 12.1b, reference dimensions to be verified on the assembled test ring include outer and inner diameters (at least in two axes), outer circumference (to be measured in three planes), and joint assembly misalignment. ÖVBB 2011, in addition, has joint opening and joint misalignment as other system tolerances to be verified in the test ring. Although standard practice is based on dimensional control at the segment casting plant, for a good start to production, it is crucial to carry out 3-D testing of each form and testing ring at the formwork manufacturer's plant before shipping the forms to precasters. A 10-measurement system shown in Fig. 12.3b has been presented as an alternative formwork tolerance measurement method to individual

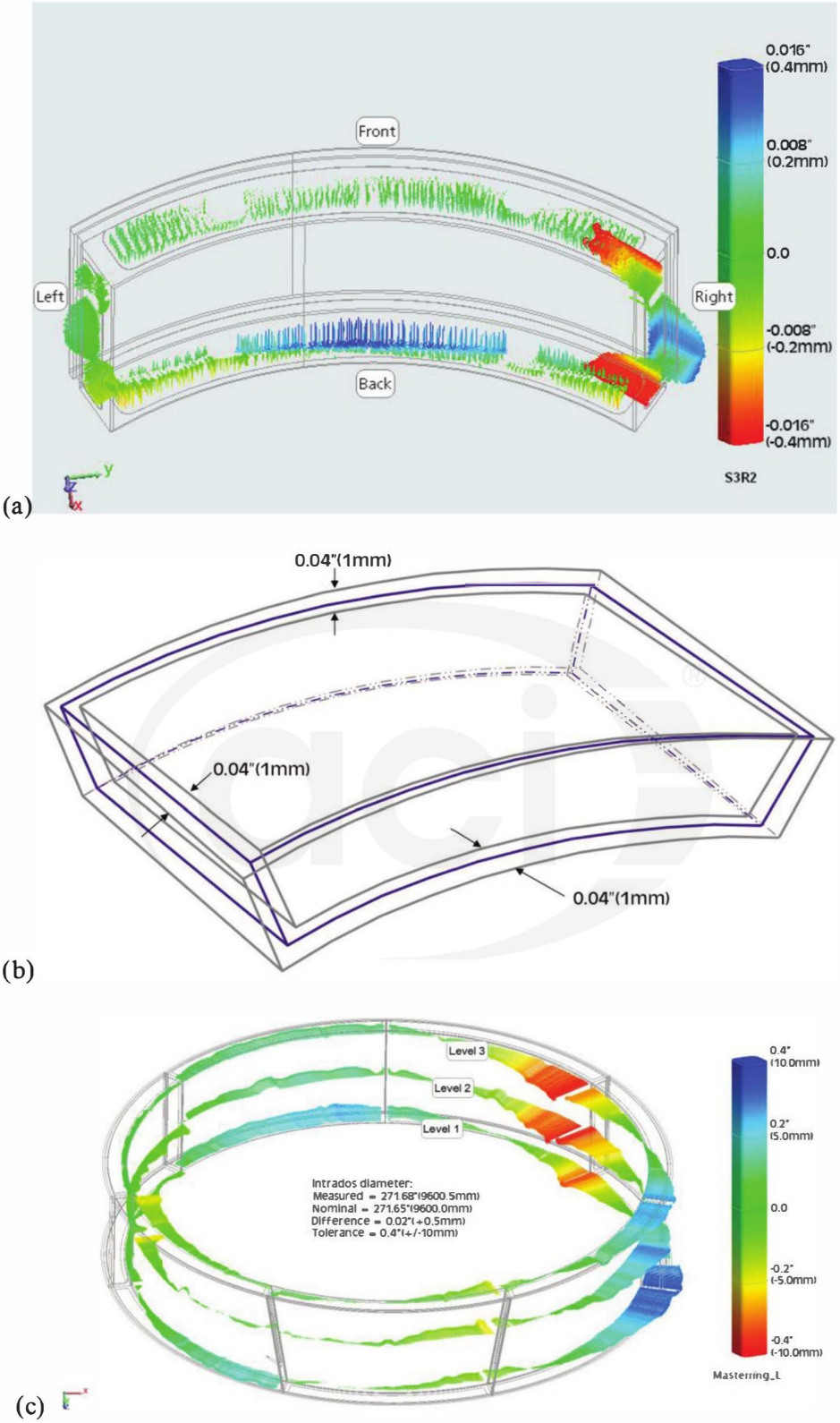

Fig. 12.2b—Spatial analyzer 3-D graphical software platform output: (a) typical segment tolerances; (b) best-fit of external surfaces and typical deviations from referenced dimensions; and (c) tolerances on virtual (test) ring build.

reference dimensions in Fig. 12.1 and Table 12.1b. Both systems are acceptable, as they can assure segment dimension accuracies with Table 12.1b referencing dimension tolerances important from design perspective and Fig. 12.3b with tolerances easier for measurement procedure.

Two major factors for dimensional control during the production phase are testing objects and testing frequency.

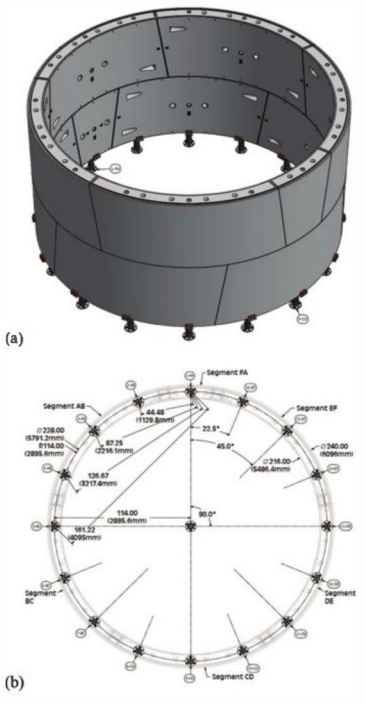

(c)

Demonstration Ring Dimensions		RING # 1		RING # 2	
Date Measured					
Date Ring Manufactured					
Internal Diameter		Nom. (inches) = 216.00		Nom. (inches) = 216.00	
Measurement Position		Measured	Deviation	Measured	Deviation
1-FA_9-CD	Top	216.07	0.07	215.90	-0.10
1-FA_9-CD	Bottom	216.13	0.13	215.88	-0.12
2-AB_1 -CD	Top	216.13	0.13	215.96	-0.04
2-AB_1 -CD	Bottom	216.00	0.00	216.14	0.14
3-AB_11-DE	Top	216.10	0.10	215.96	-0.04
3-AB_11-DE	Bottom	216.13	0.13	216.13	0.13
4-AB_12-DE	Top	216.13	0.13	215.98	-0.02
4-AB_12-DE	Bottom	216.10	0.10	216.10	0.10
5-BC_13-DE	Top	216.09	0.09	215.90	-0.10
5-BC_13-DE	Bottom	216.00	0.00	215.94	-0.06
6-BC_14-EF	Top	215.90	-0.10	215.88	-0.12
6-BC_14-EF	Bottom	216.00	0.00	215.94	-0.06
7-BC_15-EF	Top	216.00	0.00	215.88	-0.12
7-BC_15-EF	Bottom	216.00	0.00	215.94	-0.06
8-CD_16-EF	Top	216.00	0.00	215.88	-0.14
8-CD_16-EF	Bottom	216.13	0.13	215.90	-0.10
Mean Internal Diameter		216.06	0.06	215.96	-0.04
Allowable ID Tolerance			-0.125 inches		-0.125 inches
Allowable ID Tolerance			+0.125 inches		+0.125 inches

External Circumference		Nom. (inches) = 753.98		Nom. (inches) = 753.98	
		Measured	Deviation	Measured	Deviation
	Top	754.50	0.52	754.25	0.27
	Bottom	754.13	0.14	754.12	0.14
Mean External Circumference		754.31	0.33	754.19	0.20
Allowable External Circumferential Tolerance			-0.251 inches		-0.251 inches
Allowable External Circumferential Tolerance			+1.257 inches		+1.257 inches

External Diameter	Nom. (inches) = 240.00		Nom. (inches) = 240.00	
Mean External Diameter	240.11	0.11	240.06	0.06

(d)

Two Ring Overall Height (with NO shims between rings)	Nom. (inches) =	119.61
Measurement Position	Measured	Deviation
1-FA	119.62	0.01
2-AB	119.62	0.01
3-AB	119.62	0.01
4-AB	119.62	0.01
5-BC	119.62	0.01
6-BC	119.62	0.01
7-BC	119.62	0.01
8-CD	119.62	0.01
9-CD	119.62	0.01
10-CD	119.62	0.01
11-DE	119.62	0.01
12-DE	119.62	0.01
13-DE	119.62	0.01
14-EF	119.62	0.01
15-EF	119.62	0.01
16-EF	119.62	0.01
Mean Overall Height	119.62	0.012

Note: Dimensional height measured is from bottom circumferential face of bottom ring to top circumferential face of top ring.

TEST RING BUILD	
Conformance	X
Non-Conformance	

Checked By: Date

Fig. 12.3a—Two-ring test ring in preproduction phase: (a) schematics of test ring setup in isometric view; (b) typical reference locations for dimension control in plan view; (c) typical dimensional control Sheet 1 for a midsize tunnel; and (d) typical dimensional control Sheet 2. (Note: 1 in. = 25.4 mm.)

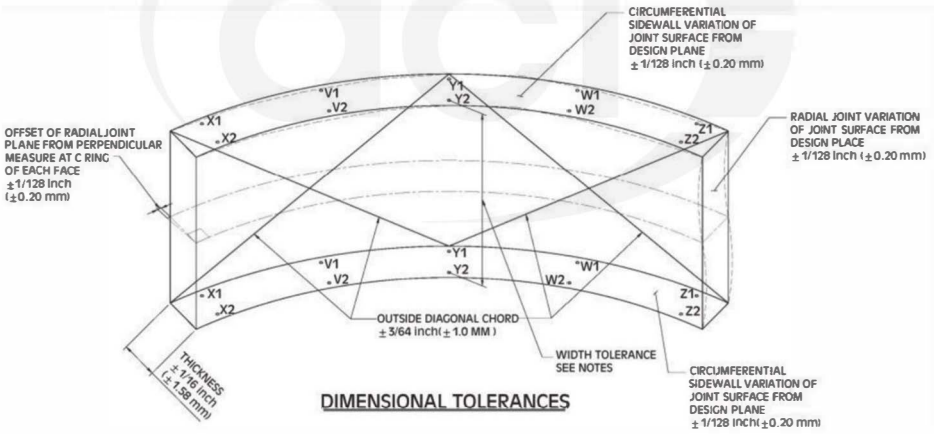

Fig. 12.3b—Alternative tolerance measurement method for formwork dimension control.

Forms, individual segments, and test rings are the three main testing objects that can be measured. Standard practice is to measure tolerances of every segment made for first to 10th casting, and then measuring every 50th segment after that. In some projects, a more frequent controlling program was adopted requesting measuring dimensions of every 10th segment. A dimensional controlling program based on monthly measurement is not recommended considering different production days in a month and working shifts per day from one precaster and one project to another. Some design documents require assembling an extra ring on the test ring after a specific number of casting. This is also not recommended considering the degree of difficulty, the high cost, and little value of such practice. When testing formwork during production, ÖVBB 2011 recommends controlling formwork dimensions after production of every 10 segments, and then after production of every 100 segments. For both segment and formwork dimension control, testing should be resumed at the initial frequency soon after detection of any inadmissible deviations. Setting formwork tolerances during the design and, later, formwork dimension control as an indirect method in preproduction as well as during production phases, can be superior to a classic approach of setting and controlling segment tolerances. This is mainly because any dimension-related problem can be detected before the segment production and can be mitigated accordingly.

12.4—Construction tolerances

Accurate segment geometry is a requirement for smooth installation of segments without any significant constraint.

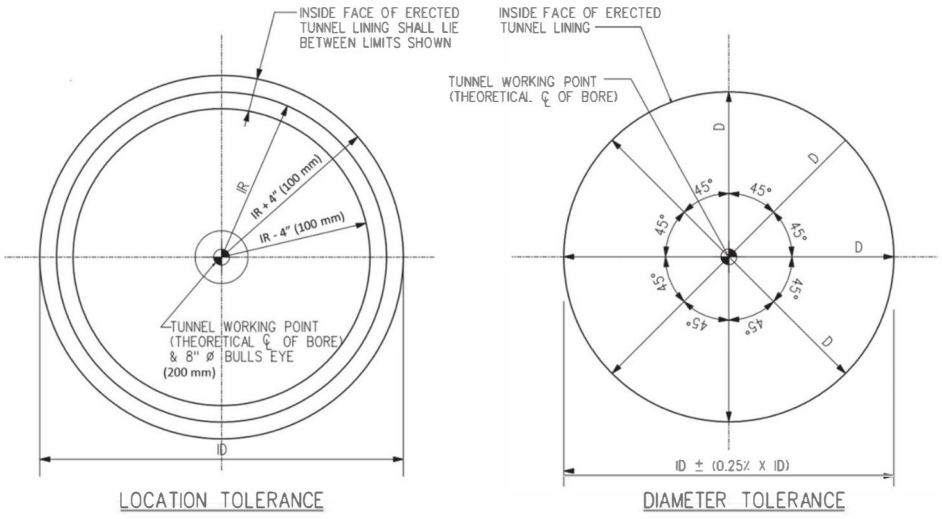

Fig. 12.4a—Typical construction tolerances in contract documents.

However, there are deviations from the nominal position of the segments during the installation phase that are independent of production accuracies and related to construction. These tolerances are referred to as construction tolerance. Ovalization of the ring and corresponding angular deviations and joint misalignment are among these unavoidable construction tolerances. Excessive construction deviations have significant implications, including reduction in quality of the finished tunnel, reduction in advance rate of tunneling, and decreased sealing performance at segment and ring joints.

At an early stage of ring assembly and due to the designed shape of joint or yielding of bolts or dowels, a newly assembled segmental ring may undergo ovalization under segment self-weight. The ovalization can also occur under loading exerted by the TBM backup equipment train that is located behind the TBM shield and used to provide a final staging area for feeding segments to the installation erectors and also carries all the mechanical, electrical, and mucking systems needed for the TBM operation. In addition, uneven beddings of segmental rings in the backfill gout or tunnel uplift during the construction after TBM passage can cause ovalization. While ovalization cannot be completely avoided, it can be limited to significantly low values through controlled ring assembly systems and self-guiding connectors such as dowels and guiding rods. To control ovalization, an allowable deviation from the nominal diameter should be specified. The allowable ovalization tolerance depends on diameter and number of segment joints in a ring, but a common requirement in different guidelines and recommendations is to keep it under 0.25 to 0.5 percent of the internal diameter. In small tunnels with diameters of 13 ft (4 m) or lower, the allowable ovalization is recommended as 1.0 percent of the internal diameter. From a design point of view, the best practice is to provide allowable ring diameter and ring location tolerances in contract documents such as Fig. 12.4a.

Joint misalignment and deviations of segment joint planes from designed full contact area with adjacent segment joint is also unavoidable but need to be limited to permissible values. Ring installation inaccuracies can have a direct impact on joint misalignment and joint opening. Also, uneven segmental ring bedding, in addition to ovalization and uncontrolled torsion in longitudinal joints, can cause joint misalignment in circumferential joints. The allowable joint misalignment depends on allowable tolerances for joint design, connecting devices, and geometry and profile of gaskets. ÖVBB 2011 recommends ±0.2 in. (±5 mm) as the joint misalignment tolerance for tunnel diameters in the range of 10 to 26 ft (3 to 8 m), whereas DAUB:2013 specifies ±0.4 in. (±10 mm). Nonetheless, allowable joint misalignment can be adjusted based on sealing performance requirement and maximum allowable offset for gaskets selected for the project.

Table 12.4—Construction tolerances for ring erection

Maximum ring roll	4 in. (±100 mm)
Ring shape (ovalization) on diameter	±0.25 percent x ID to ±0.5 percent x ID
Maximum relative ring roll	0.4 in. (±10 mm)
Step and slip (lip) due to joint misalignment	0.2 in. (±5 mm)
Maximum gap between joint contact faces	0.2 in. (±5 mm)
Tolerances on absolute vertical position of lining invert	3 in. (±75 mm)

An extensive list of construction tolerances for ring erection, along with their typical allowable values, are summarized in Table 12.4. Figure 12.4b demonstrates different types of joint misalignments. As shown in this figure, maximum relative ring roll, defined as rolling of every ring relative to adjacent rings, corresponds to circumferential joint misalignment whereas step or slips (lips) are related to longitudinal joint misalignment. Maximum allowed gap between joint contact faces corresponds to joint opening and is often specified as 0.2 in. (5 mm) for best gasket performance. Tolerances on absolute vertical position of lining invert is especially important in subsea and river crossings, projects where the tunnel lining is under excessive uplift

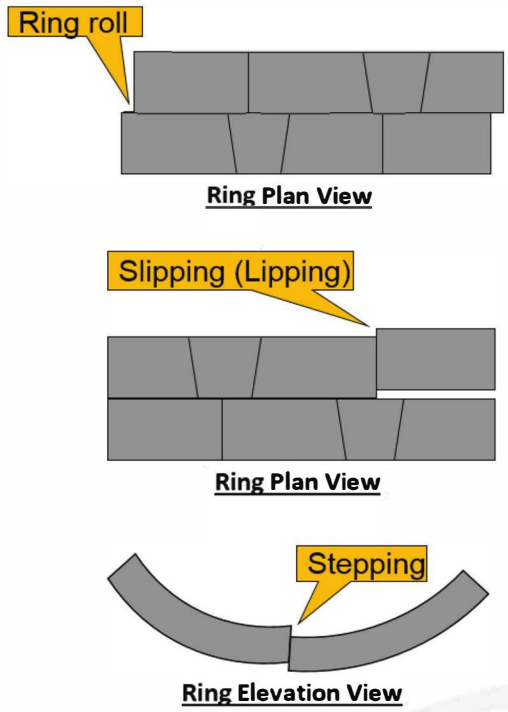

Fig. 12.4b—Schematics of ring roll, slip (lip), and step as different type of joint misalignment in segmental lining system.

pressure, or in transportation tunnels with high demand on accurate location of top of rail or profile grade line. Other tolerances that are not related to ring erection but should be considered among construction tolerances include eccentricity of the locations of the stack supports during storage and transportation phases, and eccentricity of jack pads with respect to the centroid of segments during the stage of TBM thrust jacking force. These eccentricities are discussed in the previous chapters.

Current tolerances specified in practice are evaluated through referencing results of finite element method (FEM) simulation studies on segment joints, and effects of tolerances on contact deficiencies to evaluate consequential structural damages (Cavalaro et al. 2012). With a focus on longitudinal joint deviation and segment width tolerances, results show that the allowable tolerances obtained with the recommended inverse analysis method are above the recommendation found in the contract documents and guidelines. Such results shed a light to the possibility of loosening currently specified tolerances, providing further research studies confirm similar results.

CHAPTER 13—REPAIR OF DEFECTS

Structurally damaged and misaligned segments should be repaired or replaced to maintain structural integrity, durability, and watertightness of the segmental lining system. Minor damage to concrete segments before erection can be repaired by removing the defective or damaged area to sound concrete and patching with materials and procedures reviewed and approved by the project engineer. A table, such as Table 13, should be provided covering procedures for repair of segment defects. This table should include a description of the type and extent of damage, and corresponding repair procedures in accordance with ACI 224.1R and ACI 546R, or the basis for rejection of segments. All oil-stained and unsightly rings should be cleaned before erection. All the rings that have been stained during or after erection should be cleaned as well. For detailed information about types, causes, mitigation, and repair of damages of segmental lining, refer to SIG WG N. 2:2019.

CHAPTER 14—DURABILITY

Tunnels, as important underground structures, are typically designed for a service life of more than 100 years. Mechanized tunneling, with tunnel boring machines (TBMs) as the most common excavation method, is often associated with continuous installation of precast concrete segmental rings behind TBM cutterheads. In these tunnels, the durability of a tunnel is directly related to the durability of the concrete segments acting as both the initial support and the tunnel final lining. In this chapter, the most-frequent degradation mechanisms of concrete linings are briefly discussed. This includes corrosion of reinforcement by chloride attack and carbonation, as well as sulfate and acid attacks as major deterioration processes caused by external agents. Alkali-aggregate reactions caused by internal chemical reactions and frost attack and freezing-and-thawing damage are also discussed. Stray current-induced corrosion is one of the major durability concerns specific to railway and subway tunnel linings. Mitigation methods for stray current corrosion, including use of fiber-reinforced concrete (FRC) segments, are presented and durability of segments under coupling effects of stray current with other conventional degradation factors are explained. The prescriptive approach for durability design is based on BS EN 206-1:2013, BS EN 1992-1-1:2004, and ACI 318. These codes are explained and comparison is made between the methods. Exposure classes related to environmental actions as the main inputs to the prescriptive approaches are explained separately. Using these standards, recommendations made on concrete strength class, maximum water-cement ratio (w/c), minimum cement content, minimum air content, and other requirements to ensure typical service life of tunnels are explained.

14.1—Conventional degradation mechanisms in tunnel linings

Durability issues of bored tunnels need to be addressed from the perspective of degradation mechanisms specific to tunnel segmental linings. Due to different geological environments surrounding tunnels and the specific use of each tunnel, tunnel linings are exposed to different aggressive environments. Possible degradation and damage mechanisms in bored tunnels include corrosion of reinforcement by chloride attack and carbonation, sulfate and acid attacks, alkali-aggregate reactions, and freezing-and-thawing damages. These mechanisms will be briefly discussed.

14.1.1 *Reinforcement corrosion*—Unprotected steel materials tend to corrode quickly. However, steel bars embedded in concrete as reinforcement are protected by a passive layer

Table 13—Procedures for repair of segment defects*

Class of damage/ defect	Description	Location	Extent	Remedy
Class A1 nonstructural patching	Blowholes and air voids	All locations except gasket groove, intrados, and caulking groove	Diameter > 3/4 in. (20 mm) or depth > 3.8 in. (10 mm)	Repair Procedure 2A
Class A2 nonstructural patching		Intrados, caulking groove, and gasket groove	Diameter > 3/4 in. (20 mm) or depth >3/16 in. (5 mm)	Repair Procedure 2A
Class B nonstructural patching		Gasket groove	Depth or diameter > 3/32 in. (2 mm)	Repair Procedure 1
Class C nonstructural cosmetics	Chipping and spalling	Gasket groove edges	Area: Length > 3/4 in. (20 mm) Depth > 3/16 in. (5 mm)	Use Procedure 2A or 2B
Class D nonstructural cosmetic		All locations except gasket groove edges	Area: Length > 1-1/2 in. (40 mm) or Depth > 9/16 in. (15 mm)	Use Procedure 2A or 2B
Class E1 surface irregularities	Local protrusions	Nonformed surfaces	>3/16 in. (5 mm)	Stone-rubbed or ground
Class E2 surface irregularities		Joint faces	>0.04 in. (0.5 mm) high	Stone-rubbed or ground, check mold
Class F localized surface cracking and crazing	Minor nonstructural local defects	Gasket groove and extrados edge on joint faces	Cracks > 0.008 in. (0.3 mm) wide to be assessed by examination	Review for approval of repair procedure
Class G1 structural cracks	Localized structural cracking	Longitudinal joint bearing areas only	Any crack	Review for approval of repair procedure
Class G2 structural cracks		Circumferential joint bearing area only	Cracks < 0.002 in. (0.05 mm) wide	No repair
Class G3 structural cracks		All locations except as noted in Class G1 and G2	Cracks > 0.002 in. (0.05 mm) and < 0.008 in. (0.2 mm) wide that do not cross the gasket groove	Use Procedure 3
Class G5 structural cracks		All locations	Multiple cracks > 0.008 in. (0.2 mm) wide emanating from a single source and producing a wedge pattern on the bearing face	Reject segment
Class H structural cracks	Cracking through segment	All locations	Full depth	Reject segment
Class J1 honeycombing	Exposed aggregate/ poor consolidation	At locations within proximity of circumferential and longitudinal joints (bearing areas)	Maximum 2 in. (50 mm) depth > 2 in. (50 mm) to be assessed by examination	Reject segment
Class J2 honeycombing		All locations except as noted in Class J1	Maximum 2 in. (50 mm) depth > 2 in. (50 mm) to be assessed by examination	Use Procedure 3
Class K structural damage	Damage exposing reinforcing bars	All surfaces except longitudinal joints	To be assessed by examination	Review for approval of repair procedure

formed on the surface of the steel due to high alkalinity of hydrated cement in concrete (pH of 12 to 13). Without the passive layer, the steel corrodes at rates at least 1000 times higher than when embedded in concrete (ACI 222R). The destruction of the passive layer and rapid reinforcement corrosion occurs when the alkalinity of the concrete is reduced by carbonation or when the chloride concentration in concrete at the level of reinforcement is increased to corrosion threshold level. Chloride ions, oxygen, and moisture should also be available to sustain this reaction. As a result, pitting corrosion reduces the size of the steel bar and uniform corrosion leads to cracking and spalling of the concrete.

14.1.1.1 *Reinforcement corrosion of reinforcement induced by chloride attack*—Chloride-induced corrosion of reinforcement is the main cause of degradation in tunnels lined with reinforced concrete (RC). As shown in Table 14.1.1.1, ITA Working Group on Maintenance and Repair of Underground Structures (1991) presents 13 tunnels that have been significantly damaged due to corrosion by chloride ingress before 1991 (Abbas 2014).

Chloride-induced corrosion is even a greater durability issue specifically in subsea, sea outfall, and road/rail tunnels.

Table 13, (cont.)—Procedures for repair of segment defects*

*REPAIR PROCEDURE 1
MATERIAL: Type II cement; Silica sand
Mix at the rate of 1 part cement to 2.5 parts sand, with 0.4 *w/c*.

PROCEDURE:
1. Clean and wire brush off all dirt and dust from areas to be filled. Dampen repair area with water.
2. Measure and mix cement and sand with water in accordance with the instructions. Do not retemper mixture with water.
3. Fill the repair area and sack rub the finished surface immediately.

REPAIR PROCEDURES 2A & 2B
MATERIAL 2A To be used in areas less than 1-1/2 in. (40 mm) long and 9/16 in. (15 mm) deep.
Epoxy mortar.
The properly mixed epoxy can be mixed with oven-dried silica sand as recommended by the manufacturer to obtain desired consistency. Mix until uniform consistency is achieved. Do not mix quantities larger than can be used within the work life of the material.

PROCEDURE:
1. Repair area should be dry. Remove any dust, laitance, grease, oils, or loose materials from the area to be repaired and wire brush.
2. Place mixed materials into the void, working the material by trowel or spatula to ensure bond. Strike off level to existing concrete.
3. Cure the epoxy mortar at a minimum temperature of 40°F (4°C).
4. Ensure accurate profile by removing any excess mortar by grinding.

MATERIAL 2B To be used on area in excess of 1-1/2 in. (40 mm) long and 9/16 in. (15 mm) deep.
Prepackaged modified cementitious one-component patching mortar with low shrinkage, low permeability, and good freezing-and-thawing durability.

PROCEDURE:
1. Saw-cut all edges of repair to a depth of 0.6 in. (15 mm) with mechanical disc.
2. Break back to sound concrete and remove surplus material by low impact method. Clean surface to remove all loose particles, dirt, and dust from areas to be filled. Dampen surface to a saturated surface-dry condition just prior to the application of the mortar. No freestanding water.
3. Measure and mix the patching compound with water in accordance with the manufacturer's instructions. Do not retemper mixture with water.
4. Fill the repair area and finish open edges with a steel trowel and use temporary formwork when necessary, ensuring that repair material is thoroughly compacted. Strike off level to existing concrete.
5. Wet-cure for a minimum of 7 days until the patch is sufficiently cured or apply a curing compound as recommended by the manufacturer of the patch material.

REPAIR PROCEDURE 3 – Crack sealing
MATERIAL: Surface-seal epoxy injection gel.
Mix in accordance with the manufacturer's recommendation. Do not mix more materials than can be used within the material work life.

PROCEDURE:
1. Concrete will be clean and sound. Remove dust, laitance, grease, oil, and foreign matter or other contaminants that will affect the bond of the material.
2. Mix injection gel as recommended by the manufacturer. Inject gel from coaxial cartridges with a static mixing head and discharge a small amount until proper blending is achieved.
3. Work the material into the crack to seal it.
4. Remove excess resin from the surface, adjacent to the crack.
5. Allow to harden before removing any remaining excess material with a rubbing stone.

Table 14.1.1.1—Damaged/corroded tunnels due to chloride ingress (ITA Working Group on Maintenance and Repair of Underground Structures 1991; Abbas 2014)

Tunnels	Location	Tunnel type	Diameter, ft (m)	Completion year
Basel/Olten Hauenstein	Switzerland	Railway	—	1916
Northern Line Old Street to Moorgate	United Kingdom	Metro	11.5 (3.5)	1924
Shimonoseki/Moji Kanmon	Japan	Railway	—	1944
Mikuni National Route 17	Japan	Highway	25 (7.6)	1959
Uebonmachi-Nipponbashi	Japan	Railway	32.8 (10)	1970
Dubai	United Arab Emirates	Road	11.8 (3.6)	1975
Tokyo Underground	Japan	Road	—	1976
Berlin Tunnel Airport	Germany	Road	—	1978
Second Dartford	United Kingdom	Road	31.5 (9.6)	1980
Mass Transit Railway	Hong Kong	Metro	18.4 (5.6)	1980
Ahmed Hamdi	Egypt	Road	34.1 (10.4)	1980
Stockholm Underground	Sweden	Metro	—	1988

In subsea and outfall tunnels, and tunnels exposed to brackish groundwater, the intrusion of chloride ions present in salt water can cause steel embedded in concrete to corrode. In cold region road/rail tunnels, the major durability issue is the ingress of chloride ions present in deicing salts used during snowfalls. Chloride-induced corrosion due to water infiltration initiates from the lining extrados whereas corrosion due to deicing salts sprayed from vehicle tires starts from lining intrados.

When the chloride concentration in concrete exceeds the threshold level between 0.15 and 0.6 percent by mass of cement (ACI 318), in a half-cell oxidation (anodic) reaction as shown in Fig. 14.1.1.1a, iron atoms lose electrons and move into the surrounding concrete as ferrous ions, where they react with chloride ions.

Anode:

$$2Fe \rightarrow 2Fe^{2+} + 4e^{-} \quad (14.1.1.1a)$$

$$Fe^{2+} + 2Cl^{-} \rightarrow FeCl_2 \quad (14.1.1.1b)$$

Electrons remaining in the bar flow to cathodes on the reduction reaction side and react with water and oxygen in the concrete to form hydroxide (OH^{-}). Figure 14.1.1.1a shows that the ferrous ions (Fe^{2+}) in the shape of ($FeCl_2$) migrate through concrete pores to cathodes to maintain electrical neutrality, where they combine with hydroxide to form iron hydroxides, $Fe(OH)_2$, also known as rust.

Cathode:

$$2H_2O + O_2 + 4e^{-} \rightarrow 4OH^{-} \quad (14.1.1.1c)$$

$$2Fe^{2+} + 4OH^{-} \rightarrow 2Fe(OH)_2 \quad (14.1.1.1d)$$

The chloride-induced corrosion reaction in cathodes has also been presented (Romer 2013) as

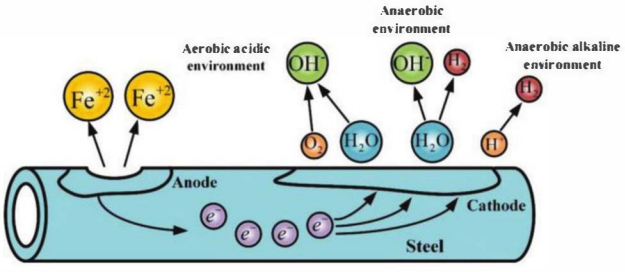

Fig. 14.1.1.1a—Electrochemical corrosion reactions in cathode and anode in steel bar (Wang et al. 2018).

$$FeCl_2 + 2H_2O \rightarrow 2Fe(OH)_2 + 2HCl \quad (14.1.1.1e)$$

Rust as the reaction product has a greater volume than the steel and causes expansion, resulting in the tensile stresses of the concrete to exceed its tensile strength, causing cracking, delamination, and spalling in the concrete (Fig. 14.1.1.1b).

14.1.1.2 *Corrosion of reinforcement induced by carbonation*—Carbonation-induced corrosion, in general, is considered as a minor durability issue in RC structures compared to chloride-induced corrosion. This is mainly due to the limited impact area of carbonation and reduced strength, which is limited to the extreme outer layer. In bored tunnels, carbonation is unlikely to occur due to the fact that the extrados of tunnel lining is permanently wet and the intrados is constantly dry. It is well-known that high rates of carbonation occur when the relative humidity is maintained between 50 and 75 percent (PCA IS536). In low relative humidity, the degree of carbonation is insignificant and above this range and moisture in concrete pores restricts penetration of CO_2 (ACI 201.2R). In tunnels, only portal areas and entrance zones can maintain a relative humidity in the aforementioned range as lining in such areas is exposed to cyclic wet and dry conditions. Also, a high rate of carbonation requires elevated atmospheric carbon dioxide (CO_2) levels, which is only a case in heavily trafficked road runnels because of CO_2 emission from car exhaust. Therefore, carbonation is a major durability factor in portal areas and entrance zones of heavily trafficked road runnels. Carbonation can also occur in tunnel linings exposed to bicarbonate (HCO_3) ground water, which often formed by the reaction of carbon dioxide with water and carbonate bedrocks such as limestone and dolomite.

When carbon dioxide from the air penetrates the concrete, it reacts with hydroxides from the cement paste (for example, calcium hydroxide) to form carbonates such as calcium carbonate (PCA IS536).

$$CO_2 + H_2O \rightarrow CO_3^{2-} + 2H^{+} \quad (14.1.1.2f)$$

$$CO_3^{2-} + 2H^{+} + Ca(OH)_2 \rightarrow CaCO_3 + 2H_2O \quad (14.1.1.2g)$$

Calcium carbonate is deposited in concrete pores in the presence of free water and, as shown in Fig. 14.1.1.2, it reduces the pH of the pore solution from 12 to 13 to as low as 8 to 9 in carbonated region (BTS ICE 2004). When alkalinity of concrete close to the steel reduces to this level, the passive layer on the steel surface become unstable and destroyed. With depassivation and in the presence of water

Fig. 14.1.1.1b—Loss of reinforcement section and cracks caused by chloride-induced steel corrosion (PCA IS536; Romer 2013).

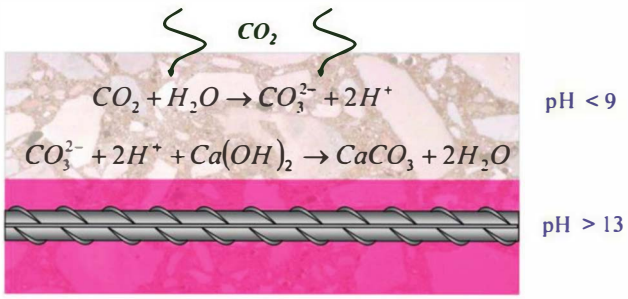

Fig. 14.1.1.2—CO_2 from the air reacts with cement hydration products such as calcium hydroxide and $Ca(OH)_2$, and reduces the pH of concrete from approximately 13 to less than 9.

and oxygen, the rate of steel corrosion increases by three orders of magnitude or higher (ACI 222R).

Both chloride-induced and carbonation-induced corrosion can be mitigated by using a concrete with low *w/c*, high compressive strength, and high cement content. This, in conjunction with a sufficient concrete cover over reinforcement, provide high-quality and dense concrete that can delay the initiation time of corrosion, also known as propagation time, beyond the service life of the structure. Further details regarding code recommendations to reduce chloride attack are provided in Section 14.5. Other effective mitigation methods that are not in the codes include using cements with high amount of C_3A and the addition of corrosion inhibitors to concrete mixture.

14.1.2 *Sulfate attack*—Sulfate attack is a major durability issue for concrete structures in contact with soil or water containing deleterious amounts of water-soluble sulfate ions. Tunnels as underground structures, regardless of their specific use, can be exposed to external sulfate attack from common sources such as sulfates of sodium, potassium, calcium, or magnesium found in the surrounding ground or dissolved in natural groundwater. Ancient sedimentary clays and the weathered zone (less than 32.8 ft [10 m]) of other geological strata, as well as contaminated ground and groundwater, generally contain significant sulfate concentrations (BTS ICE 2004). In tunnel linings exposed to such conditions, sulfate attack is a major concrete degradation mechanism.

As sulfate ions penetrate in the cement paste, they react with unconstrained aluminate phases, mainly calcium aluminate monosulfate (AFm or Al_2O_3-Fe_2O_3-mono phase), calcium hydroxide, or both. The reaction products are ettringite, gypsum, and thaumasite only at low temperatures between 32 and 50°F (0 and 10°C). In tunnels, ettringite and gypsum can usually be produced as a result of a sulfate attack that in turn results in expansion of the cement paste. The reason is that the ettringite and gypsum by-products have higher volume than reactants (for example, ettringite volume is approximately 2.2 times higher). As a result, as shown in Fig. 14.1.2, concrete cracking and spalling are likely to occur. In case of magnesium sulfate attacks, in addition to ettringite and gypsum, brucite or magnesium hydroxide may also form on concrete surface. Brucite drops the pH of a pore solution due to consumption of calcium hydroxide and results in decomposition of the calcium silicate hydrates or CSH, which is the main product resulting from cement hydration and is the compound responsible for the concrete strength.

Note that there is also another type of sulfate attack, known as internal sulfate attack, which is caused by sulfate present in cement and commonly related to delayed ettringite formation (DEF). DEF, however, is observed in concrete when initial concrete curing temperature is high due to hot aggregates (greater than 160°F [70°C]), or in cases of mass concrete with excessive heat of hydration. Project specifications usually prohibit such high curing temperatures for precast concrete tunnel segments. Therefore, it is expected that damages in tunnel linings due to sulfate attack start on segment extrados and at the interface between lining and the ground where sulfate from ground or groundwater can penetrate the concrete.

Sulfate attack can be mitigated by using cements with low amount of C_3A (less than 8 percent), use of high content of active mineral components, low *w/c*, and use of blended cements with pozzolans. Codes and standard recommendations (ACI 318; BS EN 206-1:2013; BS EN 1992-1-1:2004) to mitigate sulfate attack are based on using a concrete with low *w/c*, high compressive strength, and high cement content. In addition, codes require use of sulfate-resisting cements such as Type II portland cement (ASTM C150/C150M) or in severe cases Type V (ASTM C150/C150M) plus pozzolan or slag cement.

14.1.3 *Acid attack*—Acid attack is a chemical attack that can be a major durability issue when a concrete structure is exposed to high concentrations of aggressive acids with high degrees of dissociation. The deterioration of concrete by acids is primarily the result of decomposition of the hydration products of the cementitious paste (ACI 201.2R). Sulfuric, hydrochloric, and nitric acids are the main inorganic (mineral) acids, and acetic, formic, and lactic acid are main organic acids with rapid rate of attack on concrete at ambient temperature. Acids reduce the pH or alkalinity of the concrete, and once the pH reduces to less than 5.5 to 4.5, severe damage is imminent. Cement hydration products such as Portlandite (CH, $Ca(OH)_2$) and C-S-H starts to decompose when pH drops to approximately 12 and 10 (ACI 201.2R). This is the main reason that concrete materials do not have a good resistance to acids.

In tunnels, the concrete lining can be attacked from external sources in the surrounding ground and groundwater as well as from internal sources within the tunnels. Concerning external sources, acidic materials may be found on polluted sites used for industrial waste; agricultural applications; animal feed and manure; or from natural sources such as peat soils, clay soils, and alum shales. These geological strata, for example, contain sulfide bearing minerals such as pyrite that produce sulfuric acid on oxidation (ACI 201.2R). The rapid deterioration of concrete, however, only occurs when concrete is subject to the action of highly mobile acidic water (BTS ICE 2004).

Regarding internal sources for acid attack, flow of acid-containing runoff from outside the tunnel is not a major

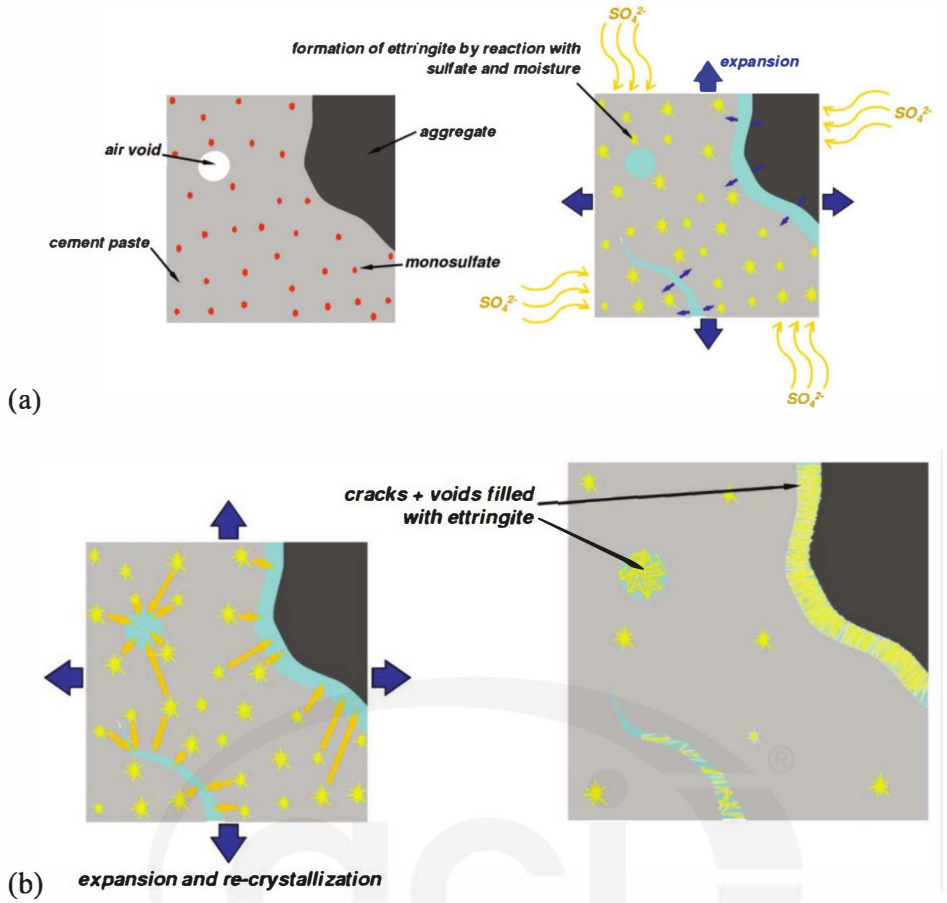

Fig. 14.1.2—External sulfate attack damage process: (a) formation of ettringite by reaction with sulfate and moisture; and (b) expansion and recrystallization causing cracks and voids filled with ettringite (Helsing and Mueller 2013).

concern. However, sulfuric acid solutions result from decay of organic matter by bacterial action in sewage and wastewater tunnels can have these degradation mechanisms. This is due to the high attack rate of sulfuric acid and continuous movement of the acidic materials inside the tunnel as gravitational flow of sewage in these tunnels is always guaranteed. Note that sewage is not aggressive to concrete buy itself, but hydrogen sulfide produced by anaerobic bacteria reaction within the sludge is subsequently oxidized by aerobic bacteria to form sulfuric acid. In addition to decomposition of the cement hydration products, sulfuric acid is particularly aggressive to concrete because the calcium sulfate formed from the acid reaction may drive sulfate attack of adjacent concrete that was unaffected by the initial acid attack (ACI 201.2R; PCA IS536).

Acid attacks can be mitigated by providing a dense and high-quality concrete, lowering the *w/c* and increasing compressive strength and cement content. Codes and standards (ACI 318; BS EN 206-1:2013; BS EN 1992-1-1:2004) provide specific limits to achieve very high density and relatively impermeable concrete to reduce the damage due to acid attack. Type of cement has an insignificant role on mitigation of acid attack. When concrete is exposed to acid attack, a surface protection method such as coatings, waterproofing membranes, or a sacrificial layer should be considered.

14.1.4 *Alkali-aggregate reaction*—Alkali-aggregate reaction (AAR) is a chemical reaction between reactive aggregates and cement. In most concrete, aggregates are chemically inert or nonreactive. However, AAR as a chemical attack can be a major durability concern when aggregates contain materials that can be reactive with alkali hydroxides in the cement phase. The AAR generates expansive products and may result in damaging deformation and cracking of concrete over a period of years. AAR has two main forms: alkali-silica reaction (ASR) and alkali-carbonate reaction (ACR). ASR is often a major concern compared to ACR, as aggregates containing reactive silica are more common (PCA IS536), whereas aggregates susceptible to ACR are less common and usually unsuitable for use in concrete. Reactive forms of silica can be found in aggregates such as chert, volcanic glass, quartzite, opal, chalcedony, and strained quartz crystals. Damage to concrete typically occurs when concrete alkali content is high, aggregate contains an alkali-reactive constituent, and concrete is under wet conditions (BTS ICE 2004). ASR reactions can be summarized as

$$\text{alkalis} + \text{reactive silica} \rightarrow \text{gel reaction product}$$

$$\text{gel reaction product} + \text{moisture} \rightarrow \text{expansion}$$

Fig. 14.2a—Extensive corrosion of the outer reinforcement layer in Bucharest Metro on segments taken from Gorgului station prior to reconstruction and repair of the station (Buhr et al. 1999).

Because sufficient moisture is needed to promote destructive expansion, PCA IS536 reports the internal relative humidity of 80 percent as a threshold, below which the alkali-silica reactivity can be virtually stopped.

Concrete tunnel linings are not different from general types of concrete elements as far as AAR sources, which are internal reactive aggregates. Therefore, the degradation mechanism of AAR does not depend on the specific use of each tunnel. Subsea tunnels may be more susceptible due to exposure to warm seawater containing dissolved alkalis that may aggravate ASR. AAR can be mitigated by using inert aggregate, controlling the amount of soluble alkalis in concrete, and using blended cements with pozzolans.

14.1.5 *Frost attack and freezing-and-thawing damage*—Frost attack and freezing-and-thawing damage are durability concerns in concrete structures built in cold regions. Water expands by approximately 9 percent when it freezes and, as a result, the moisture in concrete capillary pores exerts pressure on the concrete solid skeleton. This leads to development of excessive tensile stresses in the concrete and rupture of cavities. Successive cycles of freezing and thawing can disrupt paste and aggregate and eventually cause significant expansion and cracking, scaling, and crumbling of the concrete (PCA IS536). Frost damage is considerably accelerated by deicing salts (ACI 201.2R).

Frost damage at early ages is not noted in precast concrete produced under high-quality control conditions. In well-cured concrete with durable aggregate, surface scaling—that is, the loss of paste and mortar from the surface of the concrete—is the most common form of frost damage. Therefore, surface scaling is the only frost damage that can occur in precast tunnel segments. Because the increase in volume when water turns to ice is approximately 9 percent, more than 90 percent of the capillary pore volume needs to be filled with water for internal stresses to be induced by ice formation (BTS ICE 2004). Moisture content near saturation level is usually the case for tunnel linings as tunnels are often built under the water table and concrete lining can be near saturation level. However, along most of the tunnel alignment, the temperature rarely falls under the freezing point because the tunnel is embedded in the ground. Tunnel entrances, portals, and shafts are parts of the tunnel system that should be designed for exposure to cycles of freezing and thawing because of saturation level and exposure to freezing temperatures.

Freezing and thawing attacks are mitigated by controlling *w/c*, compressive strength, and cement content. However, the most effective method to mitigate the freezing-and-thawing attacks is controlling the air content in the mixture to a minimum value of 4 percent using air-entraining admixtures. Codes and standards (ACI 318; BS EN 206-1:2013; BS EN 1992-1-1:2004) often provide limits for maximum *w/c* and minimum compressive strength. Certain codes, in addition, require use of frost-resistant aggregate (BS EN 206-1:2013).

14.2—Stray current corrosion in segmental tunnel linings

Stray current corrosion is a type of corrosion specific to rail tunnels where corrosion is caused by traction current resulting in the accelerated oxidation of metals and rapid migration of the chloride ions (ITA Working Group on Maintenance and Repair of Underground Structures 1991). As shown in Fig. 14.2a, inspection of removed segments from tunnels with high conductivity between running rails and lining reinforcement has shown extensive corrosion of the outer reinforcement layer (Buhr et al. 1999).

Electric trains consume at least 20 percent less power than diesel-powered trains (Kemp 2007), have a lower carbon footprint during operation, and provide sustainable solutions to public transportation. Therefore, government agencies around the world are promoting electric trains and modern railway systems are taking advantage of railway electrification. Power transmission is provided by overhead catenary wire or a conductor rail also known as a third rail. Due to construction limitations and maintenance costs, the running rail connected to nearby substations is often used as a traction loop through which the return circuit is made. Therefore, running rails in modern railway systems are used for the purpose of mechanical support and guideways as well as electric conductors in the traction and signaling circuits (Brenna et al. 2010). Running rails have a limited conductivity, and insulation between the rail and the ground is sometimes reduced or constructed poorly from the beginning. This causes a fraction of the traction current to leave the rail, leak into the ground, and flow back along the running rail on the return path to the traction substation by the earth diversion, which is referred to as stray current. Figure 14.2b(a) shows a simplified electronic circuit of the electric railway system for modeling the stray current. Based on this simplified model, stray current (I_s) can be determined as follows

$$I_s = \frac{R_R I_T}{R_T + R_R + R_S} \tag{14.2a}$$

where I_T is the train (overhead catenary system) current; R_R is the running rail resistance; R_S is the ground resistance at

the traction substation; and R_T is the ground resistance as seen at the train. This equation further presents the effect of insulation problems between the rail and ground as reduced R_T or R_S, which results in increased stray current. When trains run in a lined tunnel, stray current leaks to the tunnel lining and through the concrete reinforcement. This is shown schematically in Fig. 14.2b(b) with a cathode formed at reinforcement, where stray current enters the reinforcing bar and an anode is formed where stray current leaves the reinforcing bar and flows back to the substation. Corrosion and severe damage to concrete are anticipated due to hydrogenation and the accumulation of corrosion products. As shown in Fig. 14.2b(c), in a cathode, the reinforcing bar is disengaged from the concrete due to trapped hydrogen isostatic pressure and, in the anode, the reinforcing bar is oxidized in contact with electrolytic material—that is, the concrete, and accumulation of corrosion products exerts excessive pressure leading to cracking. The following reaction equations were presented by Wang et al. (2018) (Fig. 14.1.1.1b) and depend on the reduction reaction environment.

Cathode: hydrogen evolution corrosion

$$4H^+ + 4e^- = 2H\uparrow \text{ (Anaerobic alkaline environment)} \quad (14.2b)$$

$$4H_2O + 4e^- = 4OH\_ + 2H_2\uparrow \text{ (Anaerobic environment)} \quad (14.2c)$$

Anode: Oxygen absorption corrosion

$$O_2 + 2H_2O + 4e^- = 4OH\_ \text{ (Aerobic acidic environment)} \quad (14.2d)$$

Note that this type of corrosion is not limited to the reinforcement in the concrete lining, but severe corrosion can occur in metal utilities and steel pipelines embedded in the ground has been observed in the proximity of tracks.

14.3—Mitigation methods for stray current corrosion

Major mitigation methods for stray current corrosion include decreasing rail resistance; improving rail-to-ground insulation using isolated rail fastening systems or pads, keeping the substation as close to the point of maximum current as possible; and developing monitoring systems, devices, and measurement apparatus (Brenna et al. 2010). All these measures are effective for reducing the amount of stray current and therefore are considered as general measures for stray current corrosion mitigation of all metals embedded in the ground or reinforcement in both cast-in-place and precast segmental linings.

Brenna et al. (2010) used finite element method (FEM) simulations to study specific cases of reinforcement corrosion in precast segments due to stray current. In their simulations, stray current was assumed to be developed by the traction power of surface tramway lines in close proximity to the tunnel, and not from the catenary system of the subway train inside the tunnel (Fig. 14.3a(a)). While this simulation pertains to a particular subway line under construction in Milan located under already-existing and working surface tramway line, results of this study can be extended to general segmentally lined tunnels. Figure 14.3a(b) shows the conduction field in the ground and equipotential surfaces around the segmental ring under a tramway track voltage of 8 V corresponding to rush-hour conditions. As shown in Fig. 14.3a(c), the contact between two adjacent segments is a particularly critical aspect of the model. The current leaves the upper segment (Segment #6), flows into the ground, and then returns to the adjacent segment (Segment #5). Parts of the reinforcement where current leaves the reinforcing bar constitute the anode in which corrosion can initiate, depending on the reinforcement-to-ground potential difference. For example, in this research, the difference of potential between reinforcing bars and ground for Segment #6 as a result is greater than or close to the maximum value

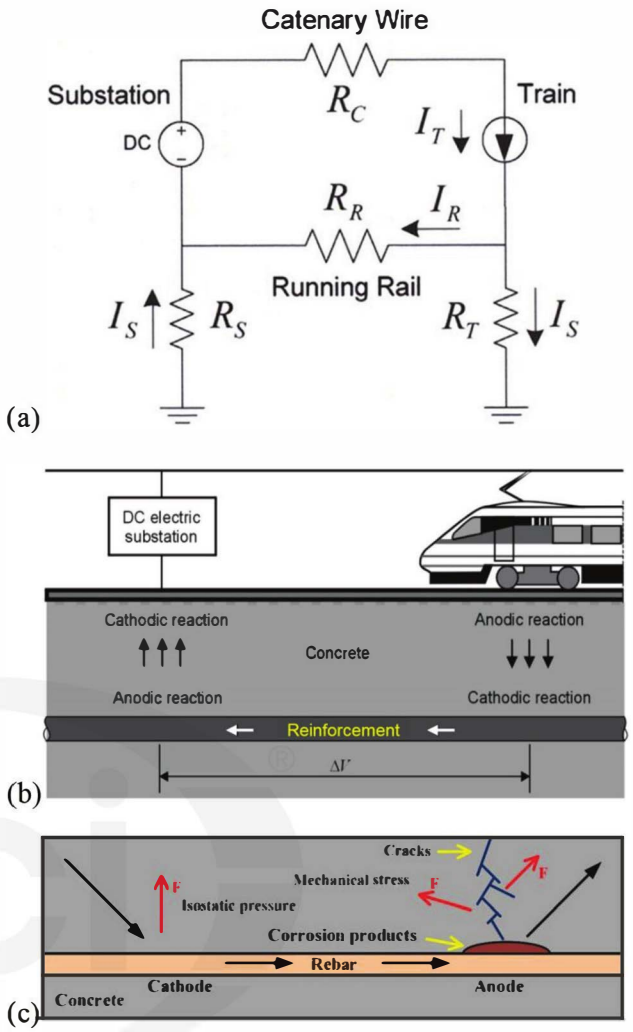

Fig. 14.2b—(a) Modeling stray current leakage with simplified electronic circuit of the electric railway system (Niasati and Gholami 2008); (b) schematics of stray current from a train catenary system picked up by steel reinforcement in concrete (Bertolini et al. 2007); and (c) corrosive effect of stray current on reinforced concrete (Wang et al. 2018).

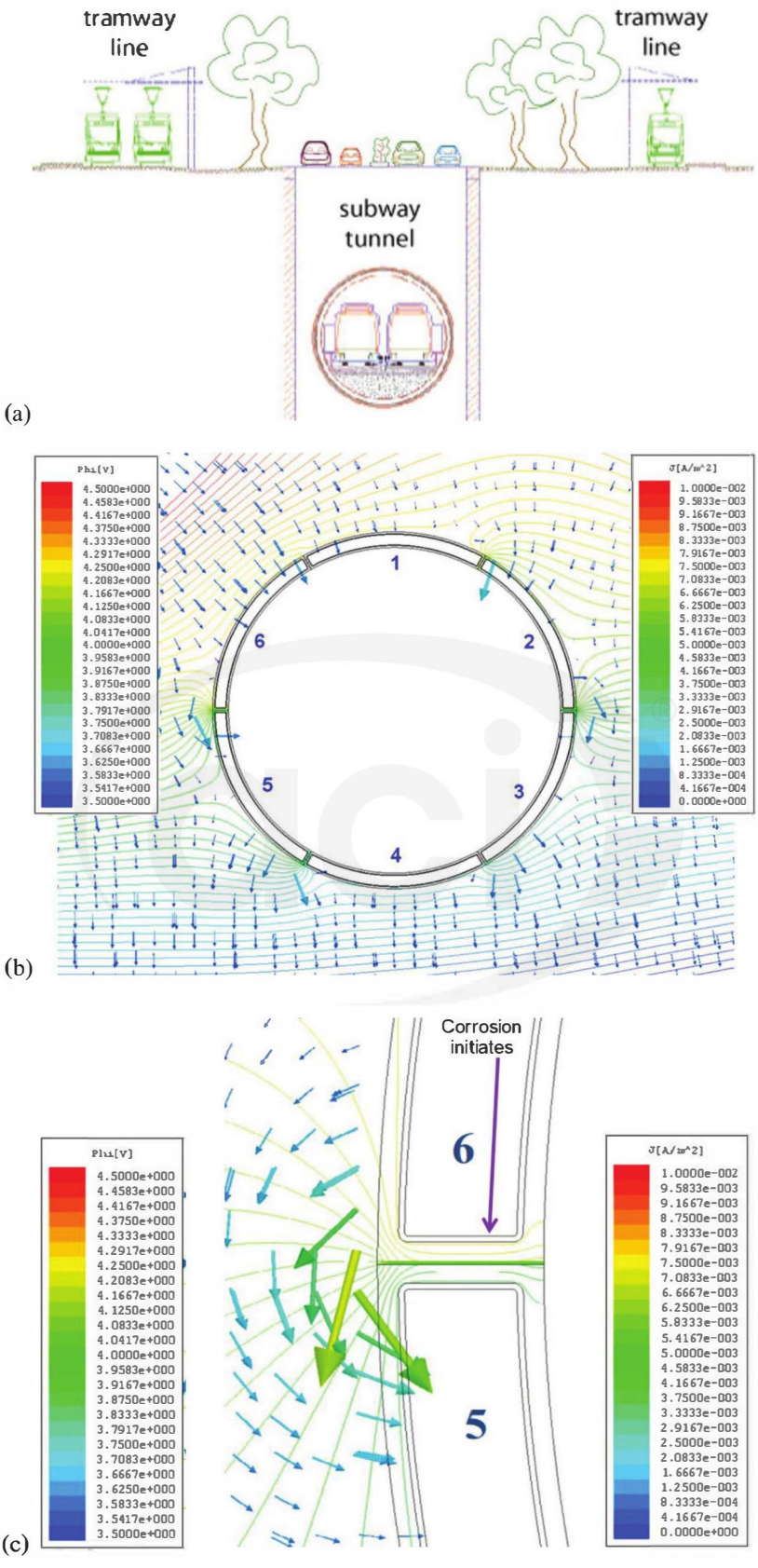

Fig. 14.3a—Brenna et al. (2010) FEM simulation: (a) typical tunnel section used for simulation of stray current in the lining due to surface tramway line traction power; (b) conduction field in the ground and equipotential surfaces around segmental ring as results of simulation; and (c) equipotential surfaces and current field in the lining and in the ground near contact area of segments.

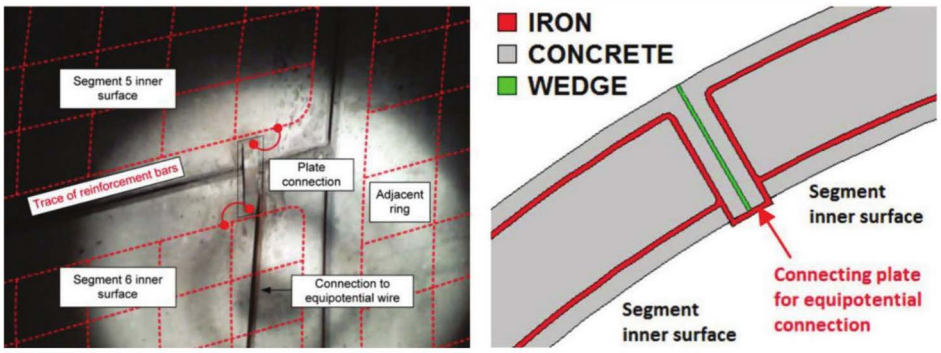

Fig. 14.3b—Stray current mitigation using equipotential connection provided by copper plates/straps connecting reinforcement cages of segments by Dolara et al. (2012).

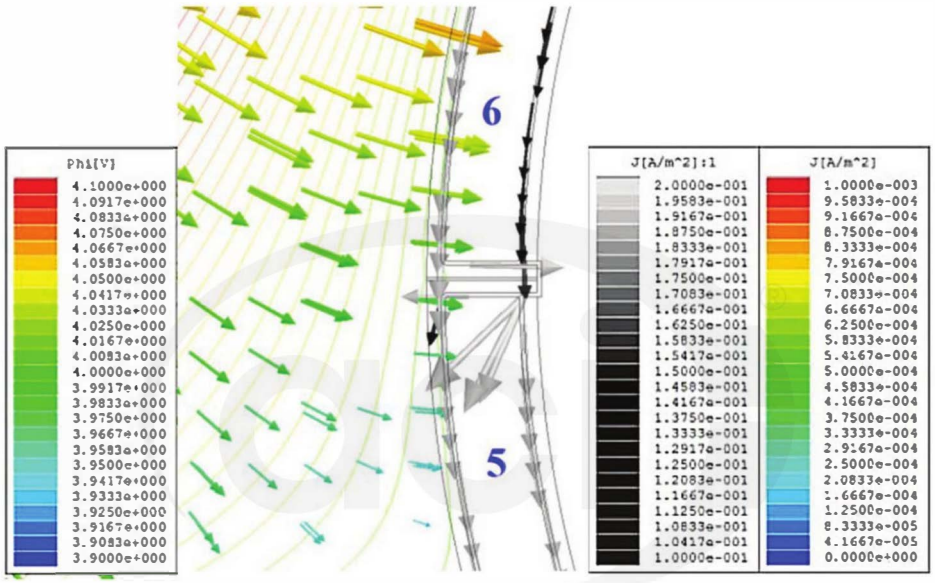

Fig. 14.3c—Effect of connection plates between adjacent segment reinforcement cages on equipotential surfaces and current field near contact area of segments as results of FEM simulation by Dolara et al. (2012).

allowed by BS EN 50122-2:2010, indicating the possibility of corrosion initiation. Therefore, a potential mitigation method for stray current corrosion in precast segments is an equipotential connection between reinforcing bars of adjacent segments and of adjacent rings to avoid zones with high output current density. As shown in Fig. 14.3b, Dolara et al. (2012) modeled this solution using copper plates connecting reinforcement cages of segments together for the same tramway line project studied by Brenna et al. (2010). The traces of reinforcing bars in adjacent segments were depicted with red dashed lines connected together with a plate connection. The equipotential connections between the reinforcing bars of all segments in a ring constitute a path with extremely low electrical resistance that allows the current to flow from a segment to the adjacent one without passing into the ground. FEM simulation by Dolara et al. (2012) presented in Fig. 14.3c shows that stray current flows from a segment to adjacent one without passing into the ground. Electrically connected bars behave like a cylindrical metallic shield that allows the stray current to be distributed in an almost uniform way both in entering from the top and leaving from the bottom of the tunnel. In this case, the anode is the ring outer surface near the invert and the maximum potential difference between the bars and ground is reduced by more than 15 times. The conclusion is that equipotential connection reduces bar-to-ground voltage to values well below the standard limits (BS EN 50122-2:2010) for corrosion initiation and provides an effective method to prevent stray current corrosion in segments.

Another mitigation method for stray current-induced corrosion is the use of fiber-reinforced concrete (FRC) segments (Tang 2017; Solgaard et al. 2013). Results of studies on stray current corrosion of FRC show that steel bars are more likely to pick up current than short steel fibers under the same conditions (Edvardsen et al. 2017). This can be due to the fact that the chloride threshold for the corrosion of steel bars in concrete is between 0.15 and 0.6 percent by mass of cement (ACI 318). However, steel FRC demonstrates a higher corrosion resistance compared to steel bar reinforced with a chloride threshold level for corrosion at 4 percent by mass of cement, which is above that of the reinforcing bar by more than 10 times (Tang 2017). The discon-

Table 14.4—Durability factors for tunnel linings, sources, and mitigation methods

Degradation mechanism	Type of tunnels susceptible to this factor	Main sources of degradation	Specific location of tunnel prone to factor	Mitigation method
Chloride-induced corrosion	Subsea tunnels	Sea/salt water	Lining extrados	Delay corrosion initiation by: a) Sufficient cover over reinforcing bar b) Dense/high-quality concrete: i. Low *w/c* ii. High compressive strength iii. High cement content c) Cement with high C_3A content d) Use of corrosion inhibitors
	Sea outfall tunnels	Sea/salt water		
	Transportation tunnels in cold regions	Chloride ions present in deicing salts used during snow falls		
Carbonate-induced corrosion	Heavily trafficked roadway tunnels	CO_2 emission from car exhaust	Lining intrados near portals, entrance zones, shafts	
	All types of tunnels embedded in carbonate bedrock such as limestone or dolomite	Bicarbonate (HCO_3) groundwater formed by the reaction of water and carbonate bedrocks	Lining extrados	
External sulfate attack	All types of tunnels embedded in ancient sedimentary clays	Formation of ettringite due to sulfate reacting with calcium aluminates or $Ca(OH)_2$	Lining extrados	a) Dense/high-quality concrete: i. Low *w/c* ii. High compressive strength iii. High cement content b) Cement with low C_3A content (less than 8 percent) c) Pozzolans/Blended cement
	All types of shallow tunnels exposed to weathered zone (less than 32 ft [10 m]) of other geological strata			
	All types of tunnels exposed to sulfate contamination			
Internal acid attack	Sewage/Wastewater	Formation of H_2S and oxidization to sulfuric acid	Lining intrados	a) Dense/high-quality concrete b) Coatings c) Sacrificial layers d) Use calcareous aggregates
Alkali aggregate reaction (AAR)	All types of tunnels built with reactive silica aggregate	Volcanic glass Opal/chalcedony Deformed quartz	No specific location	a) Use inert aggregate b) Control amount of soluble alkalis in concrete c) Pozzolans/blended cement
	Subsea tunnels	Warm seawater containing dissolved alkalis	Lining extrados	
Frost attack/ Freezing and thawing	All types of tunnels in cold regions	Surface scaling due to increase in volume when water turns to ice near saturation	Lining intrados near portals, entrance zones, shafts	a) Dense/high-quality concrete: i. Low *w/c* ii. High compressive strength iii. High cement content b) Air-entraining admixture
Stray current corrosion	Subway tunnels	OCS current leaking into lining when returning from running rail	Near reinforcing bar	a) Reduce amount of current: i. Decrease rail resistance ii. Improve rail/ground insulation iii. Substation close to maximum current b) Use of straps connecting bars c) Use fiber reinforcement
	Railway tunnels			

tinuous and discrete nature of steel fibers or the length effect is the main factor to be accounted for this higher corrosion resistance, as fibers rarely touch each other and there is no continuous conductive path for stray currents through the concrete (ACI 544.1R).

14.4—Durability under coupling multi-degradation factors

Precast concrete tunnel segments may be subjected to the coupling effects of degradation factors such as carbonation and sulfate and chloride-induced corrosion of steel bars by groundwater and surrounding ground (Bakhshi and Nasri 2018d). For electrical subway tunnels, stray current is another major factor that accelerates the steel corrosion. A summary of these different major degradation mechanisms together with their mitigation methods are shown in Table 14.4.

A literature review on experiments conducted on coupled effect of stray current and other degradation factors reveals that the majority of previous work (Srikanth et al. 2005; Xiong 2008; Geng 2008) has been focused on the material scale level, which cannot truly reflect the durability aspects of full-size concrete members (Zhu and Zou 2012; Geng and Ding 2010). The study conducted by Li et al. (2014), however, pertains to the durability of concrete tunnel segments on a large scale and considers various factors of

carbonation, sulfate, and chloride penetration coupled with stray-current corrosion. Their research consists of groups of samples nearly the size of full-size segments used in the practice. Figure 14.4(a) shows the dimension of segments and arrangement of reinforcement. Figure 14.4(b) shows schematics of the test setup demonstrating series connections between several segment samples in a group to ensure equal current flow of 1A among all segments. Segment reinforcement is the anode and a stainless-steel tube placed in corrosion pools is the cathode, and the segments were connected to DC power supply to simulate the stray current. For simulation of chloride and sulfate penetration from the surrounding ground and groundwater, the extrados side of the segment was immersed in a solution of 3.5 percent NaCl and 3.5 percent NaCl + 5 percent Na_2SO_4. The intrados side of the segments was exposed to a relative humidity of 70 ± 5 percent and a temperature of 20 ± 5 degrees representing the inside environment of the tunnel. For segment samples studied for the coupled effect of carbonation, the intrados side of the segments was exposed to a carbonation setup simulating a CO_2 environment with concentration of 20 percent, temperatures of 20 ± 5 degrees, and relative humidity of 70 ± 5 percent (Fig. 14.4(c)). Segments are made of concrete with a *w/c* of 0.28 to 0.33, a compressive strength of 8700 to 10,000 psi (60 to 70 MPa), and steel bars of 1/4 in. (6.5 mm) diameter with yield and ultimate strengths of 68 and 85 ksi (472 and 586 MPa), respectively. After casting and standard curing, samples were placed in a corrosion solution for 18 days and were exposed to a carbonation setup for 28 days. Free chloride ion was determined from powder samples collected using drilling at 0.2 in. (5 mm) intervals along the segment thickness. Results show that stray current accelerates the migration of chloride ions and changes the penetration distribution of chloride ion in the section. In the absence of stray current, the largest concentration of chloride ions is near the exposure surface to corrosion solution. However, results of the Li et al. (2014) study reveals that the presence of stray current causes the chloride ions to gradually gather

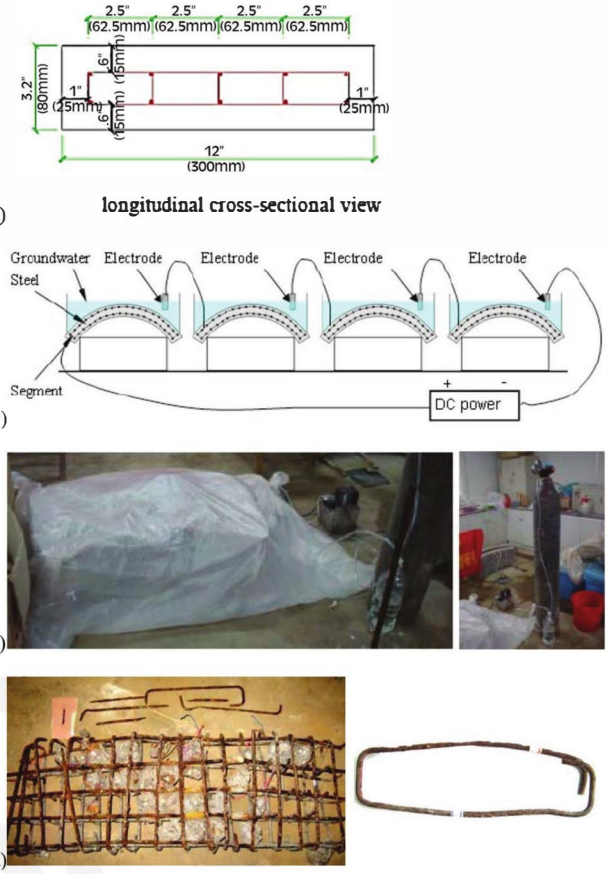

Fig. 14.4—Li et al. (2014) study on stray current coupled with multiple degradation factors: (a) size and layout of experimental segment samples and reinforcement (in inches [mm]); (b) schematics of test setup for combined effect of corrosion solution and stray current (note that all baths contain same solution and all connected segments represent specimen replicates of same sample; (c) views of carbonation test device; and (d) steel bar corrosion in main reinforcement and stirrups.

Table 14.5a—Recommended structural classification by BS EN 1992-1-1:2004

Criterion	Structural class						
	Exposure class according to Table 4.1 in BS EN 1992-1-1:2004 (Table 14.5b herein)						
	X0	XCl	XC2/XC3	XC4	XD1	XD2/XS1	XD3/XS2/XS3
Design working life of 100 years	increase class by 2	increase class by 2	increase class by 2	increase class by 2	increase class by 2	increase class by 2	increase class by 2
Strength class according to BS EN 1992-1-1:2004	≥C30/37* reduce class by 1	≥C30/37* reduce class by 1	≥C35/45† reduce class by 1	≥C40/50‡ reduce class by 1	≥C40/50‡ reduce class by 1	≥C40/50‡ reduce class by 1	≥C45/55§ reduce class by 1
Member with slab geometry (position of reinforcement not affected by construction process)	reduce class by 1	reduce class by 1	reduce class by 1	reduce class by 1	reduce class by 1	reduce class by 1	reduce class by 1
Special quality control of the concrete production ensured	reduce class by 1	reduce class by 1	reduce class by 1	reduce class by 1	reduce class by 1	reduce class by 1	reduce class by 1

*The strength class C30/37 based on BS EN 1992-1-1:2004 is equivalent to concrete with f_c' = 4350 psi (30 MPa).

†The strength class C35/45 based on BS EN 1992-1-1:2004 is equivalent to concrete with f_c' = 5100 psi (35 MPa).

‡The strength class C40/50 based on BS EN 1992-1-1:2004 is equivalent to concrete with f_c' = 5800 psi (40 MPa).

§The strength class C45/55 based on BS EN 1992-1-1:2004 is equivalent to concrete with f_c' = 6550 psi (45 MPa).

Table 14.5b—Exposure classes (BS EN 1992-1-1:2004; BS EN 206-1:2013)

Class designation	Description of the environment	Informative examples where exposure classes may occur
1. No risk of corrosion or attack		
X0	For concrete without reinforcement or embedded metal: all exposures except where there is freezing and thawing, abrasion, or chemical attack. For concrete with reinforcement or embedded metal: very dry	Concrete inside buildings with very low air humidity.
2. Corrosion induced by carbonation		
Where concrete containing reinforcement or other embedded metal is exposed to air and moisture, the exposure should be classified as follows:		
XC1	Dry or permanently wet	Concrete inside buildings with low air humidity: concrete permanently submerged in water
XC2	Wet, rarely dry	Concrete surfaces subject to long-term water contact; Many foundations
XC3	Moderate humidity	Concrete inside buildings with moderate or high air humidity; External concrete sheltered from rain
XC4	Cyclic wet and dry	Concrete surfaces subject to water contact, not within exposure Class XC2
3. Corrosion induced by chlorides other than from seawater		
Where concrete containing reinforcement or other embedded metal is subject to contact with water containing chlorides, including deicing salts, from sources other than from seawater, the exposure should be classified as follows:		
XD1	Moderate humidity	Concrete surfaces exposed to airborne chlorides
XD2	Wet, rarely dry	Swimming pools; Concrete exposed to industrial waters containing chlorides
XD3	Cyclic wet and dry	Parts of bridges exposed to spray containing chlorides. Pavements, car park slabs
4. Corrosion induced by chlorides from seawater		
Where concrete containing reinforcement or other embedded metal is subject to contact with chlorides from seawater or air carrying salt originating from seawater, the exposure shall be classified as follows:		
XS1	Exposed to airborne salt but not in direct contact with seawater	Structures near to or on the coast
XS2	Permanently submerged	Parts of marine structures
XS3	Tidal, splash, and spray zones	Parts of marine structures
5. Freezing-and-thawing attack with or without deicing agents		
Where concrete is exposed to significant attack by freezing-and-thawing cycles while wet, the exposure should be classified as follows:		
XF1	Moderate water saturation, without deicing agent	Vertical concrete surfaces exposed to rain and freezing
XF2	Moderate water saturation, with deicing agent	Vertical concrete surfaces of road structures exposed to freezing and airborne deicing agents
XF3	High water saturation, without deicing agent	Horizontal concrete surfaces exposed to rain and freezing
XF4	High water saturation, with deicing agent or sea water	Road and bridge decks exposed to deicing agents; Concrete surfaces exposed to direct spray containing deicing agents and freezing splash zones of marine structures exposed to freezing
6. Chemical attack		
Where concrete is exposed to chemical attack from natural soils and ground water, the exposure should be classified as follows:		
XA1	Slightly aggressive chemical environment according to BS EN 206-1:2013, Table 2	Concrete exposed to natural soil and groundwater
XA2	Moderately aggressive chemical environment according to BS EN 206-1:2013, Table 2	Concrete exposed to natural soil and groundwater
XA3	Highly aggressive chemical environment according to BS EN 206-1:2013, Table 2	Concrete exposed to natural soil and groundwater

to the surface of steel bar, resulting in the largest concentration of chloride ions at the reinforcement level and a parabolic distribution from the extrados side to intrados through the thickness. One major conclusion is that chloride ion concentration is higher for segments immersed in chloride solutions (Cl^-) than the ones immersed in solution with both

Table 14.5c—Recommended characteristics of concrete by BS EN 206-1:2013

	Exposure classes																
	No risk of corrosion or attack	Carbonation-induced corrosion				Chloride-induced corrosion						Freezing-and-thawing attack				Aggressive chemical environments		
						Seawater			Chloride other than water									
	X0	XC 1	XC2	XC3	XC4	XS1	XS2	XS3	XD1	XD2	XD3	XF1	XF2	XF3	XF4	XA 1	XA 2	XA 3
Maximum *w/c*	—	0.65	0.60	0.55	0.50	0.50	0.45	0.45	0.55	0.55	0.45	0.55	0.55	0.5	0.45	0.55	0.50	0.45
Minimum strength class according to BS EN 1992-1-1:2004	C12/15*	C20/25†	C25/30‡	C30/37§	C30/37§	C30/37§	C35/45‖	C35/45‖	C30/37§	C30/37§	C35/45‖	C30/37§	C25/30‡	C30/37§	C30/37§	C30/37§	C30/37§	C35/45‖
Minimum cement content, lb/yd³ (kg/m³)	—	440 (260)	470 (280)	470 (280)	505 (300)	505 (300)	540 (320)	575 (340)	505 (300)	505 (300)	540 (320)	505 (300)	505 (300)	540 (320)	575 (340)	505 (300)	540 (320)	575 (340)
Minimum air content, %	—	—	—	—	—	—	—	—	—	—	—	—	4.0	4.0	4.0	—	—	—
Other requirements	—	—	—	—	—	—	—	—	—	—	—	Aggregate in accordance with EN 12620 with sufficient freezing-and-thawing resistance					Sulfate-resisting cement	

*The strength class C12/15 based on BS EN 1992-1-1:2004 is equivalent to concrete with f_c' = 1750 psi (12 MPa).

†The strength class C20/25 based on BS EN 1992-1-1:2004 is equivalent to concrete with f_c' = 2900 psi (20 MPa).

‡The strength class C25/30 based on BS EN 1992-1-1:2004 is equivalent to concrete with f_c' = 3600 psi (25 MPa).

§The strength class C30/37 based on BS EN 1992-1-1:2004 is equivalent to concrete with f_c' = 4350 psi (30 MPa).

‖The strength class C35/45 based on BS EN 1992-1-1:2004 is equivalent to concrete with f_c' = 5100 psi (35 MPa).

Table 14.5d—Values of minimum cover over reinforcement steel (BS EN 1992-1-1:2004)

	Environmental requirement for $c_{min,dur}$, in. (mm)						
	Exposure class according to Table 4.1 in EN 1992-1-1:2004 (Table 14.5a herein)						
Structural class	X0	XC1	XC2/XC3	XC4	XD1/XS1	XD2/XS2	XD3/XS3
S1	0.4 (10)	0.4 (10)	0.4 (10)	0.6 (15)	0.8 (20)	1 (25)	1.2 (30)
S2	0.4 (10)	0.4 (10)	0.6 (15)	0.8 (20)	1 (25)	1.2 (30)	1.4 (35)
S3	0.4 (10)	0.4 (10)	0.8 (20)	1 (25)	1.2 (30)	1.4 (35)	1.6 (40)
S4	0.4 (10)	0.6 (15)	1 (25)	1.2 (30)	1.4 (35)	1.6 (40)	1.8 (45)
S5	0.6 (15)	0.8 (20)	1.2 (30)	1.4 (35)	1.6 (40)	1.8 (45)	2 (50)
S6	0.8 (20)	1 (25)	1.4 (35)	1.6 (40)	1.8 (45)	2 (50)	2.2 (55)

chloride and sulfate ($Cl^- + SO_4^{2-}$). This may be due to the concrete pores being filled with ettringite produced by reaction of SO_4^{2-} ions in the solution with hydration products, resulting in obstruction of channels through which chloride ions migrate. Another argument is that SO_4^{2-} ions first react with C_3A producing ettringite. This reaction reduces the amount of free C_3A leading to reduce its reaction with Cl^- ions. As a result, it is more likely that Cl^- ion to be absorbed by C-S-H, altering the combination form of Cl^- ions (Li et al. 2014). Another outcome is that carbonation depth is only 0.04 to 0.15 in. (1 to 4 mm), leading to a conclusion that carbonation is not a controlling durability factor for concrete segments compared with the chloride and sulfate ions and stray-current corrosion. A typical corroded steel cage under coupled durability factors using this setup is shown in Fig. 14.4(d). Other results specific to reinforcement include more significant corrosion of the reinforcement layer near the extrados but at the level of reinforcement compared to intrados, and more corrosion damage on stirrups than main transverse reinforcing bars. Considering results of this study, one can conclude that coupling factors of chloride ion penetration and stray current has the most detrimental effect on the durability of concrete tunnel segments.

14.5—Prescriptive-based approaches

Durability design according to prescriptive approaches is often performed in accordance with major national and international structural codes. Such codes specify characteristics of concrete such as concrete strength or maximum *w/c* based on exposure or environmental classes to which the concrete element is exposed. BS EN 206-1:2013, in combination with BS EN 1992-1-1:2004, is one of the world's most well-known codes and provides the most comprehensive prescriptive-based specifications for concrete exposed to environmental actions. According to BS EN 1992-1-1:2004, main exposure classes are XC for risk of carbonation-induced corrosion, XD for risk of chloride-induced corrosion from other sources than seawater, XS for risk of chloride-induced corrosion from seawater, XF for risk of freezing and thawing and frost attack, and XA for chemical attacks. Depending

Table 14.5e—Exposure categories and classes by ACI 318

Category	Class	Condition	
Freezing and thawing (F)	F0	Concrete not exposed to freezing-and-thawing cycles	
	F1	Concrete exposed to freezing-and-thawing cycles with limited exposure to water	
	F2	Concrete exposed to freezing-and-thawing cycles with frequent exposure to water	
	F3	Concrete exposed to freezing-and-thawing cycles with frequent exposure to water and exposure to deicing chemicals	
Sulfate (S)		Water-soluble sulfate (SO_4^{2-}) in soil, percent by mass*	Dissolved sulfate (SO_4^{2-}) in water, ppm†
	S0	$SO_4^{2-} < 0.10$	$SO_4^{2-} < 150$
	S1	$0.10 \le SO_4^{2-} < 0.20$	$150 \le SO_4^{2-} < 1500$ or seawater
	S2	$0.20 \le SO_4^{2-} \le 2.00$	$1500 \le SO_4^{2-} \le 10{,}000$
	S3	$SO_4^{2-} > 2.00$	$SO_4^{2-} > 10{,}000$
In contact with water (W)	W0	Concrete dry in service Concrete in contact with water and low permeability is not required	
	W1	Concrete in contact with water and low permeability is required	
Corrosion protection of reinforcement (C)	C0	Concrete dry or protected from moisture	
	C1	Concrete exposed to moisture but not to an external source of chlorides	
	C2	Concrete exposed to moisture and an external source of chlorides from deicing chemicals, salt, brackish water, seawater, or spray from these sources	

*Percent sulfate by mass in soil shall be determined by ASTM C1580.

†Concentration of dissolved sulfates in water, in ppm, should be determined by ASTM D516 or ASTM D4130.

on the severity of exposure, ranges of XC1 to XC4, XD1 to XD3, XS1 to XS3, XF1 to XF4, and XA1 to XA3 are provided, along with description of environment for each subclass, and informative examples where exposure classes may occur. For specific cases of tunnel linings, suggested exposure classes according to Helsing and Mueller (2013) for CO_2 carbonation are XC3 to XC4, for seawater chloride-induced corrosion are XS2 to XS3, for deicing salt chloride-induced corrosion are XD2 to XD3, for frost exposure are XF3 to XF4, and for harmful ions other than chloride (Mg^{2+}, SO_4^{2-}) are XA1 to XA3. The concrete requirement specified by BS EN 1992-1-1:2004 includes the assumption of an intended design service life of 50 years. However, almost all tunnels are designed for a service life of over 100 years. To take the longer required service life into account, Table 4.3N of BS EN 1992-1-1:2004 can be adopted, recommending an increase in exposure class by 2 for all environmental conditions to consider the requirement for a service life of 100 years. Main specified requirements by BS EN 206-1:2013 and BS EN 1992-1-1:2004 corresponding to these exposure classes include maximum *w/c*, minimum strength class, and minimum cement content. This is due to the fact that density and quality of concrete outer layer (cover) as the main protection layer is achieved by controlling the maximum *w/c* and minimum cement content, and may be related to a minimum strength class of concrete (BS EN 1992-1-1:2004). The range of specified requirements and minimum air content for freezing-and-thawing attack can be found in BS EN 206-1:2013, Table F.1. This table also presents other requirement such as aggregate characteristics for XF exposure classes, and sulfate-resisting cement for XA exposure classes. For corrosion protection of steel reinforcement when concrete is exposed to carbonation (XC classes) or chloride ions (XD/XS classes), values of minimum concrete cover required by BS EN 1992-1-1:2004, Table 4.4N, for Structural Class S4 should be considered. For extreme classes of XC4 and XD3/XS3, which are usually the case for tunnel lining designed for 100-year service life, minimum required covers are 1.2 in. (30 mm) and 1.8 in. (45 mm), respectively.

ACI 318 is another well-known and widely-used concrete code in the world that can be used for durability requirements of tunnel segments. ACI 318 approach, similar to BS EN 206-1:2013 and BS EN 1992-1-1:2004, is also based on Exposure Categories F, S, W, and C defined in ACI 318-14 Table 19.3.1.1, and requirements in Table 19.3.2.1. However, a few major differences exist between the ACI and European (EN) codes. First, ACI 318 has an additional exposure category, W, which is defined for durability of concrete in general in contact with water but not exposed to freezing and thawing, chlorides, or sulfates. Second, Exposure Category C applies to concrete exposed to all conditions that require protection against corrosion of reinforcement. Therefore, Category C in ACI 318 can be compared to XC and XD/XS exposure classes in BS EN 206-1:2013 and BS EN 1992-1-1:2004, which provide much more insight into how the specified requirements are set differently as related to the sources of corrosion. Third, ACI 318 only considers sulfate attack requirements corresponding to Category S, whereas BS EN 206-1:2013 and BS EN 1992-1-1:2004 cover a wide range of chemical attacks to different types of ions and acids, not only sulfate. Another major difference is that ACI 318 does not have any requirements for minimum cement content. Also, in contrast to BS EN 1992-1-1:2004, for corrosion protection of reinforcement, minimum concrete cover required by ACI 318 is a function of casting type—that is, cast-in-place or precast concrete manufactured under plant conditions. For precast segments, ACI 318 only categorizes the minimum cover based on two exposure classes of exposed or

Table 14.5f—Requirements for concrete by exposure class by ACI 318

Exposure class	Maximum *w/cm**	Minimum f_c', psi (MPa)	Additional requirements			Limits on cementitious materials
			Air content			
F0	NA	2500 (17.2)	NA			NA
F1	0.55	3500 (24.1)	Table 19.3.3.1			NA
F2	0.45	4500 (31.0)	Table 19.3.3.1			NA
F3	0.40†	5000† (34.5)	Table 19.3.3.1			26.4.2.2(b)
			Cementitious materials‡ — Types			Calcium chloride admixture
			ASTM C150/C150M	ASTM C595/C595M	ASTM C1157/C1157M	
S0	NA	2500 (17.2)	No type restriction	No type restriction	No type restriction	No restriction
S1	0.50	4000 (27.6)	II§‖	Types IP, IS, or IT with (MS) designation	MS	No restriction
S2	0.45	4500 (31.0)	V‖	Types IP, IS, or IT with (HS) designation	HS	Not permitted
S3	0.45	4500 (31.0)	V plus pozzolan or slag cement#	Types IP, IS, or IT with (HS) designation plus pozzolan or slag cement#	HS plus pozzolan or slag cement#	Not permitted
W0	NA	2500 (17.2)	None			
W1	0.50	4000 (27.6)	None			
			Maximum water-soluble chloride ion (Cl^-) content in concrete, percent by weight of cement**		Additional provisions	
			Nonprestressed concrete	Prestressed concrete		
C0	NA	2500 (17.2)	1.00	0.06	None	
C1	NA	2500 (17.2)	0.30	0.06		
C2	0.40	5000 (34.5)	0.15	0.06	Concrete cover††	

*The maximum *w/cm* limits in ACI 318-19, Table 19.3.2.1, do not apply to lightweight concrete.

†For plain concrete, the maximum *w/cm* should be 0.45 and the minimum f_c' should be 4500 psi (31 MPa).

‡Alternative combinations of cementitious materials to those listed in ACI 318-19, Table 19.3.2.1, are permitted when tested for sulfate resistance and meeting the criteria in 26.4.2.2(c).

§For seawater exposure, other types of portland cements with tricalcium aluminate (C_3A) contents up to 10 percent are permitted if *w/cm* does not exceed 0.40.

‖Other available types of cement such as Type I or Type III are permitted in Exposure Classes S1 or S2 if the C_3A contents are less than 8 percent for Exposure Class S1 or less than 5 percent for Exposure Class S2.

#The amount of the specific source of the pozzolan or slag cement to be used should be at least the amount that has been determined by service record to improve sulfate resistance when used in concrete containing Type V cement. Alternatively, the amount of the specific source of the pozzolan or slag cement to be used should be at least the amount tested in accordance with ASTM C1012/C1012M and meeting the criteria in 26.4.2.2(c).

**Water-soluble chloride ion content that is contributed from the ingredients including water, aggregates, cementitious materials, and admixtures should be determined on the concrete mixture by ASTM C1218/C1218M at age between 28 and 42 days.

††Concrete cover should be in accordance with 20.6.

not exposed to weather or in contract with the ground. Other considerations in ACI 318 are member types categorized as walls or others, and size of reinforcing bars for concrete exposure to weather or in contact with the ground. Because steel bars smaller than No. 6 (No. 19) are commonly used in segments, for all different exposure classes of precast segments, ACI 318 specifies a constant minimum cover of 1.5 in. (38 mm). This is in contrast with BS EN 1992-1-1:2004, which requires different minimum concrete covers ranging from 0.4 to 1.8 in. (10 to 45 mm) based on the sources of corrosion that can range from carbonation, chloride ions other than seawater, and seawater exposure.

Despite all the differences between ACI and EN approaches, a case example for an extreme exposure class/category, such as concrete exposed to chloride-induced corrosion, can provide some insight into how different the requirement can be between these codes. For this purpose, requirements of ACI 318, Category C2, is compared with EN Class XS3/XD3. ACI would require a maximum *w/c* of 0.4 and a minimum compressive strength of 5000 psi (35 MPa) whereas EN would require a maximum *w/c* of 0.45, a minimum compressive strength of 5000 psi (35 MPa), and a minimum cement content of 575 lb/yd^3 (340 kg/m^3). Concrete cover specified by ACI 318 as a minimum of 1.5 in. (38 mm) for reinforcement No. 6 (No. 19) or smaller can be compared with 1.8 in. (45 mm) required by BS EN 1992-1-1:2004. Such an example shows that despite all aforementioned differences between the two methods, the concrete requirements set forth would be very similar and most likely would result in a concrete specification with similar, if not identical, quality (Bakhshi and Nasri 2018c).

Prescriptive design methodologies provide similar recommendations to achieve a very dense high-quality concrete. However, the major flaw of prescriptive approaches is the lack of connection between the limiting requirements and main source of degradation mechanisms for each specific type of concrete damage. In contrast, performance-based design approaches, despite all challenges related to these methods, provides significant benefits to designers by focusing on the specific sources of concrete damages in a project-specific fashion (SIA 262). Future studies are needed to develop a performance-based design approach with reference to different major tunnel segment projects, including a combined sewer overflow tunnel, a subway tunnel, and a subsea road tunnel. Additionally, durability recommendations of national and international tunnel segment guidelines should be analyzed and compared, including BS PAS 8810 2016, DAUB:2013, AFTES:2005, ÖVBB (2011), and LTA 2010.

CHAPTER 15—REFERENCES

Committee documents are listed first by document number and year of publication followed by authored documents listed alphabetically.

American Association of State Highway and Transportation Officials (AASHTO)

AASHTO DCRT-1-2010—Technical Manual for Design and Construction of Road Tunnels—Civil Elements

American Concrete Institute (ACI)

ACI 201.2R-16—Guide to Durable Concrete

ACI 222R-01(10)—Protection of Metals in Concrete Against Corrosion

ACI 224.1R-07—Causes, Evaluation, and Repair of Cracks in Concrete Structures

ACI 318-19—Building Code Requirements for Structural Concrete and Commentary

ACI 544.1R-96(09)—Report on Fiber Reinforced Concrete

ACI 544.7R-16—Report on Design and Construction of Fiber-Reinforced Precast Concrete Tunnel Segments

ACI 546R-16—Guide to Concrete Repair

ASTM International

ASTM A615/A615M-18—Standard Specification for Deformed and Plain Carbon-Steel Bars for Concrete Reinforcement

ASTM A706/A706M-16—Standard Specification for Deformed and Plain Low-Alloy Steel Bars for Concrete Reinforcement

ASTM A820/A820M-16—Standard Specification for Steel Fibers for Fiber-Reinforced Concrete

ASTM A1064/A1064M-18—Standard Specification for Carbon-Steel Wire and Welded Wire Reinforcement, Plain and Deformed, for Concrete

ASTM C150/C150M-18—Standard Specification for Portland Cement

ASTM C595/C595M-19—Standard Specification for Blended Hydraulic Cements

ASTM C1012/C1012M-18b—Standard Test Method for Length Change of Hydraulic-Cement Mortars Exposed to a Sulfate Solution

ASTM C1157/C1157M-17—Standard Performance Specification for Hydraulic Cement

ASTM C1218/C1218M-17—Standard Test Method for Water-Soluble Chloride in Mortar and Concrete

ASTM C1580-15—Standard Test Method for Water-Soluble Sulfate in Soil

ASTM C1609/C1609M-12—Standard Test Method for Flexural Performance of Fiber-Reinforced Concrete (Using Beam With Third-Point Loading)

ASTM D412-16—Standard Test Methods for Vulcanized Rubber and Thermoplastic Elastomers—Tension

ASTM D516-16—Standard Test Method for Sulfate Ion in Water

ASTM D2240-15—Standard Test Method for Rubber Property—Durometer Hardness

ASTM D4130-15—Standard Test Method for Sulfate Ion in Brackish Water, Seawater, and Brines

ASTM E119-18—Standard Test Methods for Fire Tests of Building Construction and Materials

Austrian Society for Concrete and Construction Technology

ÖVBB 2011—Guideline for Concrete Segmental Lining Systems

British Standards Institution (BSI)

BS EN 206-1:2013—Concrete–Specification, Performance, Production and Conformity

BS EN 1991-1-1:2002—Eurocode 1: Actions on Structures

BS EN 1992-1-1:2004—Eurocode 2: Design of Concrete Structures—Part 1-1: General Rules and Rules for Buildings

BS EN 14651:2005+A1:2007—Test Method for Metallic Fibre Concrete. Measuring the Flexural Tensile Strength (Limit of Proportionality (LOP), residual)

BS EN 50122-2:2010—Railway applications - Fixed Installations – Electrical Safety, Earthing and the Return Circuit Part 2: Provisions Against the Effects of Stray Currents Caused by D.C. Traction Systems

BS PAS 8810:2016—Tunnel Design—Design of Concrete Segmental Tunnel Linings—Code of Practice

British Tunneling Society and The Institution of Civil Engineers

BTS ICE 2004—Tunnel Lining Design Guide

Concrete Society

CS TR63:2007—Guidance for the Design of Steel-Fibre-Reinforced Concrete

French Ministry for the Economy and Finance - Béton armé états limites

BAEL 91 Révisé 99:2007—Règles techniques de conception et de calcul des ouvrages et constructions en béton armé suivant la méthode des états limites

French Tunneling and Underground Space Association (AFTES)

AFTES:2005—Recommendation for the Design, Sizing and Construction of Precast Concrete Segments Installed at the Rear of a Tunnel Boring Machine (TBM)

AFTES-WG7:1993—Considerations on the Usual Methods of Tunnel Lining Design

Working Group No.7—Temporary Supports and Permanent Lining

German Committee for Structural Concrete within German Institute for Standardization

DAfStB Stahlfaserbeton:2012-11—Richtlinie Stahlfaserbeton/Technical Guidelines for Steel Fiber Reinforced Concrete, Part 1-3

German Federal Ministry of Transport and Digital Infrastructure

ZTV-ING:2007—Zusätzliche Technische Vertragsbedingungen und Richtlinien für den Bau von Straßentunneln (ZTV-ING)—Teil 5, Tunnelbau, Abschnitt 3 Maschinelle Schildvortriebsverfahren

German Railway Standards

Ril 853:2011—Richtlinie Eisenbahntunnel planen, bauen und in Stand halten

DS 853:1993—Eisenbabntunnel planen, bauen und instandhalten

German Research Association for Underground Transportation Facilities

STUVAtec:2005—STUVA Recommendations for Testing and Application of Sealing Gaskets in Segmental Linings

German Society for Concrete and Construction Technology (DBV)

DBV:2001—Guide to Good Practice—Steel Fibre Concrete

German Tunneling Committee (DAUB)

DAUB:2005—Recommendations for Static Analysis of Shield Tunnelling Machines

DAUB:2013—Lining Segment Design: Recommendations for the Design, Production, and Installation of Segmental Rings

International Federation for Structural Concrete (fib)

MC2010—Model Code for Concrete Structures 2010

International Organization for Standardization

ISO 834-11:2014—Fire Resistance Tests — Elements of Building Construction — Part 11: Specific Requirements for the Assessment of Fire Protection to Structural Steel Elements

ISO 11346:2004—Rubber, Vulcanized or Thermoplastic—Estimation of Life-Time and Maximum Temperature of Use

International Tunneling Association

ITA WG2 2000—Guidelines for the design of shield tunnel lining

ITA WG6 2004—Guidelines for structural fire resistance for road tunnels

International Union of Laboratories and Experts in Construction Materials, Systems and Structures (RILEM)

RILEM TC 162-TDF:2003—Test and Design Methods for Steel Fibre Reinforced Concrete. s–e Design Method: Final Recommendation

Italian National Research Council (CNR)

CNR DT 204/2006:2007—Guidelines for the Design, Construction and Production Control of Fibre Reinforced Concrete Structures

Italian Tunnelling Society

SIG WG N. 2:2019—Report No. 1 – Damages of Segmental Lining

Japanese Railway Technical Research Institute

RTRI 2008—Design Standards for Railway Structures and Commentary (Shield Tunnels)

Japan Society of Civil Engineers (JSCE)

JSCE 2007—Standard Specifications for Tunneling: Shield Tunnels

Los Angeles County Metropolitan Transportation Authority

LACMTA 2013—Metro Rail Design Criteria—Section 5 Structural/Geotechnical

Portland Cement Association (PCA)

PCA IS536:2002—Types and Causes of Concrete Deterioration

Royal Netherlands Standardization Institute (NEN)

NEN 6720:1995—Regulations for Concrete—Structural Requirements and Calculation Methods

Singapore Land Transport Authority

LTA 2010—Civil Design Criteria for Road and Rail Transit Systems

Spanish Ministry of Public Works and Transport

EHE-08 2010—Code on Structural Concrete, ANNEX 14—Recommendations for Using Concrete with Fibres

Swiss Society of Engineers and Architects

SIA 262:2003—Concrete Structures

U.S. Army Corps of Engineers

USACE EM 1110-2-2901:1997—Tunnels and Shafts in Rock

Authored documents

Abbas, S., 2014, "Structural and Durability Performance of Precast Segmental Tunnel Linings," PhD dissertation, University of Western Ontario, London, ON, Canada.

Alder, A.; Dhanda, D.; Hillyar, W.; and Runacres, A., 2010, "Extending London's Docklands Light Railway to Woolwich," *Proceedings of the ICE-Civil Engineering*, V. 163, No. 2, pp. 81-90. doi: 10.1680/cien.2010.163.2.81

Bakhshi, M.; Barsby, C.; and Mobasher, B., 2014, "Comparative Evaluation of Early Age Toughness Parameters in Fiber Reinforced Concrete," *Materials and Structures*, V. 47, No. 5, pp. 853-872. doi: 10.1617/s11527-013-0098-1

Bakhshi, M., and Nasri, V., 2013a, "Latest Developments in Design of Segmental Tunnel Linings," *Proceedings of the Canadian Society for Civil Engineering General Conference (CSCE 2013)*, Montréal, QC, Canada.

Bakhshi, M., and Nasri, V., 2013b, "Practical Aspects of Segmental Tunnel Lining Design," *Underground—The Way to the Future: Proceedings of the World Tunnel Congress 2013*, G. Anagnostou and H. Ehrbar, eds., Geneva, Switzerland.

Bakhshi, M., and Nasri, V., 2013c, "Structural Design of Segmental Tunnel Linings," *Proceedings of 3rd International Conference on Computational Methods in Tunneling and Subsurface Engineering: EURO: TUN 2013*, Ruhr University, Bochum, Germany, pp. 131-138.

Bakhshi, M., and Nasri, V., 2014a, "Review of International Practice on Critical Aspects of Segmental Tunnel Lining Design," *Proceedings of the 2014 North American Tunneling (NAT) Conference*, Los Angeles, CA, pp. 274-282.

Bakhshi, M., and Nasri, V., 2014b, "Guidelines and Methods on Segmental Tunnel Lining Analysis and Design—Review and Best Practice Recommendation," *Proceedings of the World Tunnel Congress*, Iguassu Falls, Brazil.

Bakhshi, M., and Nasri, V., 2014c, "Developments in Design for Fiber Reinforced Concrete Segmental Tunnel Lining," *2nd FRC International Workshop (1st ACI-fib Joint Workshop) on Fibre Reinforced Concrete*, Montreal, QC, Canada, pp. 441-452.

Bakhshi, M., and Nasri, V., 2014d, "Design Considerations for Precast Tunnel Segments According to International Recommendations, Guidelines and Standards," TAC 2014, Vancouver, BC, Canada.

Bakhshi, M., and Nasri, V., 2015a, "Design of Segmental Tunnel Linings for Serviceability Limit State," ITA World Tunnel Congress (WTC) 2015, Dubrovnik, Croatia.

Bakhshi, M., and Nasri, V., 2015b, "Cracking Serviceability Limit State for Precast Concrete Tunnel Segments," Canadian Society of Civil Engineers (CSCE) 2015 General Conference, Regina, SK, Canada.

Bakhshi, M., and Nasri, V., 2017a, "Design of Steel Fiber-Reinforced Concrete Segmental Lining for the South Hartford CSO Tunnel," *Rapid Excavation Tunneling Conference (RETC) 2017*, San Diego, CA, pp. 706-717.

Bakhshi, M., and Nasri, V., 2017b, "Reduction of Water Inflow by Controlling Cracks in Tunnel Segmental Linings using Fiber Reinforcement," SP-319, *Reduction of Crack Width with Fiber*, C.-M. Aldea and M. Ekenel, eds., American Concrete Institute, Farmington Hills, MI. (CD-ROM)

Bakhshi, M., and Nasri, V., 2018a, "Tunnel Segment Gasket Design-Solutions and Innovations," *Proceedings of the Canadian Society for Civil Engineering General Conference (CSCE 2018)*, Fredericton, NB, Canada.

Bakhshi, M., and Nasri, V., 2018b, "Guide for Optimized Design of Tunnel Segmental Ring Geometry," *North American Tunneling (NAT) 2018 Proceedings*, Washington, DC, pp. 541-549.

Bakhshi, M., and Nasri, V., 2018c, "Durability Design of Segmental Linings for Intended Service Life of Tunnels," *Proceedings of Sixth International Conference on Durability of Concrete Structures*, Leeds, UK.

Bakhshi, M., and Nasri, V., 2018d, "Tunnel Segmental Lining Durability," *Proceedings of TT2018-TAC/NASTT-NW Tunnelling and Trenchless Conference*, Edmonton, AB, Canada.

Bakhshi, M., and Nasri, V., 2018e, "Tunnel Segmental Lining Geometry, Tolerance and Measurement," *Proceedings of TT2018-TAC/NASTT-NW Tunnelling and Trenchless Conference*, Edmonton, AB, Canada.

Barros, J. A. O.; Cunha, V. M. C. F.; Ribeiro, A. F.; and Antunes, J. A. B., 2005, "Postcracking Behaviour of Steel Fibre Reinforced Concrete," *Materials and Structures*, V. 38, No. 1, pp. 47-56. doi: 10.1007/BF02480574

Beňo, J., and Hilar, M., 2013, "Steel Fibre Reinforced Concrete for Tunnel Lining-Verification by Extensive Laboratory Testing and Numerical Modelling," *Acta Polytechnica*, V. 53, No. 4, pp. 329-337.

Bertolini, L.; Carsana, M.; and Pedeferri, P., 2007, "Corrosion Behaviour of Steel in Concrete in the Presence of Stray Current," *Corrosion Science*, V. 49, No. 3, pp. 1056-1068. doi: 10.1016/j.corsci.2006.05.048

Blom, C. B. M., 2002, "Design Philosophy of Concrete Linings for Tunnels in Soft Soil," PhD dissertation, Delft University Press, Delft, the Netherlands, Dec.

Brenna, M.; Dolara, A.; Leva, S.; and Zaninelli, D., 2010, "Effects of the DC Stray Currents on Subway Tunnel Structures Evaluated by FEM Analysis," Power and Energy Society General Meeting, 2010 IEEE, pp. 1-7.

Buhr, B.; Nielsen, P. V.; Bajernaru, F.; and McLeish, A., 1999, "Bucharest Metro: Dealing with Stray Current Corrosion," *Proceedings of the Tunnel Construction and Piling Conference*, Institution of Mining and Metallurgy, pp. 275-286.

Caan, C. P.; Jansen, J. A. G.; Heijmans, R. W. M. G.; and van der Put, J. L., 1998, "High Speed Line – South: The Groene Hart Tunnel- Lining Design," *Reference Design*, Report No. 9G4 0001 981028, 52 pp.

Caratelli, A.; Meda, A.; and Rinaldi, Z., 2012, "Design According to MC2010 of a Fibre-Reinforced Concrete Tunnel in Monte Lirio, Panama," *Structural Concrete*, V. 13, No. 3, pp. 166-173. doi: 10.1002/suco.201100034

Cavalaro, S. H. P.; Blom, C. B. M.; Aguado, A.; and Walraven, J. C., 2012, "New Design Method for the Production Tolerances of Concrete Tunnel Segments," *Journal of Performance of Constructed Facilities*, ASCE, V. 26, No. 6, pp. 824-834. doi: 10.1061/(ASCE)CF.1943-5509.0000291

Çimentepe, A. G., 2010, "Evaluation of Structural Analysis Methods Used for the Design of TBM Segmental

Linings," MSc thesis, Middle East Technical University, Ankara, Turkey.

Clarke-Hackston, N.; Messing, M.; Loh, D.; and Lott, R., 2006, "Modern High Precision High Speed Measurement of Segments and Moulds," *Tunnelling and Underground Space Technology*, V. 21, No. 3, p. 258 doi: 10.1016/j.tust.2005.12.119

Colombo, M.; Martinelli, P.; and di Prisco, M., 2015, "A Design Approach for Tunnels Exposed to Blast and Fire," *Structural Concrete*, V. 16, No. 2, pp. 262-272. doi: 10.1002/suco.201400052

Curtis, D. J.; Hay, M.; and Croydon, A., 1976, "discussion on 'The Circular Tunnel in Elastic Ground,'," *Geotechnique*, V. 26, No. 1, pp. 231-237. doi: 10.1680/geot.1976.26.1.231

Deere, D. U.; Peck, R. B.; Monsees, J. E.; and Schmidt, B., 1969, "Design of Tunnel Liners and Support Systems," *Highway Research Record 889*, Final Report to Urban Mass Transit Administration, U.S. Department of Transportation, Washington, DC.

Dolara, A.; Foiadelli, F.; and Leva, S., 2012, "Stray Current Effects Mitigation in Subway Tunnels," *IEEE Transactions on Power Delivery*, V. 27, No. 4, pp. 2304-2311. doi: 10.1109/TPWRD.2012.2203829

Duddeck, H., and Erdmann, J., 1982, "Structural Design Models for Tunnels," *Tunneling '82-Proceedings of the Third International Symposium, Institute of Mining and Metallurgy*, London, UK, pp. 83-91.

Edvardsen, C.; Müller, S.; Nell, W.; and Eberli, M., 2017, "Steel Fibre Reinforced Concrete for Tunnel Lining Segments – Design, Durability Aspects and Case Studies on Contemporary Projects," *Proceedings of STUVA Conference 2017* (49 Forschung + Praxis: STUVA-Tagung 2017), Stuttgart, Germany, pp. 184-189.

fib Working Party 1.4.1, 2017, "Tunnels in Fiber Reinforced Concrete," fib *Bulletin*, No. 83, Fédération Internationale du Béton, Lausanne, Switzerland, Oct.

Francis, O., and Mangione, M., 2012, "Developments in Joint Design for Steel Fibre Reinforced Concrete Segmental Tunnel Linings," *Proceedings of the World Tunnelling Congress* 2012, Bangkok, Thailand.

Fukui, K., and Okubo, S., 2003, "TBM Cutting Forces with Particular Reference to Cutter and Tunnel Diameters," *ISRM 2003–Technology Roadmap for Rock Mechanics*, South African Institute of Mining and Metallurgy, Johannesburg, South Africa.

Geng, J., 2008, "The Research on the Deteriorated Mechanisms of Reinforced Concrete in Stray Currents and Chloride Ion Coexisted Corrosion Environment," PhD dissertation, Wuhan University of Technology, Wuhan, China.

Geng, J., and Ding, Q. J., 2010, "Transport Characteristics of Chloride Ion in Concrete with Stray Current," *Journal of Building Materials*, No. 1, pp. 121-124.

Groeneweg, T., 2007, "Shield Driven Tunnels in Ultra High Strength Concrete: Reduction of the Tunnel Lining Thickness," MSc thesis, Delft University of Technology, Delft, the Netherlands.

Guglielmetti, V.; Grasso, P.; Mahtab, A.; and Xu, S., 2007, *Mechanized Tunnelling in Urban Areas: Design Methodology and Construction Control*, CRC Press, Boca Raton, FL, 528 pp.

Handke, D., 2012, "High-Precision Segments: Prerequisite for a High-Quality Monocoque Tunnel," *Tunnel*, V. 8, No. 42.

Harding, A., and Francis, O., 2013, "Designing at the Limit: Brisbane Airport Link Segmental Lining," Rapid Excavation Tunneling Conference (RETC) 2013, Washington, DC, pp. 834-843.

Helsing, E., and Mueller, U., 2013, "Beständighet av cement och betong i tunnelmiljö (Resistance to Cement and Concrete in Tunnel Environment)," *Seminarium Vatten i anläggningsbyggande (Seminar on Water in Construction)*, Göteborg, Sweden.

Hoek, E., and Brown, E. T., 2018, "The Hoek-Brown Failure Criterion and GSI: 2018 Edition," *Journal of Rock Mechanics and Geotechnical Engineering*, doi: 10.1016/j.jrmge.2018.08.001

ITA Working Group 2, 2016, "Twenty Years of FRC Tunnel Segments Practice: Lessons Learnt and Proposed Design Principles," *Report* No. 16, International Tunnelling and Underground Space Association, Apr., pp. 71.

ITA Working Group on Maintenance and Repair of Underground Structures, 1991, "Report on the Damaging Effects of Water on Tunnels During their Working Life," *Tunnelling and Underground Space Technology*, V. 6, No. 1, pp. 11-76. doi: 10.1016/0886-7798(91)90005-O

ITA Working Group on General Approaches to the Design of Tunnels, 1988, "Guidelines for the Design of Tunnels," *Tunnelling and Underground Space Technology*, V. 3, No. 3, pp. 237-249. doi: 10.1016/0886-7798(88)90050-8

Iyengar, K. T., 1962, "Two-Dimensional Theories of Anchorage Zone Stresses in Post-Tensioned Beams," *ACI Journal Proceedings*, V. 59, No. 10, Oct., pp. 1443-1466.

Janssen, P., 1983, "Load Capacity of Segment Joints," PhD dissertation, Braunschweig University of Technology, Braunschweig, Germany.

Kemp, R., 2007, "Traction Energy Metrics," *Rail Safety and Standards Board*, Lancaster University, UK.

Kirschke, D.; Schälicke, H.; and Fraas, D., 2013, "Finne Tunnel: Innovative Targeted Resealing of Segment Bore Joints—Part 2," *Tunnel*, pp. 30-40.

Lee, T., and Choi, T., 2017, "Numerical Analysis of Cross Passage Opening for TBM Tunnels," *Proceedings of the 19th International Conference on Soil Mechanics and Geotechnical Engineering*, Seoul, South Korea.

Li, Q.; Yu, H.; Ma, H.; Chen, S.; and Liu, S., 2014, "Test on Durability of Shield Tunnel Concrete Segment under Coupling Multi-Factors," *The Open Civil Engineering Journal*, V. 8, No. 1, pp. 451-457. doi: 10.2174/1874149501408010451

Mashimo, H.; Isago, N.; Yoshinaga, S.; Shiroma, H.; and Baba, K., 2002, "Experimental Investigation on Load-Carrying Capacity of Concrete Tunnel Lining," *Proceedings of AITES-ITA 2002 - 28th General Assembly & World Tunnelling Congress 2002*, Sydney, Australia, pp. 1-10.

Mendez Lorenzo, M. G., 1998, "Reliability Analysis of a Steel Fibre Reinforced Concrete Tunnel Lining,"

master's thesis, Delft University of Technology, Delft, the Netherlands.

Mobasher, B.; Bakhshi, M.; and Barsby, C., 2014, "Back-calculation of Residual Tensile Strength of Regular and High Performance Fiber Reinforced," *Construction and Building Materials*, V. 70, pp. 243-253. doi: 10.1016/j.conbuildmat.2014.07.037

Moccichino, M.; Romualdi, P.; Perruzza, P.; Meda, A.; and Rinaldi, Z., 2010, "Experimental Tests on Tunnel Precast Segmental Lining with Fiber Reinforced Concrete," ITA 2010 World Tunnel Congress, Vancouver, BC, Canada.

Morgan, H. D., 1961, "A Contribution to the Analysis of Stress in A Circular Tunnel," *Geotechnique*, V. 11, No. 1, pp. 37-46. doi: 10.1680/geot.1961.11.1.37

Muir Wood, A. M., 1975, "The Circular Tunnel in Elastic Ground," *Geotechnique*, V. 25, No. 1, pp. 115-127. doi: 10.1680/geot.1975.25.1.115

Neun, E., 2012, "Structural Fire Safety Engineering—Eurocode Approach and Practical Application," *Proceedings of the World Tunnelling Congress 2012*, Bangkok, Thailand.

Niasati, M., and Gholami, A., 2008, "Overview of Stray Current Control in DC Railway Systems," *International Conference on Railway Engineering - Challenges for Railway Transportation in Information Age*, ICRE, pp. 1-6.

Ninić, J., and Meschke, G., 2017, "Simulation Based Evaluation of Time-Variant Loadings Acting on Tunnel Linings during Mechanized Tunnel Construction," *Engineering Structures*, V. 135, pp. 21-40. doi: 10.1016/j.engstruct.2016.12.043

Peck, R. B., 1969, "Deep Excavation and Tunnelling in Soft Ground, State of the Art Report," 7th International Conference on Soil Mechanics and Foundation Engineering, Mexico City, Mexico, pp. 225-290.

Plizzari, G., and Tiberti, G., 2009, "Tunnel Linings Made by Precast Concrete Segments," *Construction Methodologies and Structural Performance of Tunnel Linings*, G. A. Plizzari, ed., Brescia, Italy, pp. 136-131.

Poh, J.; Tan, K. H.; Peterson, G. L.; and Wen, D., 2009, "Structural Testing of Steel Fibre Reinforced Concrete (SFRC) Tunnel Lining Segments in Singapore," *Proceedings of the World Tunnelling Congress*, Budapest, Hungary.

Romer, M., 2013, "Durability of Underground Concrete," Workshop on Underground Infrastructures: Challenges and Solutions, LTA, Singapore.

Rostami, J., 2008, "Hard Rock TBM Cutterhead Modeling for Design and Performance Prediction," *Geomechanics and Tunnelling*, V. 1, No. 1, pp. 18-28. doi: 10.1002/geot.200800002

Sinha, R. S., 1989, *Underground Structures: Design and Instrumentation,* Elsevier Science, New York, NY, 500 pp.

Solgaard, A. O. S.; Carsana, M.; Geiker, M. R.; Küter, A.; and Bertolini, L., 2013, "Experimental Observations of Stray Current Effects on Steel Fibres Embedded in Mortar," *Corrosion Science*, V. 74, pp. 1-12. doi: 10.1016/j.corsci.2013.03.014

Soranakom, C., and Mobasher, B., 2007, "Closed Form Solutions for Flexural Response of Fiber Reinforced Concrete Beams," *Journal of Engineering Mechanics*, ASCE, V. 133, No. 8, pp. 933-941. doi: 10.1061/(ASCE)0733-9399(2007)133:8(933)

Srikanth, S.; Sankaranarayanan, T. S. N.; Gopalakrishna, K.; Narasimhan, B. R. V.; Das, T. V. K.; and Das, S. K., 2005, "Corrosion in a Buried Pressurised Water Pipeline," *Engineering Failure Analysis*, V. 12, No. 4, pp. 634-651. doi: 10.1016/j.engfailanal.2004.02.006

Talmon, A. M., and Bezuijen, A., 2011, "Analytical Model for the Beam Action of a Tunnel Lining During Construction," *International Journal for Numerical and Analytical Methods in Geomechanics*, V. 37, No. 2, pp. 181-200. doi: 10.1002/nag.1092

Tang, K., 2017, "Stray Current Induced Corrosion of Steel Fibre Reinforced Concrete," *Cement and Concrete Research*, V. 100, pp. 445-456. doi: 10.1016/j.cemconres.2017.08.004

Tintelnot, G.; Lindenbauer, K.-H.; and Sinelnikow, M., 2018, "New Joint Sealing Process for Segment Tunnels," *Tunnel*, pp. 54-59.

Vandewalle, L., 2000, "Cracking Behaviour of Concrete Beams Reinforced with a Combination of Ordinary Reinforcement and Steel Fibers," *Materials and Structures*, V. 33, No. 3, pp. 164-170. doi: 10.1007/BF02479410

Wang, C.; Li, W.; Wang, Y.; Xu, S.; and Fan, M., 2018, "Stray Current Distributing Model in the Subway System: A Review and Outlook," *International Journal of Electrochemical Science*, V. 13, pp. 1700-1727. doi: 10.20964/2018.02.16

Xiong, W., 2008, "Study on Deterioration Characteristics of Reinforced Concrete in the Presence of Stray Current and Chloride Ion," PhD dissertation, Wuhan University of Technology, Wuhan, China.

Yao, Y.; Bakhshi, M.; Nasri, V.; and Mobasher, B., 2018a, "Interaction Diagrams for Design of Hybrid Fiber-Reinforced Tunnel Segments," *Materials and Structures*, V. 51, No. 1, 17 pp.

Yao, Y.; Bakhshi, M.; Nasri, V.; and Mobasher, B., 2018b, "Closed-Form Solutions for Interaction Diagrams of Hybrid Fiber-Reinforced Tunnel Segments," *Proceedings of FRC2018 - 3rd ACI-fib-RILEM on Fibre Reinforced Concrete: from Design to Structural Applications*, Lake Garda, Italy.

Zhong, X.-C.; Liu, Q.-W.; and Zhao, H., 2011, "Study on the Grouting Pressure of Shield Tunnel," *ASCE Geotechnical Special Publication*, V. 215, pp. 183-190.

Zhu, Y. H., and Zou, Y. S., 2012, "Influence of Stray Current on Chloride Ion Migrates in Concrete," *Journal of Wuhan University of Technology—Materials Science Edition*, V. 7, pp. 32-36.

American Concrete Institute
Always advancing

As ACI begins its second century of advancing concrete knowledge, its original chartered purpose remains "to provide a comradeship in finding the best ways to do concrete work of all kinds and in spreading knowledge." In keeping with this purpose, ACI supports the following activities:

- Technical committees that produce consensus reports, guides, specifications, and codes.
- Spring and fall conventions to facilitate the work of its committees.
- Educational seminars that disseminate reliable information on concrete.
- Certification programs for personnel employed within the concrete industry.
- Student programs such as scholarships, internships, and competitions.
- Sponsoring and co-sponsoring international conferences and symposia.
- Formal coordination with several international concrete related societies.
- Periodicals: the ACI Structural Journal, Materials Journal, and Concrete International.

Benefits of membership include a subscription to Concrete International and to an ACI Journal. ACI members receive discounts of up to 40% on all ACI products and services, including documents, seminars and convention registration fees.

As a member of ACI, you join thousands of practitioners and professionals worldwide who share a commitment to maintain the highest industry standards for concrete technology, construction, and practices. In addition, ACI chapters provide opportunities for interaction of professionals and practitioners at a local level to discuss and share concrete knowledge and fellowship.

American Concrete Institute
38800 Country Club Drive
Farmington Hills, MI 48331
Phone: +1.248.848.3700
Fax: +1.248.848.3701

www.concrete.org

American Concrete Institute
Always advancing

38800 Country Club Drive
Farmington Hills, MI 48331 USA
+1.248.848.3700
www.concrete.org

The American Concrete Institute (ACI) is a leading authority and resource worldwide for the development and distribution of consensus-based standards and technical resources, educational programs, and certifications for individuals and organizations involved in concrete design, construction, and materials, who share a commitment to pursuing the best use of concrete.

Individuals interested in the activities of ACI are encouraged to explore the ACI website for membership opportunities, committee activities, and a wide variety of concrete resources. As a volunteer member-driven organization, ACI invites partnerships and welcomes all concrete professionals who wish to be part of a respected, connected, social group that provides an opportunity for professional growth, networking and enjoyment.

9 781641 950978